UNIVERSITY OF OKLAHOMA

GRADUATE COLLEGE

EFFECT OF LIPID MODIFICATION AND ACRA-LIPID INTERACTIONS ON THE STRUCTURE AND OLIGOMERIZATION OF ACRA

A DISSERTATION

SUBMITTED TO THE GRADUATE FACULTY

in partial fulfillment of the requirements for the

Degree of

DOCTOR OF PHILOSOPHY

By

QIANG GE
Norman, Oklahoma
2009

EFFECT OF LIPID MODIFICATION AND ACRA-LIPID INTERACTIONS ON THE STRUCTURE AND OLIGOMERIZATION OF ACRA

A DISSERTATION APPROVED FOR THE
DEPARTMENT OF CHEMISTRY AND BIOCHEMISTRY

BY

_____
Dr. Helen I. Zgurskaya, Chair

_____
Dr. Valentin V. Rybenkov

_____
Dr. Ann H. West

_____
Dr. Robert P. Houser

_____
Dr. Anne K. Dunn

Acknowledgements

The writing of a dissertation is a relatively isolating experience, yet it is definitely not possible without the support from numerous people. Therefore my sincere gratitude goes to everyone whoever helped and supported me during the last six years.

I wish to thank my advisor Dr. Helen I. Zgurskaya, for her continuous support in the Ph.D. program. She was always there to listen and to give advice. She taught me how to ask and address questions. Without her encouragement and constant guidance, I could not finish this dissertation. Special thanks to Dr. Valentin Rybenkov for his constructive criticism and sound advice. His deep insight into the science always motivated me to explore my research. I would like to thank my current committee members (Dr. Ann H. West, Dr. Robert P. Houser, and Dr. Anne K. Dunn) as well as previous committee members (Dr. Richard W. Taylor, Dr. Marvin Whiteley, and Dr. Han Wang) for their consistent suggestion and support in my study.

I also appreciate the help and encouragement from all members in Dr. Zgurskaya's and Dr. Rybenkov's lab. Special thanks to Dr. Elena Tikhonova, who taught me a lot of basic biochemical techniques in the beginning of my research. Dr. Zoya Petrushenko, Dr. Lusine Demirkhanyan, Dr. Qinhong Wang, Dr. Yuanbo Cui and Dr. Yoichi Yamada provided me with their support. Thanks to my friends in the lab: Dr. Sze Yi Lau, Vishakha Devroy, Girija Dhamdhere, Sita Devi Modali, Shou Lu, Yun Liu, Feng Xia, Ganesh Krishnamoorthy, Kostyantyn Bobyk, Weifeng She, and Nick Huffmaster.

I want to dedicate this dissertation to my parents, Liyun Ge and Zhihui Feng for giving me life, for educating me, for unconditional love and encouragement to pursue my

interests. Thanks to my parents-in-law for their support and help. I also want to thank my lovely wife, Juan Peng, for her love and trust, for standing behind me all the time without complaint. Thanks to my dear sister Hai Ge, for listening to my frustrations, and for believing in me. Last but not least, I give special thanks to my baby son, Alan Ge, who brings me so much happiness and inspiration, who always amazes me and gives me strength.

Table of Contents

List of Tables

II. Materials and Methods

Chapter 1

Chapter 3

Lists of Figures

I. Introduction

Chapter 1

Chapter 2

Chapter 3

Abstract

A wide range of antibacterial agents including antibiotics can be expelled out of the cell by AcrAB-TolC complex. In this complex, the membrane fusion protein AcrA is located in the periplasm and essential for drug efflux. Although AcrA is generally considered to be a physical linker that strengthens the weak interaction between the RND type transporter AcrB and the outer membrane channel TolC, the molecular mechanism of AcrA is still not well understood. To elucidate how AcrA functions in the multidrug efflux complex AcrAB-TolC, we characterized the structure of AcrA. Using the *in vitro* limited proteolysis approach, we demonstrated that both the N-terminal lipid modification and *E. coli* polar lipids affect the accessibility of AcrA to trypsin. In addition, we found that the cleavage sites are located in the conserved membrane proximal (MP) domain of AcrA. We next used these sites as a map to characterize the structure of AcrA in the periplasm. Our *in vivo* study showed that the overall structure of over-expressed AcrA *in vivo* is similar to that of the purified AcrA. However, the trypsin cleavage of the chromosomally encoded AcrA demonstrated that the tripartite AcrAB-TolC assembly protects the MP domain of AcrA. This result thus suggests that the MP domain of AcrA is required for the functional assembly of the multidrug efflux complex AcrAB-TolC.

The oligomeric state of AcrA is still uncertain. Here we used formaldehyde cross-linking and size exclusion chromatography to study the oligomerization of AcrA. We found that, in contrast to the monomeric form of soluble AcrA ($AcrA^{S}$-His), the lipidated AcrA ($AcrA^{L}$-His) exists as an oligomer, mostly as a trimer. This result indicates that lipid modification promotes oligomerization of AcrA. In addition, soluble AcrA can form

an oligomer in the presence of *E. coli* polar lipids and low concentrations (less than 100 mM) of sodium chloride, suggesting that AcrA-lipid interaction is one of the driving forces for the oligomerization of soluble AcrA. We concluded that AcrA functions as an oligomer, possibly a trimer.

I. Introduction

I.1 AcrAB-TolC is the major multidrug efflux complex in *E. coli*

Antibiotics are the powerful means with which human beings combat bacterial infections. Although many antibiotics are still widely used and new antibiotics are developed, drug resistance in bacteria attracts more and more attention. Particularly, Gram-negative bacteria are more resistant than Gram-positive bacteria (46). Both low permeability of the unique outer membrane and drug efflux systems in Gram-negative bacteria contribute to drug tolerance in clinical isolates (31). Compared to the substrate-specific transporters, multidrug efflux transporters are capable of expelling many structurally unrelated compounds including antibiotics, dyes, detergents, organic solvents, bile salts, to the outside medium. Moreover, exposure to antibiotics can induce the over-expression of otherwise silent multi-drug efflux transporters (45).

Based on energy sources, multidrug-efflux pumps are classified into: primary transporters belonging to the ATP-Binding Cassette (ABC) family of proteins, which expel substrates at the expense of hydrolysis of ATP, and secondary pumps that utilize transmembrane electrochemical potential of proton or sodium ion as the driving force (53). These secondary transporters belong to four superfamilies of proteins: Major Facilitator Superfamily (MFS), Resistance-Nodulation-cell Division (RND) superfamily, Multidrug And Toxic compound Exporters (MATE), and Small Multidrug Resistance (SMR) family (53).

The majority of multidrug efflux transporters in Gram-negative bacteria belong to the RND superfamily (52). Seven ORFs (*acrB, acrD, acrF, yhiV, cusA, yegN and yegO*)

on the chromosomal DNA of *E.coli* are assumed to be capable of drug transport (47). However, only AcrAB-TolC is over-expressed in clinical isolates (39).

RND transporter AcrB in *E. coli* takes advantage of influx of protons (from periplasm to cytoplasm) to expel the drugs to the external medium. AcrB functions in conjunction with two accessory proteins: Outer-Membrane Factor (OMF) TolC and the periplasmic adaptor protein, AcrA (11, 37). The essential role of these components in the multidrug efflux was confirmed by the increased susceptibility to antibiotics with the deletion of any components in this complex (48). Bypassing the periplasm, AcrA-AcrB-TolC complex extrudes various substances directly into the external medium (66). The substrates include, but are not limited to, chloramphenicol, fluoroquinolones, fusidic acid, lipophilic β-lactam antibiotics, nalidixic acid, novobiocin, rifampin, tetracycline, acriflavine, ethidium bromide, bile salts, short-chain fatty acids, SDS, Triton X-100 (TX) and triclosan (51).

Biochemical studies showed the interactions between the components in this tripartite complex. AcrA interaction with AcrB and/or TolC was demonstrated in the *in vivo* and *in vitro* studies (14, 23, 66, 67, 74). Dithiobis(succinimidylpropionate) (DSP) cross-linking *in vivo* showed that AcrA associates with AcrB independently of TolC and substrates (74). A chimeric study further implied that the C-terminal residues of AcrA (290-357 a.a) are involved in the interaction with AcrB (7). Another independent study, Isothermal Titration Calorimetry (ITC) experiments, also illustrated that the C-terminal domain of AcrA (172-397 a.a) binds to AcrB (67). The interface of AcrA-AcrB was mapped in the recent *in vivo* site-specific cross-linking study (62). It showed that contiguous β-roll, β-barrel, and lipoyl domain of AcrA are physically adjacent to the

periplasmic domain of AcrB (62). On the other hand, AcrA interaction with TolC was demonstrated in several genetic and biochemical studies (14, 23, 32, 66, 67). Cross-linking of cysteine residues introduced by site-directed mutagenesis into AcrA and TolC implied that the AcrA-TolC interaction domain is located between residues on the lower α-helical barrel domain of TolC and the N-terminal α-helix of the AcrA coiled-coil (32). Although a cross-linking study showed that AcrB and TolC are spatially adjacent to each other (63), it is generally assumed that interaction between AcrB and TolC is weak, especially in the absence of AcrA (66).

On the other hand, structural studies of these three proteins in recent years greatly enhanced our understanding of the complex formation at the molecular level. Crystal structures of TolC, AcrB and AcrA were released in 2000, 2002, and 2006, respectively (28, 40, 43).

As shown in Figure I.1, the crystal structure of the OMF TolC is a cannon-like trimer with a length of about 140 Å (28). This trimer can be further divided into an outer membrane section and a periplasmic section. Four strands from each protomer assemble and form a 40 Å thick, 12-stranded β-barrel that crosses the outer membrane. The periplasmic section comprises the 100 Å long α-helical barrel and equatorial section surrounding the helical domain. The proline-containing interdomains link the right-handed β-barrel and left-handed α-helical barrel. Unlike the partially or fully occluded interior of some outer membrane proteins (5, 8, 33, 49, 57), the top of the structure, or the outer membrane section of TolC, is open and fully accessible to solvent. Nevertheless, the bottom of the α-helical barrel is closed by coiled-coils in this structure.

In the crystal structure, the RND pump AcrB is arranged as a jellyfish-like trimer

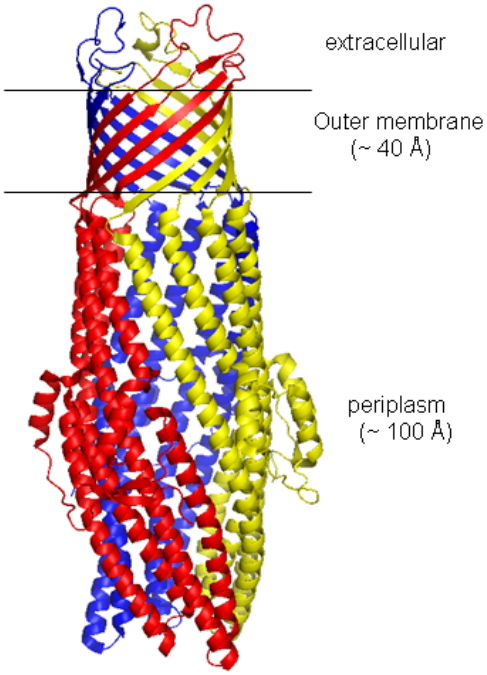

Figure I.1 Crystal structure of TolC (28). The individual protomers are colored blue, red, and yellow. The β-barrel domain of TolC transverses the bacterial OM.

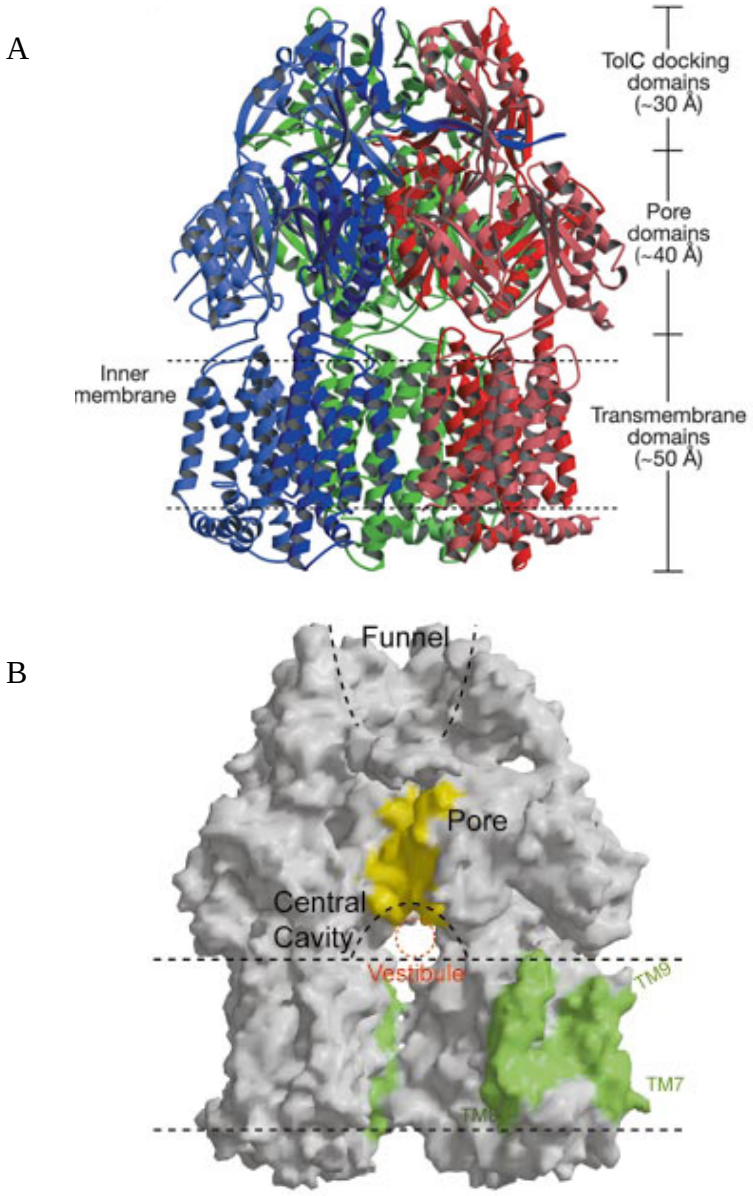

Figure I.2 Crystal structure of AcrB (43). (A) Side view of a ribbon representation of three protomers, which are individually coloured (blue, green and red). (B) A cutaway view displaying the solvent-accessible surface of AcrB. The framework of the funnel and the cavity are indicated by dotted lines. The yellow areas of the surface are coloured according to residues from Asp 99 to Leu 118 in pore helices. The pale green areas are coloured according to residues in TM7 (Gly 539–Val 557) and TM8–TM9 (Ser 869–Phe 918).

(Figure I.2) (42, 43, 58). It consists of a 50 Å transmembrane domain and a 70 Å periplasmic headpiece. This headpiece can be further divided as an upper TolC-docking domain and a lower pore domain with 30 and 40 Å thick, respectively. The trapezoidal TolC-docking part is about 70 Å wide at the bottom and 40 Å wide at the top. The cutaway view showed that this TolC-docking domain is a funnel-like structure which opens to the outside. The maximal inner diameter of this domain is about 30 Å. In addition, a long hairpin from the TolC-docking domain in each protomer inserts into the upper part in the next protomer, which possibly results in the tight packing of the headpiece in periplasm. Three α helices from each protomer, nine helices in total, form the pore domain. The bottom part of the pore domain is open to form the central cavity, which is supposed to mediate substrate trapping from periplasm. Loosely packed transmembrane domains are organized in a ring-like structure with a central hole. The site-specific mutagenesis studies (17, 43) show that there are three essential charged residues: Asp 407, Asp 408 and Lys940 in this transmembrane domain. These three residues are proposed to mediate the proton translocation through the inner membrane.

The protease-resistant fragment of AcrA (45-312 a.a) was crystallized and the core portion (53-299 a.a) was solved in 2006 (40). The protomer structure of AcrA is similar to that of MexA (1, 21), a homologous membrane fusion protein in *P. aeruginosa*. Both AcrA and MexA have the elongated sickle shape protein structures. The resolved structure displayed three domains: a β-barrel domain, a coiled-coil α-helical hairpin and a lipoyl domain between above two domains (Figure I.3 A). This result is consistent with the secondary structure prediction based on the amino acid sequence: helices domain, lipoyl domain and C-terminal hydrophobic domain (26). The β-barrel domain consists of

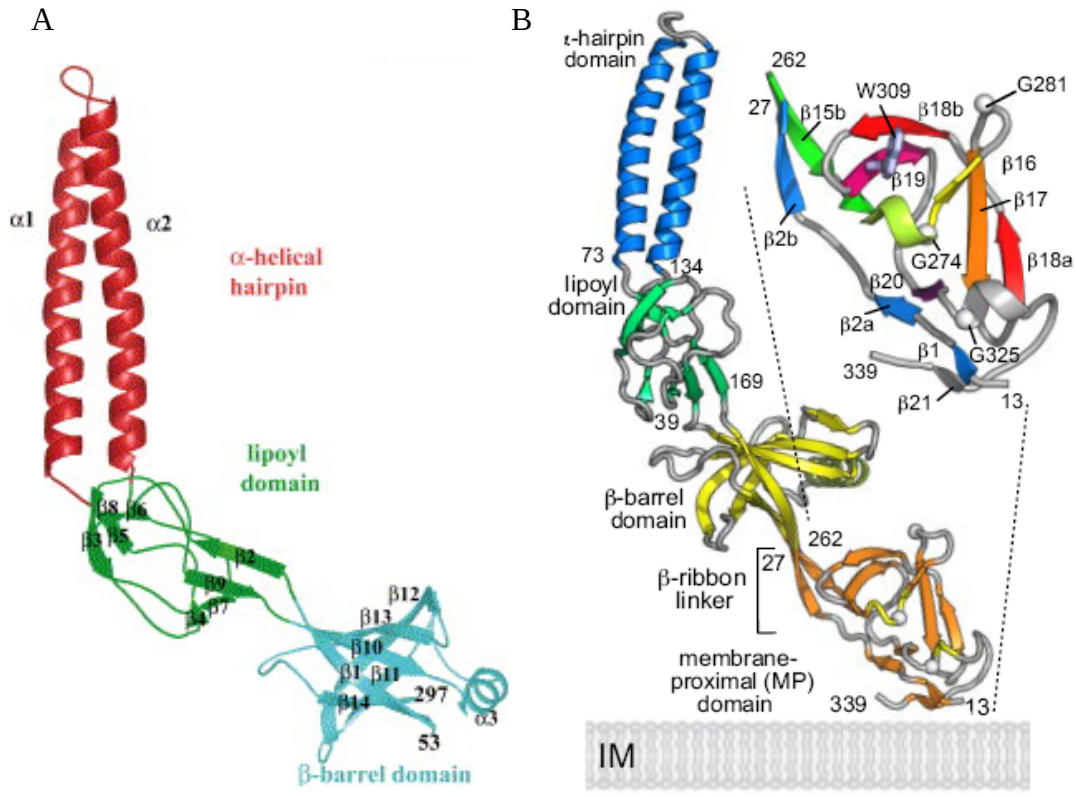

Figure I.3 Crystal structure of membrane fusion proteins. (A) Structure of AcrA (45–312)-4M (molecule C) (40), with the α-helical hairpin domain in red, lipoyl domain in green, and β-barrel domain in cyan. (B) Completed structure of the MexA including the MP domain (62). The α-hairpin domain, lipoyl domain, β-barrel domain, and MP domain are colored blue, green, yellow and orange, respectively.

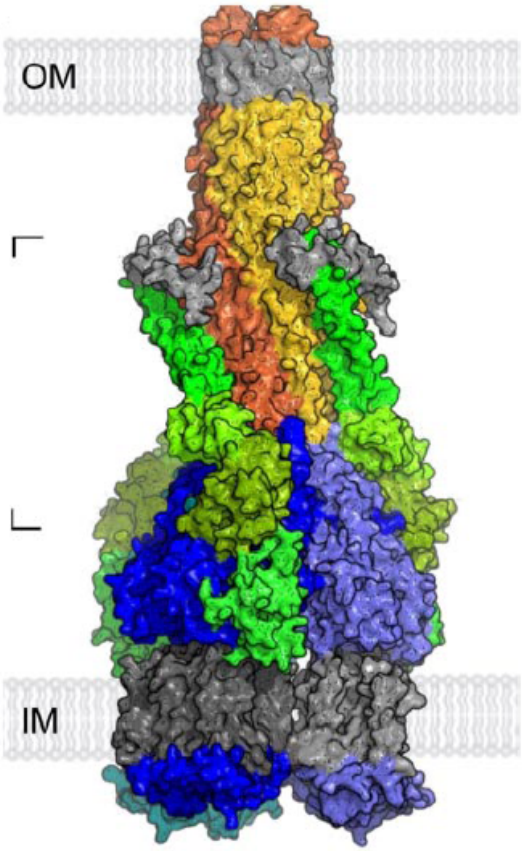

Figure I.4 Docking model of AcrAB-TolC (62). The surface rendering of the $AcrA_3$-$AcrB_3$-$TolC_3$ complex is colored by its components. The TolC trimer (orange, red, and yellow subunits with gray equatorial domains and membrane regions) is docked onto the AcrA (green)-docked AcrB trimer (blue/light blue subunits with gray membrane regions).

six antiparallel β-strands and a short α helix. The lipoyl domain includes two lipoyl half-motifs, each of which comprises four β-strands. These two half motifs interwine with one another to form a β-sandwich. The α-helical domain is composed of two helices linked by a loop. Compared to four heptad repeats in MexA (1, 21), each helix in AcrA includes five heptad units, which accounts for the length difference between AcrA (105 Å) and MexA (89 Å). More recently, the crystal structure on the N- and C-termini of MexA was recently reported (62). As demonstrated in Figure I.3 B, these ninety two residues at the termini (residues 13-27 and 262-339) form a compact β-roll extending from the β-barrel domain on a β-ribbon linker. Since this β-roll is adjacent to the inner membrane, it was named the membrane proximal (MP) domain. Given the high sequence similarity between MexA and AcrA, AcrA possibly assumes the similar structure as MexA, including four domains: β-barrel domain, coiled-coil α-helical hairpin, lipoyl domain and MP domain.

The arrangement of the complex was investigated by superimposing crystal structures of AcrB and TolC and several models have been proposed (6, 9, 62). Of them, the appealing molecular docking model is based on the cross-linking experiments with AcrA-TolC and AcrA-AcrB (62), showing that these three proteins form a tripartite $AcrA_3$-$AcrB_3$-$TolC_3$ complex (Figure I.4) (62), in which α-helical hairpins of AcrA are rotated to bind on the TolC entrance coiled coils, while the lipoyl domain, β-barrel domain, and MP domain bind to AcrB. In addition, there is a close fit between the top section of AcrB and the bottom section of TolC.

Despite the fact that more and more biochemical and biophysical (structural analysis) information about the tripartite complex reveals the interactions between

components, some open questions are still awaiting answers. For example, what is the stoichiometry of the interacting components, especially the oligomeric number of AcrA? Does AcrA interaction with AcrB and/or TolC induce conformational changes of AcrA? and if yes, how do these conformational changes coordinate with drug efflux?

I.2 AcrA, the periplasmic membrane fusion protein, is anchored into the inner membrane by lipid modification

There are 397 amino acid residues in AcrA from *E. coli*. Like other lipoproteins in the periplasm (24), AcrA has a characteristic signal peptide at the N-terminus (24 residues) shown below (40):

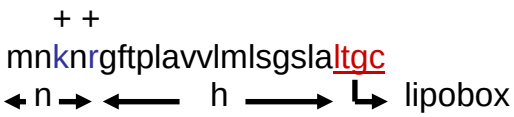

in which the N-terminal domain (n) includes two positively-charged residues, followed by the hydrophobic h-region and a lipobox from -3 to +1 position. This signal peptide directs AcrA translocation into periplasm (38). The studies of bacterial lipoprotein biosynthetic pathways in the 1970s elucidated the lipid modification of lipoproteins in periplasm (19). According to this theory, the thiol group and the N-terminal amido linkage of cysteine residue just outside the signal peptide in lipoproteins are modified to covalently link diacyglyceryl and acyl respectively, thereby anchoring matured lipoproteins into the inner membrane. The final composition of the N-terminal cysteine residue is shown in Figure I.5 A (19).

Detailed studies indicate that there are three sequential steps during this chemical

A

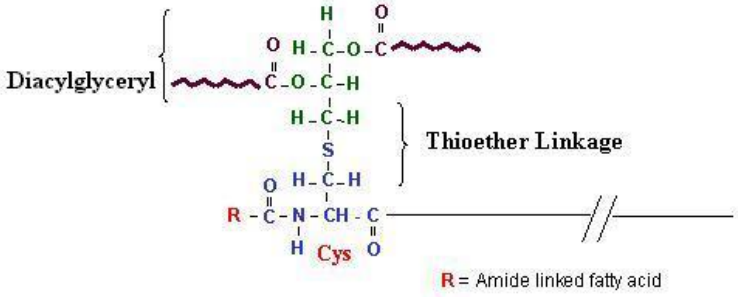

B

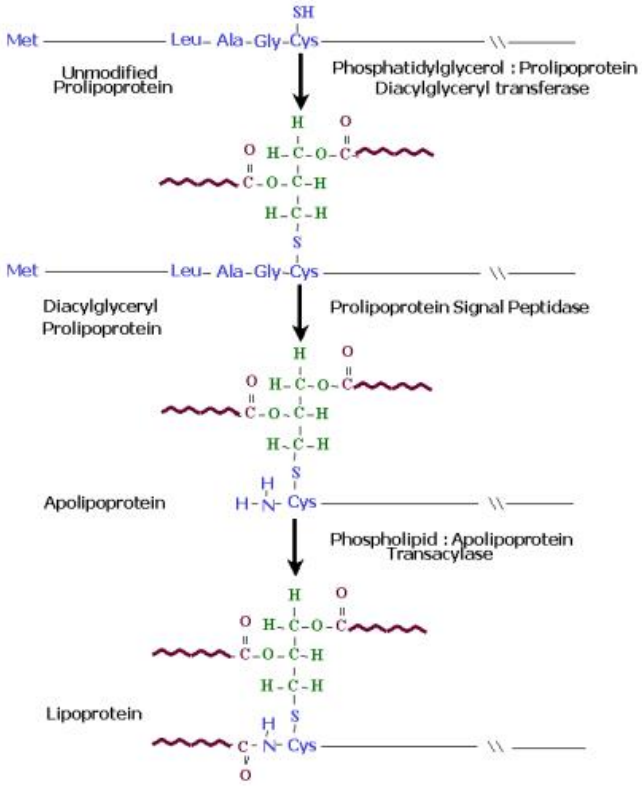

Figure I.5 Lipid modification at N-terminal Cys residue. (A) Chemical structure of modified cysteine residue (19). The diacylglyceryl group covalently attaches cysteine residue via thioether linkage, whereas the N-terminal amido linkage is modified to link fatty acyl group. (B) Biosynthetic pathway of lipid modification of lipoproteins (56). Three sequential steps are catalyzed by three enzymes.

modification: first, the thiol group in the side chain of cysteine residue is subject to diacylglyceryl modification, which is catalyzed by the enzyme diacylglyceryl transferase (30, 56). Second, the signal peptidase II cleaves at the amido site between cysteine residue and signal peptide (8, 24), thus removing the signal peptide and exposing the amino group of the cysteine residue. Third, this free amino group is acylated by fatty acid with the aid of transacylase (18, 55). These three steps are illustrated in Figure I.5 B (56).

Given that the first 24 amino acids of AcrA show features typical of a signal peptide of bacterial lipoproteins, AcrA is subject to this kind of lipid modification (40). This lipid modification of AcrA was experimentally confirmed by labeling cells with radioactive palmitic acid (72). This lipid modification at the N-terminus of AcrA results in association with the inner membrane. On the other hand, mutation of cysteine residue, regardless of deletion and substitution, abolished the membrane anchoring and made AcrA as well as the homologous MexA in *P. aeruginosa* soluble in an aqueous medium (70, 72). The functional roles of this lipid modification in AcrA and MexA were also studied. In particular, original signal peptides of AcrA and MexA were replaced with cleavable but non-lipidated OmpA and Azurin signal peptides, respectively (70, 72). The minimal inhibitory concentrations (MIC) of these soluble AcrA (OmpA-AcrA) and MexA (Azurin-MexA) are almost the same as the corresponding lipoproteins, indicating that this lipid modification is not required for drug extrusion.

I.3 Conformational flexibility of AcrA

Since AcrA is located in periplasm and functions as an adaptor protein to bridge AcrB and TolC, it is very interesting to know whether AcrA has structural flexibility and

how the conformational changes of AcrA coordinate with the drug transport by AcrB and/or TolC channel opening. Electron Paramagnetic Resonance (EPR) analysis of spin-labeled AcrA mutants demonstrated conformational changes of AcrA induced by acidic pH (25). When pH of buffer was changed from 7.0 to 5.0, AcrA was subject to substantial reversible structural changes at residue 62 (lipoyl domain) and residues 103, 146 and 172 (α-helical hairpin domain). Moreover, local protein structure in close proximity of these residues underwent conformational changes and thus these residues are in a more restricted environment under pH 5.0. On the other hand, in the solved X-ray crystal structure, four conformations of AcrA in the asymmetric unit illustrate that the structural changes are due to hinge flexibility between lipoyl domain and α-helical hairpin (40). Figure I.6 shows the superposition of AcrA monomers in which the maximal angle change of the hinge linker is 15 degrees (21 Å in distance) based on the lipoyl domain. This hinge-like conformational flexibility at the base of the α-helical domain in AcrA possibly contributes to assembly of the efflux complex and energy transition from AcrB to TolC, which is postulated to be involved in the iris-opening of the TolC. In contrast, there are no such changes in MexA crystal structure, although the molecular simulation of MexA suggested similar inter-domain motion (68).

In addition, heterogeneity of the sedimentation coefficient and polydisperisity parameter from Dynamic Laser Scattering (DLS) of AcrA implied that AcrAs without Mg cation adopt two conformations compared to the one dominant conformation in the presence of magnesium (72). This conformational transition is not due to the secondary structure change based on the similar circular dichroism spectra data.

The above *in vitro* studies showed the conformational flexibility of AcrA,

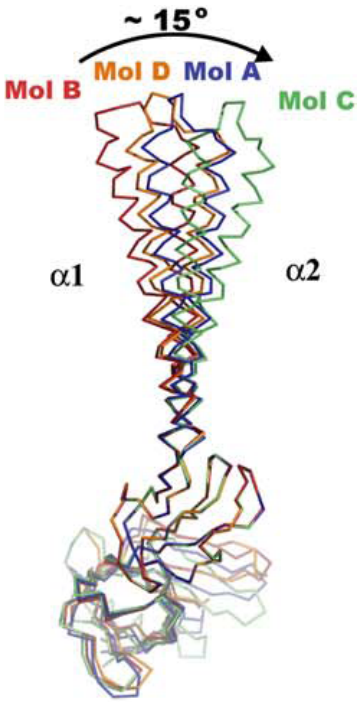

Figure I.6 Conformational flexibility of AcrA. Comparison of four conformations of AcrA (45-312)-4M observed in the crystal (40), with molecules A, B, C, and D superposed on the lipoyl domain. The greatest difference, ~15°, is between molecules B and C.

indicating that, rather than a passive linkage between AcrB and TolC, AcrA is a dynamic protein and actively participates in the drug efflux across both periplasm and outer membrane. One of the remaining questions in this field is how these conformational changes of AcrA coordinate with the efflux process.

I.4 Oligomerization of AcrA *in vivo* and *in vitro*

Unlike the integral membrane proteins such as trimers of AcrB and TolC, oligomerization of AcrA is still unclear: what is the "functional" oligomeric number of AcrA *in vivo*? How do the oligomers of AcrAs assemble with the two other components of the complex and mediate multidrug extrusion?

A hydrodynamic analysis was used to determine the oligomeric state of soluble AcrA (OmpA-AcrA-His) *in vitro*. A sedimentation equilibrium study indicated that this soluble AcrA exists as a monomer in solution (72). Moreover, the sokes radii calculated from sedimentation and Dynamic Laser Scattering showed that the axial ratio of $AcrA^{S}$-His is about 8, suggesting that the $AcrA^{S}$-His is an asymmetric elongated molecule. Similarly, most of non-lipidated MexA was shown to be monomer, although a small amount of dimer was detected in gel filtration experiment (1). Interestingly, an electron paramagnetic resonance study showed that acidic pH results in oligomerization of $AcrA^{S}$-His in solution. Disulfide cross-linking showed that $AcrA^{S}$-His oligomers are arranged in parallel (25).

In another independent study, $AcrA^{S}$-His was crystallized on lipid layers containing nickel-chelating phospholipid DOGS-NTA (2). In this experiment, AcrA was attached by the C-terminal 6His tag. Electron crystallography showed the two-

dimensional structure of AcrA at 30 Å level as layer group $P2_122$. There are four asymmetric units in the unit cell, including two tubular rings with about 150 Å in perimeter and a hole of approximately 30 Å in diameter. The contour length of a quasi-helical path is about 210 Å, which is very consistent with the length data from the hydrodynamic study (72). In contrast to the three-fold symmetry structure of the inner/outer membrane components (AcrB and TolC) (29, 45), this horse-shoe structure of AcrA is likely a dimer configuration.

Interestingly, the core portion of AcrA (45-312 a.a) was reported to assemble as a dimer of dimers in the X-ray crystal structure (40). Anti-parallel dimerization involves inter-molecular helix interaction (Figure I.7 A). The C-terminal helix from one monomer interacts with the adjacent N-terminal helix from a second monomer in classical knobs-into-holes packing manner. On the other hand, two parallel AcrA monomers extensively interact through α-helical hairpins, lipoyl domain and β-barrel domains. It should be noted that X-ray crystallography here only shows the central part of AcrA. About one third of the protein residues at both termini are missing in the protease-resistance core of AcrA. The 28 N-terminal and 98 C-terminal residues of the AcrA were not resolved. Thus, the crystal structure here does not provide the whole picture of AcrA. Although the MP domain of MexA was recently resolved (62), further experiments are needed to confirm the similar domain in AcrA and check the oligomerization status of the complete structure of AcrA.

Chemical cross-linking has been carried out to determine the oligomerization of AcrA, with and without lipid modification *in vivo* (74). It showed that lipidated AcrA forms oligomers, possibly trimers (Figure I.7 B). Unlike the monomeric status of $AcrA^S$-

His in solution, the *in vivo* cross-linking demonstrated that $AcrA^{S}$-His also forms oligomers, possibly as trimers (74). Furthermore, oligomerization of AcrA in strains with different genetic backgrounds was not affected by the existence of other two components, AcrB and TolC, indicating that AcrA oligomerization is independent on AcrB and/or TolC.

In addition, oligomerization of AcrA homologs has also been investigated. For example, in X-ray crystal structures, central parts of MexA form a tridecamer (1, 21). The six-subunit-assembly and the seven-subunit-assembly in parallel manner are organized in the head-to-head manner. However this arrangement of MexA could not fit with AcrB and TolC in complex assembly. In addition, oligomers including nine or six subunits in parallel manner have also been proposed (1, 21, 59). Another membrane fusion protein, MacA from the ABC type transporter complex MacAB-TolC, was recently crystallized (50). The X-ray crystal structure demonstrated that MacA exists as a hexamer, which is further confirmed by electron microscopy and gel filtration results (71). Additionally, trimers are dominant in the cross-linking analysis of another MFP HylD (64). Gel filtration of EmrA shows equilibrium of monomer, dimer and trimer in solution and this oligomerization is concentration-dependent (4).

Taken together, current studies showed different oligomerization status of AcrA as well as its homologs. Oligomerization transitions due to the change of pH and concentration demonstrated a dynamic nature of oligomerization of AcrA. It is thus likely that more biochemical and biophysical studies, for instance, the X-ray crystallography of the efflux complex AcrAB-TolC, are needed for deep insight into the molecular mechanism of AcrA oligomerization and further understanding of the functional complex assembly.

A

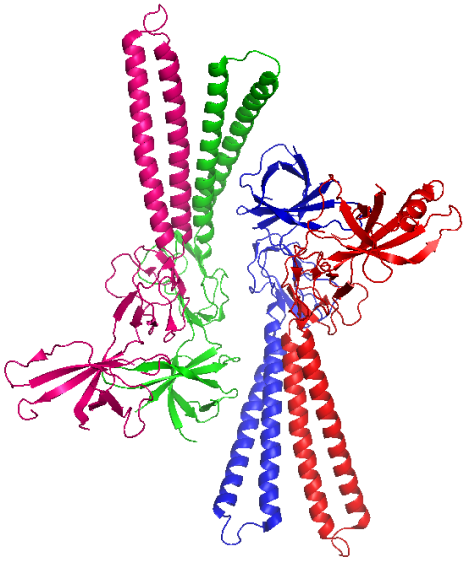

B

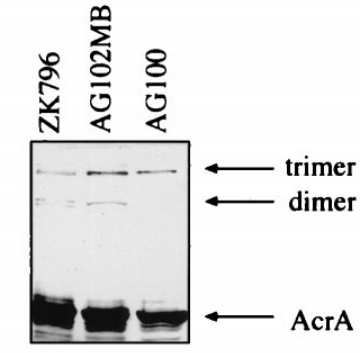

Figure I.7 Oligomers of AcrA. (A) Dimer of dimers of AcrA in the X-ray crystal structure (40). Ribbon representation of AcrA (45-312)-4M demonstrates two apparent dimers per asymmetric unit in the crystal. The protomers are shown in red, pink, blue, and green. (B) Oligomers of AcrA *in vivo* (74). Dimers and trimers of AcrA are visualized by disuccinimidyl glutarate (DSG) cross-linking *in vivo*. The oligomerization of AcrA is independent of AcrB (AG102MB is ΔacrB) and TolC (ZK796 is ΔtolC).

II Materials and Methods

II.1 Bacterial strains and plasmids, media and growth conditions

All strains and plasmids used in this study are listed in Table II.1. *E. coli* strains were grown at 37°C in Luria-Bertani (LB) broth (10 g of Bacto tryptone, 5 g of yeast extract, and 5 g of NaCl per liter). Antibiotics were added when needed to the following final concentrations: ampicillin (100 μg/ml), kanamycin (34 μg/ml), spectinomycin (50 μg/ml), tetracycline (25 μg/ml), and chloramphenicol (25 μg/ml).

II.2 Purification of AcrA, AcrB and TolC by affinity chromatography

Unless indicated otherwise, we use superscript "L" to stand for lipid modification, and superscript "S" to highlight the soluble periplasmic AcrA without lipid modification. To purify $AcrA^{L}$-His containing the N-terminal lipid moiety (AcrA-6His), AG100AX *E. coli* cells (ΔacrAB ΔacrEF) containing plasmid $pAcrA^{His}$ were grown overnight and re-inoculated into 500 ml fresh LB medium supplemented with ampicillin. The expression of protein was then induced by 0.1 mM isopropyl β-D-1-thiogalactopyranoside (IPTG) when cultures reached OD_{600} ~0.5-0.7. After three hours induction, cells were collected by low speed centrifugation (3,220 x *g*, 30 min) and resuspended in buffer containing 20 mM Tris-HCl (pH 8.0), 1 mM EDTA, and 1 mM PMSF. Lysozyme was added to final concentration of 100 μg/ml and incubated on ice for 30 min. Cells were broken by sonication, the unbroken cells were removed by low speed centrifugation at 3,220 x *g* for 15 min, and the supernatant was further centrifuged at 50,000 x g for 1 hr. The membrane pellet was resuspended in 20 mM Tris-HCl (pH 8.0) buffer containing 500 mM NaCl, 5

Table II.1 List of strains and plasmids

Strains and plasmids	Description	Source/references
E. coli strains		
AG100	K-12 argE thi-1 rpsL xyl mtl galK supE441-Δ(gal-uvrB)λ-	(13, 48)
AG102MB	argE3 thi-1 rpsL xyl mtl galK supE441-Δ(gal-uvrB)λ::	H. Nikaido
ZK796	Tet^r, same as MC4100 but tolC::Tn10	(15)
AG100AX	argE3 thi-1 rpsL xyl mtl galK supE441-Δ(gal-uvrB)λ- ΔacrAB::kan ΔacrEF::spe	(41)
ECM2112	MC4100 but ΔacrAB::kan tolC::Tn10	Lomoskaya, O
Plasmids		
pUC18	E. coli cloning vector, Amp^r	-
pUC151A	pUC 18 vector carrying the acrAB genes	(38)
pBP184	pACYC184 vector, Cm^r, expressing acrB under native promoter	(25)
$pAcrA^{His}$	His6-tagged *acrA* derivative of pUC151A plasmid	Zgurskaya H.I.
$pAcrA^{His}AcrB$	His6 between *acrA and acrB* derivative of pUC151A plasmid	Zgurskaya H.I.

pAcrB^{His}	His6-tagged *acrB* derivative of pUC151A plasmid	(66)
pTolC^{His}	His6-tagged *tolC* derivative of pTrc99A-TolC plasmid	(66)
pUZ11	pUC18 vector carrying the ompA-acrA-His fusion sequence under lac promoter	(72)
pUZ11 (A30C)	pUC11 derivative carrying single mutation in ompA-acrA-His (A30C)	(25)
pUZ11 (A39C)	pUC11 derivative carrying single mutation in ompA-acrA-His (A39C)	(25)
pUZ11 (A62C)	pUC11 derivative carrying single mutation in ompA-acrA-His (A62C)	(25)
pUZ11 (A103C)	pUC11 derivative carrying single mutation in ompA-acrA-His (A103C)	(25)
pUZ11 (A146C)	pUC11 derivative carrying single mutation in ompA-acrA-His (A146C)	(25)
pUZ11 (A172C)	pUC11 derivative carrying single mutation in ompA-acrA-His (A172C)	(25)
pUZ11 (A204C)	pUC11 derivative carrying single mutation in ompA-acrA-His (A204C)	(25)
pUZ11 (A242C)	pUC11 derivative carrying single mutation in ompA-acrA-His (A242C)	(25)
pUZ11	pUC11 derivative carrying single mutation in	(25)

(A295C)	ompA-acrA-His (A295C)	
pUZ11 (A339C)	pUC11 derivative carrying single mutation in ompA-acrA-His (A339C)	(25)
pUZ11 (A390C)	pUC11 derivative carrying single mutation in ompA-acrA-His (A390C)	(25)

mM imidazole and 1mM PMSF, then an equal volume of 10% TX in binding buffer was slowly added and incubated overnight at 4°C. The insoluble material was removed by centrifugation at 50,000 x *g* for 1 hr. Solubilized membrane proteins were loaded onto Cu^{2+} charged NTA column equilibrated with 20 mM Tris-HCl (pH 8.0) binding buffer containing 500 mM NaCl, 5 mM imidazole, 1 mM PMSF, and 3.2 mM TX. The column was washed twice, first with the above binding buffer, then the same buffer but containing 60 mM imidazole. Bound AcrA was eluted with the elution buffer containing 500 mM imidazole and 3.2 mM TX. Purified AcrA was dialyzed against buffer containing 20 mM Tris-HCl (pH 8.0), 200 mM NaCl, 3.2 mM TX, and 1 mM EDTA and stored at 4°C until needed. For prolonged storage, dialysis buffer was supplemented with 50% glycerol (v/v) and protein was stored at -20°C.

The purification of AcrB-His protein was performed as described previously (66, 73). The plasmid $pAcrB^{His}$ was transformed into AG100AX cell. The same purification steps were used as described fro the $AcrA^{L}$-His protein. The plasmid $pTolC^{His}$ was transformed into AG100AX cells to purify TolC-His protein. A similar purification protocol was followed with modifications in buffer compositions (66). In particular, after the binding buffer wash, an imidazole gradient of 60 mM and 500 mM with equilibration buffer containing 0.5% polyoxyethylene (POE) was used for the consequent washes. Purified TolC was eluted in 500 mM imidazole fractions. This fraction was dialyzed to remove imidazole, and kept in storage buffer containing 20 mM Tris-HCl (pH 7.4), 500 mM NaCl, 5 mM $MgCl_2$, 1 mM PMSF, 0.5% POE and 50% glycerol.

A similar purification protocol was followed to purify $AcrA^{S}$-His with modifications in buffer composition and membrane solubilization. Plasmid pUZ11 was

transformed into AG100AX cells. Cells were lysed in same 20 mM Tris-HCl (pH 8.0) buffer but without EDTA. The protein was purified as described by previous study (72).

II.3 SDS-polyacrylamide gel electrophoresis analysis

Protein samples were analyzed with sodium dodecyl sulfate-polyacrylamide gel electrophoresis (SDS-PAGE). Proteins samples were mixed with sample buffer (0.25M TrisCl pH 6.8, 8% SDS, 10% glycerol, 5% β-mercaptoethanol and bromophenol blue) and resolved by SDS-PAGE (8% or 12% [wt/vol] acrylamide). Protein bands were visualized with Coommassie Brilliant Blue (CBB) or silver nitrate staining (20). For immunoblotting, proteins were transferred electrophoretically to polyvinylidene difluoride (PVDF) membrane (Immobilon, Millipore) in 3-(cyclohexylamino)-1-propanesulfonic acid-NaOH (10 mM, pH 11.0) and methanol (10%), and proteins were visualized using anti-AcrA polyclonal antibody and alkaline-phosphatase-conjugated anti-rabbit antibody (Sigma).

II.4 Fluorescence labeling of AcrA *in vivo* and *in vitro*

E. coli cells carrying plasmids expressing AcrA-Cys variants were grown to OD_{600} ~0.5-0.7 and then induced with 0.1mM IPTG. Three hours after induction, cells were harvested using low speed centrifugation (3,220 x *g*, 30 min), and then washed with standard Phosphate Buffered Saline (PBS) (pH 7.4) buffer. Labeling of whole cells (*in vivo*) was done in PBS (pH 7.4) buffer containing 100 μM of fluorescein-5-maleimide (F5M). After incubation with F5M for 30 min at room temperature (RT), the labeling reaction was stopped by addition of the excess of DL-Dithiothreitol (DTT, 5mM). Cells were washed with PBS buffer to remove F5M and resuspended in the binding buffer including 20mM Tris-HCl (pH 7.5), 5mM imidazole, and 500mM NaCl. After pre-

treatment with lysozyme (100 μg/ml, 20min on ice), cells were sonicated (Branson 450 Sonifier). Unbroken cells were removed by low speed centrifugation (3,220 x *g* for 15 min) and AcrA variants were purified using metal-affinity chromatography as described above. Then, purified, labeled proteins were resolved on SDS-PAGE (10%) and fluorescence was detected using Storm 840 Imager (Molecular Dynamics) using the excitation wavelength 450 nm and the emission wavelength 520 nm. To visualize proteins and compare their amounts, after fluorescence scanning gels were stained with CBB. Fluorescence intensity and protein amount were analyzed using the ImageQuant™ TL program (Amersham Pharmacia). For each protein band the fluorescence intensity was normalized on the protein amount determined from the same gel after staining with CBB. The largest normalized fluorescence intensity was set as 100% and used to obtain the relative fluorescence intensity for each band.

For *in vitro* labeling, cells were lysed and AcrA was purified using affinity chromatography described above. After protein purification, labeling with F5M (20μM) was carried out for 30 min at RT. Reactions were terminated and fluorescence and amounts of proteins were analyzed as described above.

II.5 Limited proteolysis assay (trypsin and proteinase K)

Purified AcrA was incubated with trypsin at 19.5:1 molar ratio of AcrA:trypsin or 200: 1 molar ratio of AcrA:PK. For proteolysis in the presence of lipids, the polar fraction of *E. coli* lipids (Avanti Polar Lipids) was re-suspended to final concentration 10 mg/ml by sonication in buffer containing 20 mM Hepes (pH 7.0 or pH 6.0) and 100 mM NaCl. When needed TX was added to final concentration 3.2 mM. Purified AcrA was

mixed with lipids in amounts indicated in Figures and incubated for 20 min at room temperature. Tryptic digestion was carried out at 37°C. Aliquots were withdrawn at different time points, and reactions were terminated by boiling in the SDS-PAGE sample buffer and analyzed by SDS-PAGE followed by silver nitrate staining.

II.6 Reconstitution of proteins into proteoliposomes ("PL")

Reconstitution was done according to previous studies (9, 28)**.** *E. coli* polar lipid extract (Avanti) was sonicated in reconstitution buffer containing 20 mM Hepes (pH 7.0), 5 mM DTT to final concentration 40 mg/ml. TX was then added to final concentration 0.45% (wt). Protein was slowly added to lipid detergent solution at 1:200 (wt) of protein:lipids ratio and the sample was then incubated at RT for 30 min. After the pretreatment with methanol, water and reconstitution buffer in sequence, SM-2 Adsorbent Bio-Beads (Bio-Rad) were used to remove TX: two times of one-hour incubation at room temperature, and then one-hour incubation at 4°C. Reconstituted proteoliposomes were pelleted by high speed centrifugation (250,000 x *g*, 1 hr, 4°C) using TLA 100.3 rotor (Beckman). The proteoliposome pellet was resuspended in buffer including 20 mM Hepes (pH 7.0), 0.1 mM DTT, and 50 mM KCl. The PL samples along with bovine serum albumin (BSA) standards were then resolved on SDS-PAGE (12%) and stained with CBB. Gels were scanned and the intensity of each protein band was quantified using ImageQuant® program (Molecular Dynamics).

II.7 Identification of AcrA tryptic fragments by MALDI-TOF mass spectrometry

AcrA was digested with trypsin at a 19.5 molar ratio of AcrA/trypsin at 37ºC for

90 min. The reaction was terminated by addition of acetic acid to final concentration 2%. Ziptip C18 and C4 (large fragments) (Millipore) were used to desalt and concentrate tryptic fragments of AcrA. AcrA fragments were eluted using an aqueous solution containing 50% of acetonitrile and 0.1% trifluoroacetic acid. MALDI-TOF analysis was carried out at the Molecular Biology-Proteomics Facility, University of Oklahoma Health Sciences Center. Samples were mixed with sinapinic acid (3,5-dimethoxy-4-hydroxy-cinnamic acid) and then spotted and dried on specimen grids. MALDI-TOF Mass spectra of peptide fragments were collected in the linear mode on a Voyager-DE Pro mass spectrometer (Applied Biosystems) equipped with a delayed extraction device.

II.8 Size exclusion chromatography (SEC) in conjunction with light scattering (LS) and refractive index (RI) measurements

Light scattering refers to a process in which light from an incident polarized laser beam is scattered in all directions when it strikes a molecule or particle. There are two general techniques for the measurement of physical properties of polymers: Static light scattering and dynamic light scattering. In the static light scattering, the intensity of the scattered light from the dissolved materials was measured. The amount of light scattered is directly proportional to the product of the weight-average molar mass and the solute concentration1: LS ~ MW.c (16). To determine the molecular weight of the molecule, the analyte concentration is usually measured by refractive index. The differential refractometer detects the amount of solute in the column effluent by measuring the difference in the RI between the mobile phase and the column effluent containing the solute (3). This difference is proportional to the concentration of the solute. The observed

signal (RI), which corresponds to the deviation of the light beam, is proportional to the difference in the refractive index of the fluid in the two cells.

Based on LS and RI data, three kinds of molecular weight can be calculated using discovery® software: Mn, number average; Mw weight average; and Mp (peak molecular weight). The width of the distribution, called the polydispersity, is usually determined from the ratio of Mw/Mn. The larger the polydispersity index, the broader molecular weight. The following are the equations for these molecular weight forms:

$$M_n = \frac{\sum M_i N_i}{\sum N_i}, M_w = \frac{\sum M_i^2 N_i}{\sum M_i N_i}$$

In which, M_i stands for the molecular weight of ith molecules, N_i is the number of ith molecules with MW M_i.

In our experiment, gel filtration molecular weight markers (Sigma, product number: MW-GF-1000) were first applied on SEC column (YMC, Diol-300 column) connected with LS detector (PD 2010, Precision Detectors) and RI detector (2414, Waters). These markers consist of Carbonic Anhydrase from Bovine Erythrocytes (29,000 Da, “CA”), Albumin, Bovine Serum, (66,000 Da, “BSA”), and β-Amylase from Sweet Potato (200,000 Da, “Amy”).

The instrument setup used for SEC-light scattering experiments consisted of a SCL-10 Ai HPLC system (Shimadzu) connected in series with a light scattering detector PD2010 (Precision Detectors, MA) and refractomer detector Waters 2414 (Waters). Analytical size-exclusion chromatography was carried out at RT using a YMC-Pack Diol-300 column (YMC) equilibrated with a mobile phase containing 20 mM Tris-HCl (pH 7.5), NaCl 300 mM, and 0.05% (wt) n-dodecyl-β-D-maltoside (“DDM”), if required.

100 µl of purified protein sample at indicated concentrations (0.5 µg/µl) was injected into the column and eluted at a flow rate of 1.0 ml/min. The column effluent was monitored in-line with three detectors that simultaneously monitored UV absorption (280 nm), light scattering (90°), and refractive index, respectively. The molecular mass of the proteins was calculated from LS and RI data using Discovery® software (Precision Detectors, MA).

II.9 Cross-linking of proteins with formaldehyde *in vitro*

Purified AcrA was incubated with *E. coli* polar lipids (Avanti), as indicated, resuspended in 20 mM Hepes (pH 7.0 or 6.0) buffer with increasing concentration of NaCl for 20 min. Protein samples were then incubated with formaldehyde (37%, Sigma) at indicated final concentrations for 30 min at RT without shaking. The reaction was terminated by addition of glycine to final concentration 0.5 M. Protein samples were resolved on SDS-PAGE (8%) and visualized by silver staining.

Chapter 1

Limited Proteolysis of AcrA *in vitro*

1.1 Different cleavage profiles of purified $AcrA^{L}$-His and $AcrA^{S}$-His

A previous study has shown that $AcrA^{S}$-His complements the drug-susceptible phenotype of ΔacrA cells *in vivo* (72). This result indicates that the signal peptide of OmpA indeed guides the periplasmic translocation of AcrA, and lipid moiety which anchors to the inner membrane is not required for the efflux process, at least under over-expression conditions. However, the effect of lipid modification on the structural features of AcrA remains elusive. For example, does this lipid modification on the N-terminal Cys residue induce conformational changes in AcrA?

To investigate the structural features of proteins, a number of methods or techniques can be used. X-ray crystallography is one of the most important approaches to probe fine structure of proteins at the molecular level. However, proteins with dynamic structure could not be characterized using this technique (10). Another approach, NMR, can pinpoint the dynamic conformational transitions in solutions. Nevertheless, it needs milli molar concentrations of proteins for measurement, and lacks detailed information about partly folded and fluctuating states of proteins due to the resonance broadening as well as broad chemical shift dispersions (10).

In our studies we used limited proteolysis and fluorescence labeling to study dynamic structural changes of AcrA protein. Limited proteolysis is an important technique to investigate the tertiary structure of proteins. Three factors are generally considered crucial/important during the protease cleavage (22). First, the cleavage sites

should be located in the flexible region/domain. Second, cleavage sites exposed to medium decrease intermolecular steric hindrance for access to an enzyme's active site. Third, hydrogen bonding, disulfide linkage and van der Waals interactions mediate limited proteolysis. Overall, the domains/residues with a high level of flexibility, accessibility and extrusion are more susceptible to be degraded by proteases.

To characterize structure of AcrA, we used two proteases, proteinase K ("PK", Sigma) and trypsin. PK, a broad specificity protease cleaving at hydrophobic residues, was used to digest purified $AcrA^{S}$-His and $AcrA^{L}$-His. To purify these two AcrA proteins, we transformed plasmids $pAcrA^{His}$ or pUZ11 into *E. coli* AG100AX cells, which are deficient of *acrAB* and *acrEF* multidrug efflux pumps. The $AcrA^{S}$-His is the fusion protein in which OmpA signal peptide substitutes the original signal peptide in AcrA (72). Since OmpA signal peptide is cleavable and doesn't include cysteine residue, $AcrA^{S}$-His is soluble in aqueous medium (72).

Because of lac promoter in the plasmids, 0.1 mM of IPTG was used to induce the over-expression of AcrA proteins. Figure 1.1 shows the expression profiles of AcrAs. These two forms of AcrA were then purified using metal-affinity chromatography as described in the Materials and Method section. Purified AcrA variants (1.95 μM) were incubated with PK (9.19 nM). The cleavage reactions were terminated at different time points by addition of SDS sample buffer. The cleavage profiles of AcrA proteins were analyzed by SDS-PAGE (Figure 1.2). 90 min of PK digestion of AcrA variants produced several fragments. Compared to the mobility of standard markers, the molecular weights of these fragments were determined as 44.0 kDa, 42.0 kDa, 40.6 kDa, 37.6 kDa, 36.0 kDa, 35.0 kDa, 32.8 kDa, 27.5 kDa, 26.5 kDa, 24.5 kDa, 23.5 kDa. Among them, three

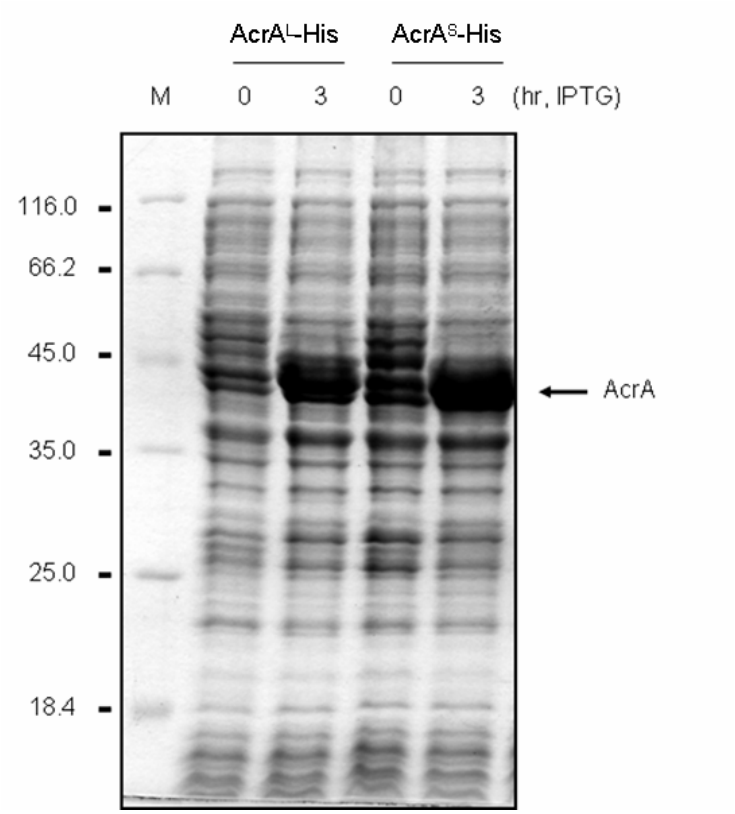

Figure 1.1 Expression of AcrA variants. AG100AX carrying pAcrA^{his} or pUZ11 were collected at three hours after IPTG (0.1 mM) induction. Whole cell extracts were resolved by 12% SDS-PAGE and stained with CBB.

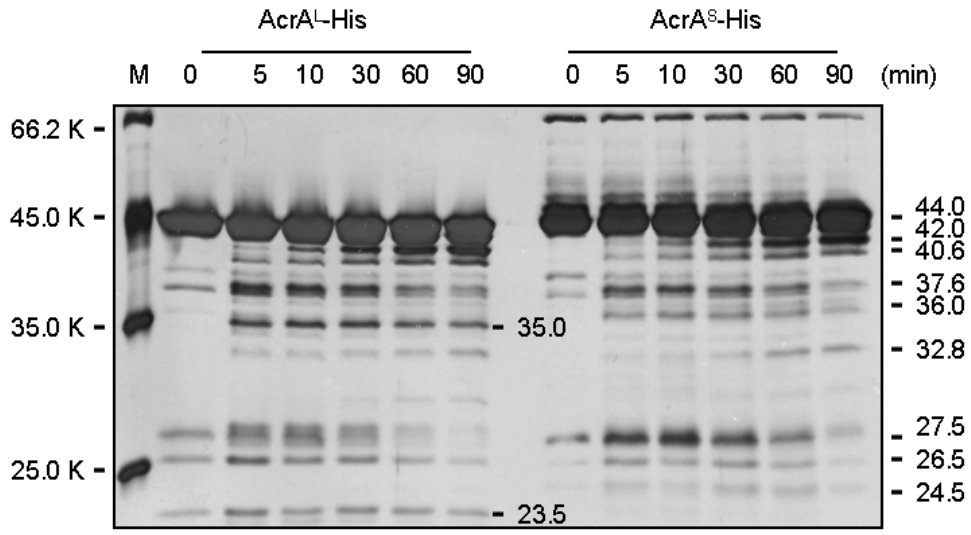

Figure 1.2 Proteinase K cleavage of purified AcrA^{L}-His and AcrA^{S}-His. Proteins (1.95 µM) were incubated with PK (9.19 nM). The digested AcrA proteins were resolved by SDS-PAGE (12%) and stained with silver nitrate. Unique fragments in AcrA^{L}-His sample are indicated.

fragments (42.0 kDa, 40.6 kDa, and 32.8 kDa) accumulated during the time course. In contrast, other fragments (37.6 kDa, 27.5 kDa, 26.5 kDa) rapidly formed in the beginning of the digestion (5 min) followed by the further degradation. Although most fragments existed in both AcrA samples, we detected some unique bands which were specific to these two AcrA variants. The 35.0 kDa and 23.5 kDa fragments were unique in $AcrA^{L}$-His sample, whereas 36.0 kDa and 24.5 kDa fragments were exclusively formed in $AcrA^{S}$-His sample. The PK cleavage profile using CBB staining also confirmed this observation (data not shown). Different cleavage fragments between $AcrA^{L}$-His and $AcrA^{S}$-His suggested that lipid modification changes accessibility of residues in AcrA.

To further examine the effect of lipid modification on accessibility of AcrA to proteases, we used another protease trypsin. Trypsin cleaves the polypeptide chain at the C-terminal side of basic residues, arginine and lysine. After trypsin digestion, cleaved AcrA fragments were resolved on SDS-PAGE (12%) and idenfied by mass spectrometry.

Mass spectrometry is a powerful tool to characterize the peptides formed in limited proteolysis (27). There are several basic mass spectrometry techniques in protein chemistry. Among them, Matrix-Assisted Laser Desorption/Ionization coupled Time-Of-Flight (MALDI-TOF) MS takes advantage of the matrix to facilitate the vaporization and ionization of biomolecules and thus has become the primary technique in identification of peptides and/or proteins in proteomics (27). Here we utilized MALDI-TOF MS to measure the m/e values of trypsin-cleaved peptides of AcrA variants, which correspond to the molecular weights of these fragments. In particular, $AcrA^{L}$-His and $AcrA^{S}$-His were treated with trypsin for 60 min as described above and those cleaved fragments were then subject to the MS measurements. Meanwhile, intact AcrA variants were used as control.

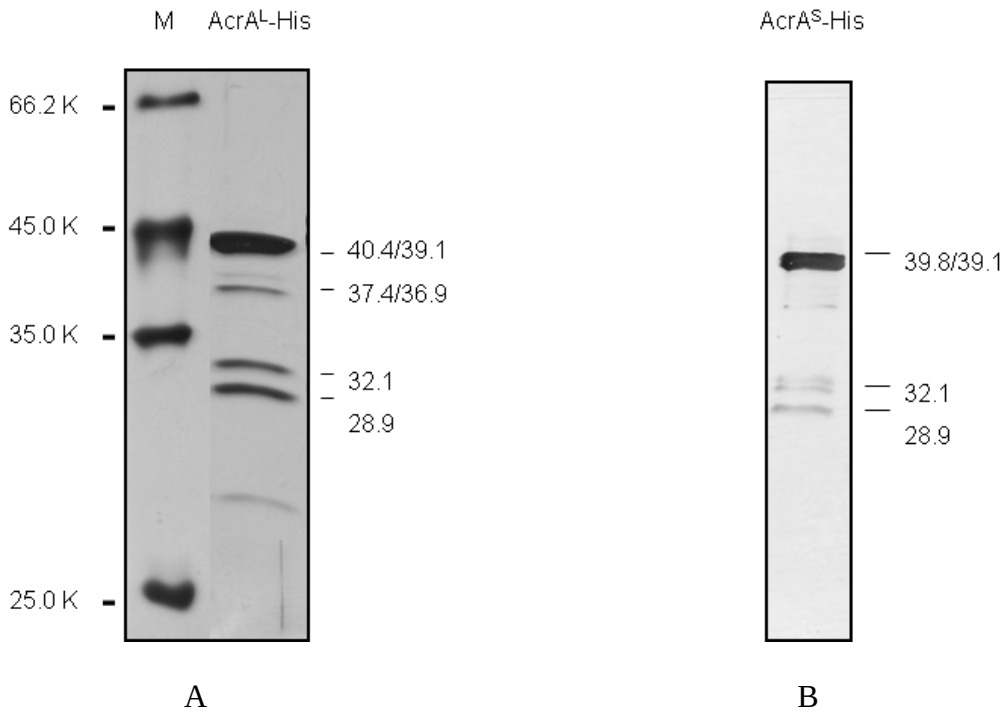

Figure 1.3 SDS-PAGE (12%) analysis of (A) $AcrA^{L}$-His and (B) $AcrA^{S}$-His digested with trypsin. The cleaved AcrA fragments were then analyzed by MOLDI-TOF MS.

A

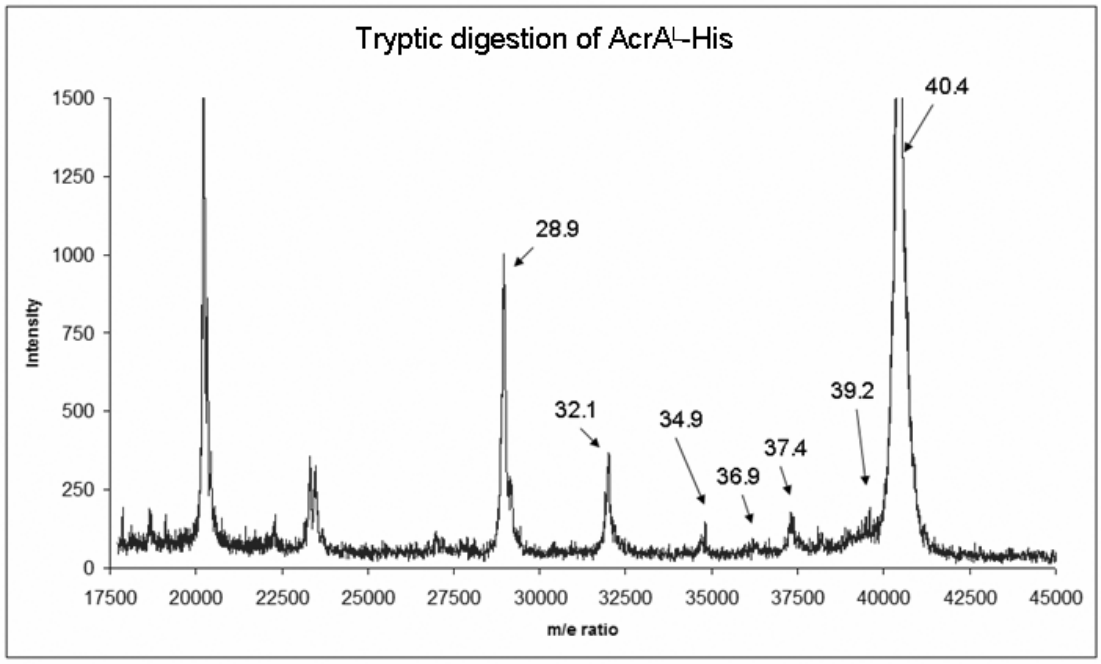

B

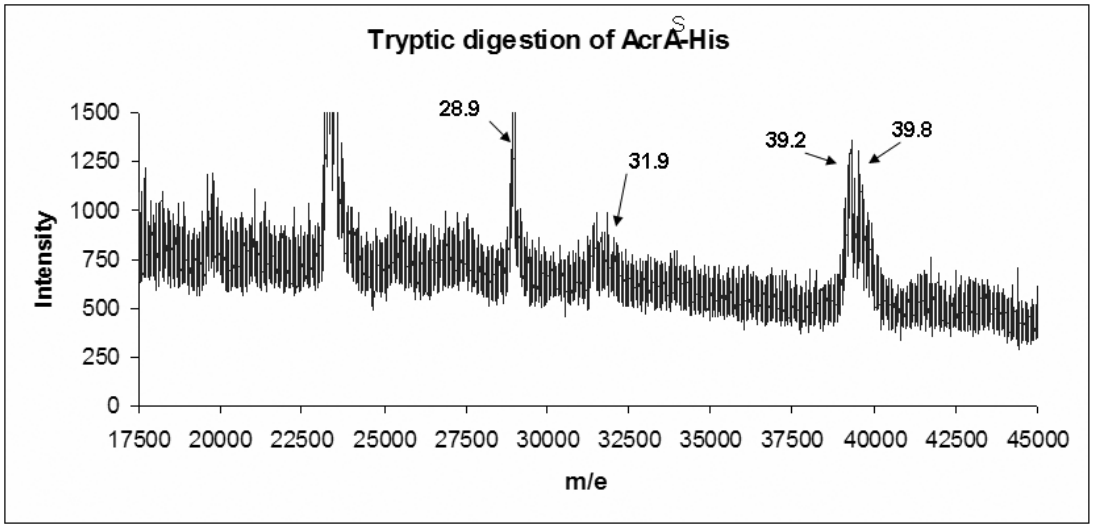

Figure 1.4 MALDI-TOF MS spectrum of trypsin cleaved (A) AcrA^{L}-His and (B) AcrA^{S}-His. After tryptic cleavage, AcrA samples were desalted and concentrated by Ziptip C18, followed by MALDI-TOF analysis.

Table 1.1 Molecular weights of intact AcrA-His and major tryptic digestion fragments

peptides	MW of $AcrA^{L}$-His and fragments (Dalton)		MW of $AcrA^{S}$-His and fragments (Dalton)	
	MALDI-TOF	From sequence (Calculated)	MALDI-TOF	From sequence (Calculated)
Whole length	41,703	41,622	41,014	40,982
N-K396	40,435	40,471	39,819	39,830
Q29-K396	39,597	39,175	39,274	39,175
T47-K396	37,389	37,367	-	37,367
Q29-K374	36,558	36,920	-	36,920
T47-K374	34,909	35,113	-	35,113
T47-K346	32,025	32,097	31910	32,097
T47-R315	28,937	28,935	28,967	28,935

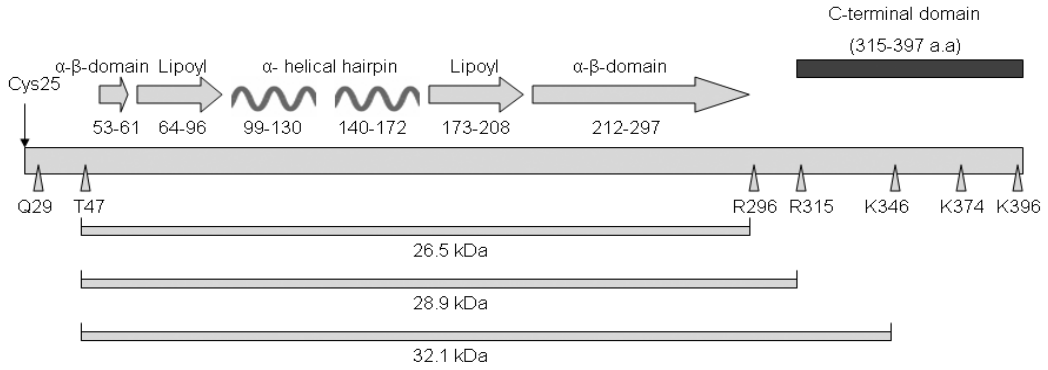

Figure 1.5 Positions of trypsin cleavage sites on the secondary structure of AcrA. The arrow on the left side shows the N-terminal Cys25 which is subject to lipid modification. Positions of amino acid residues that form the α-β-barrel, the lipoyl domain and the α-helical hairpin domains are indicated. AcrA residues cleaved by trypsin are indicated by arrowheads.

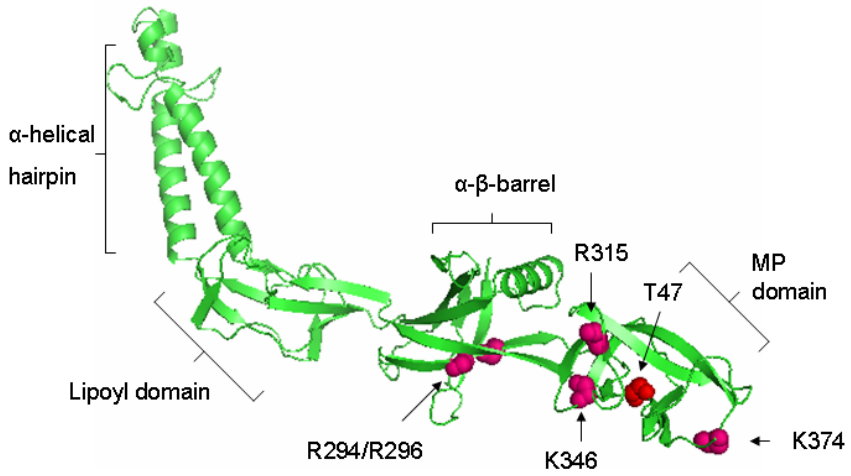

Figure 1.6 Positions of trypsin cleavage sites on the homology model of AcrA. This model was generated using Swiss-Model software (http://swissmodel.expasy.org//SWISS-MODEL.html) and the crystal structure of MexA as a template (62). Six residues including N-terminal residue T47 (red), and C-terminal residues (hotpink) R294/296, R315, K346, K374 in AcrA were labeled in spheres. Note that the residues for Q29 and K396 are not visualized in this structural model.

Figure 1.3 (A) shows the tryptic digestion profile of $AcrA^{L}$-His. Figure 1.4 (A) is the corresponding MS spectrum of $AcrA^{L}$-His. $AcrA^{L}$-His was cleaved into six bands, which were identified by MS on the basis of molecular weights (Da): 40435, 39597, 37389, 36558, 32025, and 28937. Note that there was an overlap of two peaks (40435 Da and 39597 Da) on SDS-PAGE. Figure 1.3 (B) and Figure 1.4 (B) show tryptic digestion profile of $AcrA^{S}$-His and the corresponding MS spectrum. Four trypsin-cleaved fragments of $AcrA^{S}$-His were identified based on molecular weights (Da): 39819, 39274, 31910 and 28967. The stable 28.9 kDa (T47-R315) fragment was identified in both $AcrA^{L}$-His and $AcrA^{S}$-His, which is consistent with the previous studies (40, 67).

Since trypsin cleaves at the C-terminal side of basic residues, we determined these trypsin-cleaved fragments combining the primary sequence of AcrA with the MS data. Table 1.1 lists the molecular weights (measured and calculated) of AcrA fragments and corresponding AcrA sequence ranges. In agreement with the previous studies (40, 67), AcrA was cleaved by trypsin at both termini: two cleavage sites at the N-terminus (Q29 and T47) and multiple sites at the C-terminus (K396, K374, K346 and R315). To get a clear picture of the tryptic cleavage sites on AcrA, these residues are illustrated on the secondary structure of AcrA (Figure 1.5) and labeled on the homolog model of AcrA (Figure 1.6) in which the crystal structure of MexA is used as a template (62). As shown on Figure 1.6, most cleavage sites are located in the MP domain. For example, R315 is located on the β-16 strand, K346 is located on the loop between β-18 and β-19 strands, and K374 can be found at the end of the MP domain.

After the identification of trypsin-cleaved AcrA fragments, we compared the tryptic digestion of AcrA variants in the time course (Figure 1.7). It showed that the

cleavage profile of $AcrA^S$-His was different from that of $AcrA^L$-His. First, the stable 28.9 kDa core (T47-R315) formed slower in $AcrA^L$-His than in $AcrA^S$-His. This can be interpreted that this site (R315) is protected by lipid moiety. Second, the 32.1 kDa fragment (T47-K346) in $AcrA^L$-His rapidly formed and accumulated. However, this fragment in $AcrA^S$-His formed slower, and the amount of this fragment decreased during the time course. Both observations are consistent with the principle of mass conservation. Compared to the tryptic digestion of $AcrA^S$-His, slower formation of the 28.9 kDa fragment (T47-R315) is coupled with the faster accumulation of the 32.1 kDa fragment (T47-K346) in the tryptic digestion of $AcrA^L$-His, therefore supporting the steric hindrance of lipid modification on residue R315 during the tryptic cleavage of AcrA variants.

Since oxidative phosphorylation and electron transport chain on the inner membrane of *E. coli* results in the accumulation of protons in the periplasm, the pH in the periplasm is about 6.0 (36). To characterize the effect of pH changes on the structural features of AcrA, we carried out the tryptic digestion of AcrA at pH 6.0 (Figure 1.7, B). Our result showed that the profiles under two pH conditions (pH 6.0 and pH 7.0) are very similar, suggesting that the pH change from 7.0 to 6.0 does not result in significant structural changes in AcrA. This result is also consistent with a previous study in which acidic pH 5.0 rather than pH 6.0 induces the conformational changes in AcrA (25).

Taken together, these results demonstrated that trypsin and PK cleave $AcrA^S$-His and $AcrA^L$-His differently. In the tryptic digestion, faster accumulation of the 32.1 kDa fragment (T47-K346) and slower formation of the 28.9 kDa fragment (T47-R315) of $AcrA^L$-His can be explained as a protective effect of lipid modification on residue R315.

A

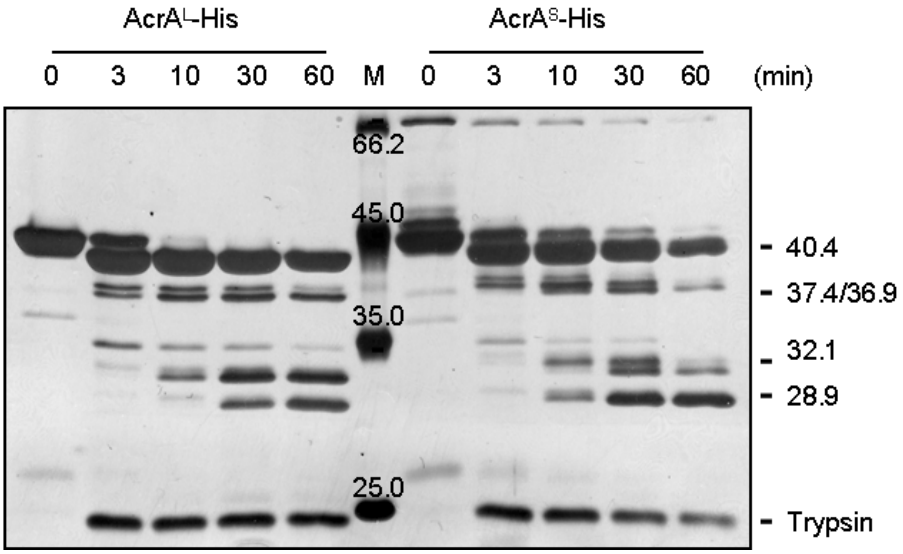

B

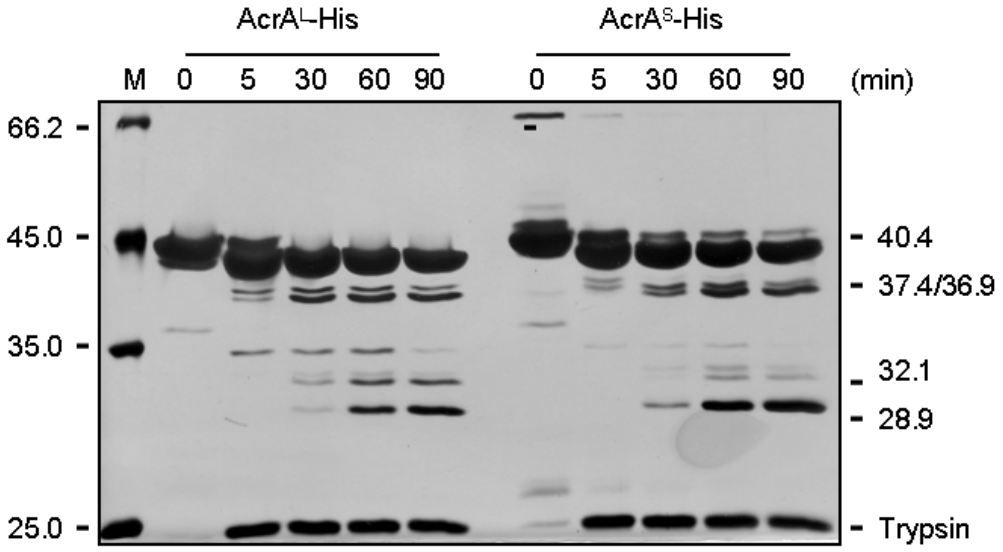

Figure 1.7 Time course of tryptic digestion of AcrA^{L}-His and AcrA^{S}-His at (A) pH 7.0 and (B) pH 6.0. Purified AcrA variants (1.95 µM) were digested with trypsin (0.10 µM). Tryptic fragments were resolved by SDS-PAGE (12 %) and stained with silver nitrate.

1.2 Effect of lipids on the accessibility of AcrA to trypsin

Membrane protein reconstitution into liposomes has been widely used to characterize the functional and structural features of membrane proteins (54). To evaluate the effect of AcrB on structure of AcrA, we reconstituted $AcrA^{L}$-His alone or together with AcrB-His into proteoliposomes. In this experiment, *E. coli* polar lipid extract (Avanti Polar Lipids, 100600) was emulsified in 20 mM Hepes (pH 7.0) buffer including 0.45% (wt) Triton X-100 (TX) and 5 mM DTT, and proteins were then added. After incubation of $AcrA^{L}$-His or $AcrA^{L}$-His together with AcrB-His in lipid samples for thirty minutes at room temperature, TX was removed by adsorption to Bio-beads (Bio-Rad). Proteins ($AcrA^{L}$-His and AcrB-His) incorporated into proteoliposomes were quantified by SDS-PAGE (12%) stained with CBB (Figure 1.8). In this experiment, BSA was used as control.

To assess whether the interaction between $AcrA^{L}$-His and AcrB-His causes the structural changes in AcrA, the reconstituted proteoliposomes were resuspended in 20 mM Hepes (pH 7.0) and 100 mM NaCl, followed by the trypsin treatment. Cleavage profiles of $AcrA^{L}$-His alone and $AcrA^{L}$-His plus AcrB-His in the proteoliposomes were very similar (Figure 1.9). Although these two proteins can form a complex *in vivo* (66, 67, 74), our result suggests that AcrA does not interact with AcrB efficiently *in vitro,* or that the AcrA-AcrB interaction does not result in the apparent conformational changes in AcrA or provide steric hindrance during the trypsin cleavage of AcrA.

When we examined the tryptic cleavage of $AcrA^{L}$-His in the presence and absence of lipids, surprisingly, we found that proteolytic profile of $AcrA^{L}$-His without lipids was different from that in the presence of lipids. First, not all $AcrA^{L}$-His in proteoliposomes

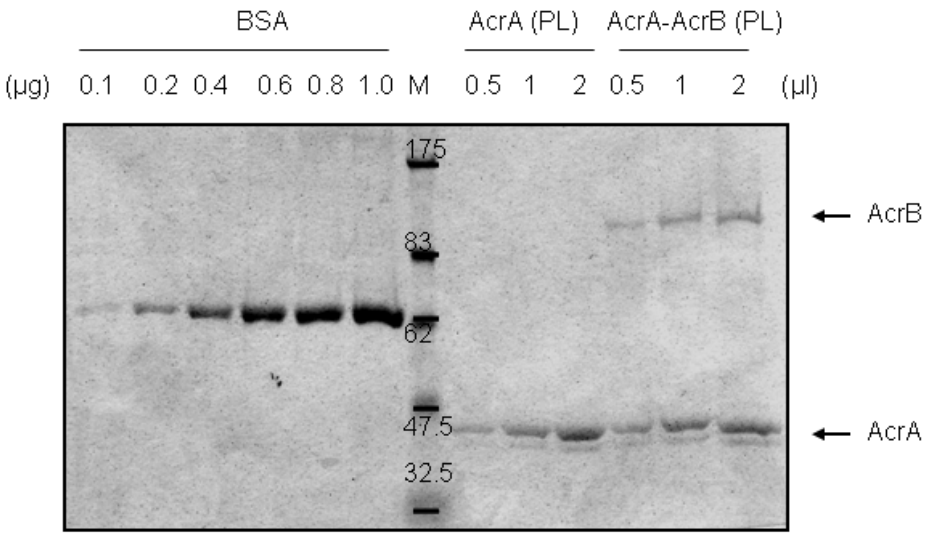

Figure 1.8 Quantification of AcrA^{L}-His and AcrB-His reconstituted into proteoliposomes. After reconstitution into proteoliposomes, proteins were resolved by SDS-PAGE (12%) and stained with CBB. AcrA^{L}-His concentrations in the AcrA^{L}-His (PL) and AcrA^{L}-His with AcrB-His (PL) are 0.173 mg/ml and 0.167 mg/ml, respectively. The AcrB-His concentration in the proteoliposomes is 0.085 mg/ml.

A

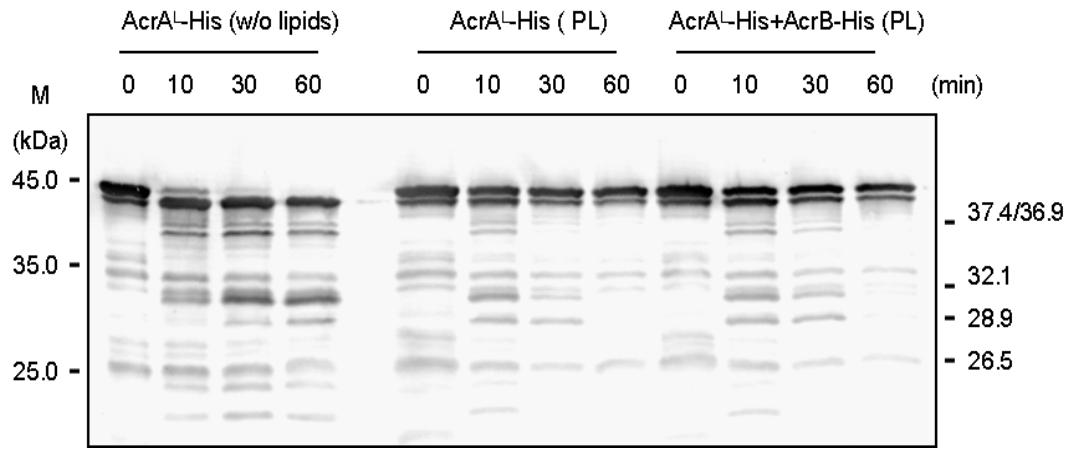

B

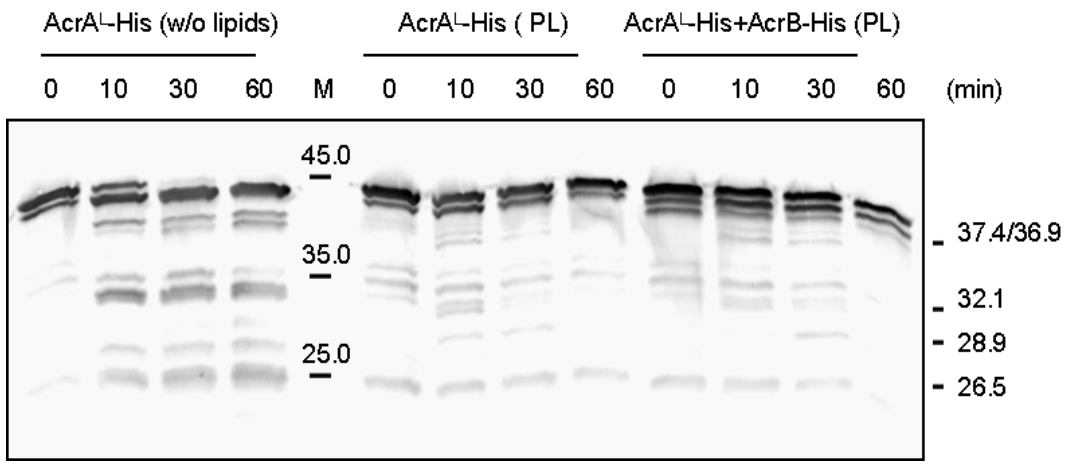

Figure 1.9 Tryptic digestion of AcrA^{L}-His-containing proteoliposome at (A) pH 7.0 and (B) pH 6.0. Purified AcrA^{L}-His was reconstituted into proteoliposomes alone or together with purified AcrB-His. Proteoliposomes were treated with trypsin, in which the concentrations of AcrA^{L}-His and trypsin are 0.73 μM, and 0.11 μM, respectively. AcrA^{L}-His in the absence of lipids was used as control (left). Tryptic fragments were resolved by 12 % SDS-PAGE and analyzed by immuno-blotting with anti-AcrA antibodies.

was cleaved during the time course. Second, we detected the 28.9 kDa fragment (T47-R315) in ten minutes in the presence of lipids and in 30 min in the absence of lipids. This result implied that the cleavage sites for this fragment are more exposed to external medium when AcrA^{L}-His is incorporated into liposomes. In addition, in the absence of lipids five fragments at 37.4 kDa (T47-K396), 36.9 kDa (Q29-K374), 32.1 kDa (T47-K346), 28.9 kDa (T47-R315) and 26.5 kDa (T47-R296) accumulated, whereas in the presence of lipids the amounts of these fragments reduced during the time course. This observation suggests that these AcrA fragments are more labile to trypsin once AcrA^{L}-His is reconstituted into liposomes.

Since the pH in the periplasm is about 6.0 (36), we next examined the pH effect (from pH 7.0 to 6.0) on AcrA digestion in the presence of lipids. Tryptic digestion was carried out as described above except at pH 6.0 (Figure 1.9 B). The presence of lipids and digestion at pH 6.0 did not change the tryptic cleavage profile of purified AcrA^{L}-His. This result suggested that there are no significant structural changes in AcrA^{L}-His due to this pH transition.

In the above experiments, the AcrA^{L}-His sample without *E. coli* polar lipids was treated with trypsin in the presence of 3.2 mM TX. To assess the effect of TX on the limited tryptic proteolysis of AcrA^{L}-His reconstituted into proteoliposomes, a similar experiment was performed in the presence of 3.2 mM TX. We found that 3.2 mM TX does not significantly affect the tryptic digestion of AcrA^{L}-His when present in the detergent-lipid mixture (data not shown).

During the above described reconstitution experiments, the lipid moiety of AcrA^{L}-His was expected to interact with *E. coli* polar lipids emulsified in detergent TX

buffer. Therefore AcrA could associate with either the inner or the outer leaflet of lipid bilayer upon the removal of TX. In this case, $AcrA^{L}$-His bound to outer leaflet is accessible to trypsin, whereas inner leaflet-bound $AcrA^{L}$-His is inaccessible. To avoid the burial of AcrA inside the liposomes, lipid(20 mM)-TX(3.2 mM) mixed vesicles were preformed before the addition of the purified $AcrA^{L}$-His without sonication. This direct incubation made all $AcrA^{L}$-His inserted into the outer leaflet of liposomes and exposed to trypsin. Similar to the reconstituted proteoliposomes, Figure 1.10 A shows that some amount, approximately 50%, of intact $AcrA^{L}$-His was not cleaved in 90 minutes, whereas the rest was cut in five minutes. When this incubation was extended to overnight, the amount of intact $AcrA^{L}$-His did not significantly decreased (data not shown). The same results were obtained in the overnight incubation of whole cells or membrane fractions with trypsin (data not shown). Trypsin-resistance of AcrA in the presence of lipid bilayers indicated that $AcrA^{L}$-His exist in, at least, two states: one is trypsin-vulnerable, and the other is trypsin-resistant. In addition, we detected the trace amount of the 32.1 kDa fragment (T47-K346) in the presence of lipids, compared to significant accumulation of this fragment in the absence of lipids (Figure 1.10 A). Besides, the 28.9 kDa fragment (T47-R315) in the presence of lipids accumulated faster than without lipids. This result illustrated the higher susceptibility of the cleavage site R315 to trypsin in the presence of lipids.

However, when $AcrA^{S}$-His was incubated with *E. coli* polar lipids followed by the tryptic digestion, the cleavage profile was the same as without lipids (Figure 1.10 B). This result implied that *E. coli* polar lipids do not induce structural changes in $AcrA^{S}$-His.

A

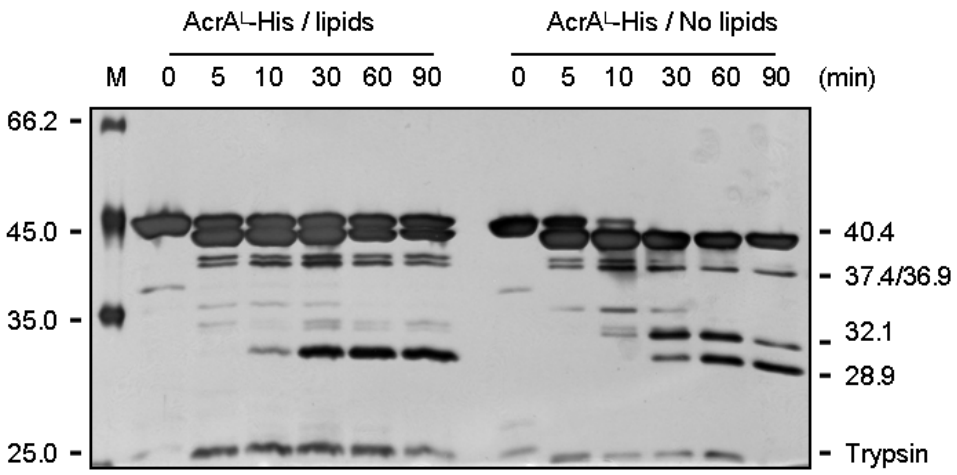

B

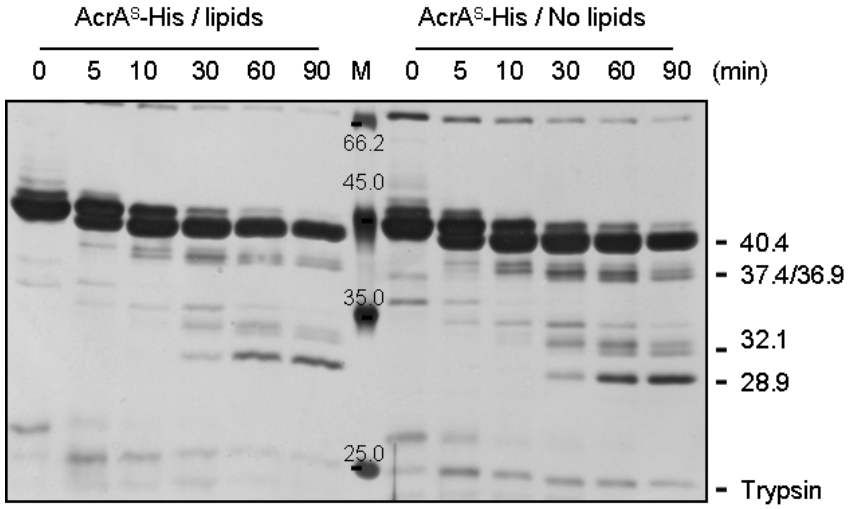

Figure 1.10 Tryptic digestion of (A) AcrA^{L}-His and (B) AcrA^{S}-His in the presence of detergent-lipid mixed vesicles. The concentration of lipids and TX are 20 mM and 3.2 mM, respectively. Purified AcrA variants (1.95 μM) were incubated with lipids (25.6 mM), followed by digestion with trypsin (0.10 μM). AcrA variants without lipids were used as control. Tryptic fragments were resolved by 12 % SDS-PAGE and analyzed by silver staining.

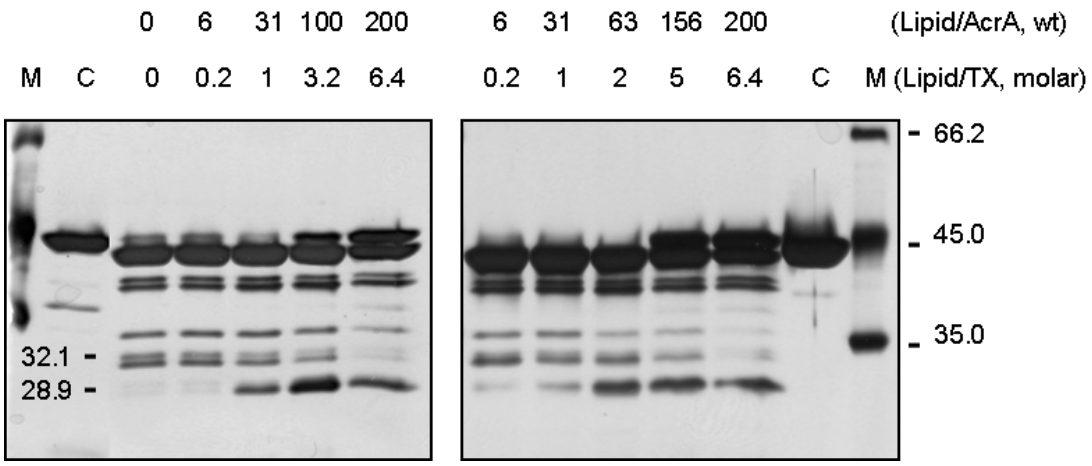

Figure 1.11 Effect of lipids on tryptic digestion of $AcrA^{L}$-His. AcrA was pre-incubated with increasing concentrations of lipids in the presence of 3.2 mM TX. After 15 min incubation with trypsin, reactions were terminated by boiling in SDS-sample buffer and analyzed by SDS-PAGE (12%).

Previous studies showed that lipids can exist as micelles and/or vesicles under different lipid:TX molar ratios (34, 65). Specifically, lipids dominantly exist in micelles when the molar ratio of lipids and TX is about 0.16, but lipid bilayers are formed as this ratio increases. Most lipids form vesicles when the ratio is increased to 1. In above experiments a large amount of *E. coli* polar lipids were incubated with AcrA variants. The molar ratio of lipids and TX was 6.4. In this case, lipids existed as vesicles even in the presence of 3.2 mM TX.

To investigate how accessibility of AcrA to trypsin changes with lipid phases, we incubated purified $AcrA^{L}$-His with different concentrations of *E. coli* polar lipid samples. The concentration of TX was set constant at 3.2 mM. Figure 1.11 shows the cleavage profile after 15 minutes incubation with trypsin. At the lowest lipid:TX ratio, the cleavage profile of $AcrA^{L}$-His was similar to that in the absence of lipids. In contrast, when lipid:TX molar ratio was increased to 1, or the lipid:AcrA ratio rose to about 30 (wt/wt), the amount of the 32.1 kDa fragment (T47-K346) decreased, whereas the 28.9 kDa fragment (T47-R315) accumulated. Moreover, when lipid:TX molar ratio was increased to 3.2 or the lipid:AcrA ratio was above 100 (wt/wt), some amount of intact $AcrA^{L}$-His became resistant to trypsin. Therefore our result demonstrated that the presence of lipid bilayers (lipid:TX molar ratio is above 1) is required to change proteolytic profiles of AcrA, especially in the formation of the 28.9 kDa fragment (T47-R315). This result suggested that interactions between $AcrA^{L}$-His and lipid bilayers increase the susceptibility of residue R315 to trypsin. On the other hand, decreased amount of the 32.1 kDa fragment (T47-K346) in the presence of lipid bilayers indicates that this fragment was rapidly cleaved into the stable 28.9 kDa core (T47-R315) or the accessibility of the

cleavage site K346 reduced. Besides, some intact $AcrA^{L}$-His is trypsin resistant when the lipid:TX molar ratio was above 3.2, suggesting that lipid vesicles protect $AcrA^{L}$-His from digestion.

Taken together, these results demonstrated that $AcrA^{L}$-His reconstituted into proteoliposomes or in the presence of detergent-lipid mixed vesicles was cleaved differently from that in the absence of lipids. In particular, the cleavage site R315 of the 28.9 kDa fragment (T47-R315) is more exposed to medium in the presence of vesicles/proteoliposomes. In addition, no significant accumulation of the 32.1 kDa fragment (T47-K346) in the presence of lipid bilayers suggests that this fragment is rapidly digested to form the stable 28.9 kDa core (T47-R315) or is formed slowly due to the reduced accessibility of the cleavage site K346. Both residues (R315 and K346) are located in the MP domain of AcrA (Figure 1.6), which is predicted to interact with the cytoplasmic membrane. Different susceptibility of the cleavage sites of AcrA to trypsin can be interpreted as the protection by lipid modification, or structural changes in AcrA. However, we did not observe the effect of *E. coli* polar lipids on the tryptic digestion of $AcrA^{S}$-His, thus lipid vesicles do not likely induce the structural variations in $AcrA^{S}$-His. In addition, when we compared proteolytic profiles of two AcrA variants in the presence of detergent-lipid vesicles, we detected the faster accumulation of the 28.9 kDa fragment (T47-R315) in $AcrA^{L}$-His than that of $AcrA^{S}$-His. This observation indicated that, compared to $AcrA^{S}$-His, the cleavage site R315 in $AcrA^{L}$-His is more exposed to aqueous medium when AcrA is associated with the lipid bilayer, given that the lipid modification and lipid bilayers do not interfere with the trypsin cleavage of $AcrA^{L}$-His. Moreover, we did not detect a significant pH effect on the structural changes under all tested conditions.

1.3 Different accessibility of AcrA-Cys mutants to thiol-reactive probes *in vitro* and *in vivo*

To compare the conformations of AcrA *in vivo* and *in vitro*, we used an approach based on fluorescence labeling (60, 69). In our study, fluorescein-5-maleimide (F5M) was used to covalently attach the fluorophore fluoresceine to a cysteine residue introduced by site-directed mutagenesis into AcrA. The reactivity of F5M was used to probe the accessibility of the Cys residue, thereby characterizing the conformational features in AcrA.

A previous study has shown that $AcrA^S$ mutants containing single Ala -> Cys substitution can complement the function as a wild type (25). These $AcrA^S$-Cys mutants include A30C, A39C, A62C, A103C, A146C, A172C, A204C, A242C, A295C, A339C, and A390C. These positions were placed in the AcrA structure which was modeled based on the crystal structure of MexA (62). As shown on Figure 1.12, A39C and A339C are located in the MP domain, A62C, A242C and A295C are positioned in the α-β barrel domain, A103C, A146C and A172C are located in the α-helical hairpin domain, and A204C are found in the lipoyl domain.

To conduct the fluorescence labeling of $AcrA^S$-Cys *in vivo*, plasmids over-expressing $AcrA^S$-Cys mutants and WT ($AcrA^S$ without Cys mutation) were transformed into AG100AX. After induction with IPTG, $AcrA^S$-Cys mutants as well as WT were treated with F5M. Labeled cells were lysed by sonication. Proteins were purified by the metal affinity chromatography and analyzed by fluorescence scanning followed by CBB staining of SDS-PAGE. Image Quant® software was then used to quantify the fluorescence as well as the amounts of proteins.

In parallel experiments, $AcrA^S$-Cys mutants were labeled *in vitro*. For this purpose, $AcrA^S$-Cys proteins were purified first, and then treated with F5M.

Figure 1.13 demonstrates the $AcrA^S$-Cys-labeling profiles *in vivo* and *in vitro*. Figure 1.14 shows the fluorescence intensities of non-lipidated $AcrA^S$-Cys mutants *in vivo* and *in vitro*. To clarify the labeling result, we organized the labeling profiles *in vivo* and *in vitro* in Table 1.2.

As seen in the Table 1.2, Cys39, Cys62, Cys103, and Cys242 are more accessible to be labeled with F5M *in vivo* than *in vitro*. Furthermore, Cys62 and Cys242 were partially labeled inside the cell but were not labeled in the purified proteins. These results suggested that these Cys residues might be located in the flexible domain of AcrA and conformational flexibility results in the accessibility heterogeneity. For example, half of these residues (Cys 62, Cys242) are accessible and the remaining 50% of the residues are inaccessible.

In addition, we found that standard derivation errors in our data are too large. Some errors are close to or even larger than the values themselves, especially in Cys 39 (*in vitro*), 62 (*in vivo*), 103 (*in vivo* and *in vitro*), and 242 (*in vivo* and *in vitro*). These significant standard derivation errors indicated that our data are not reproducible. Although our observations suggested the different accessibility of F5M to Cys in AcrA mutants, further studies are required to confirm this result.

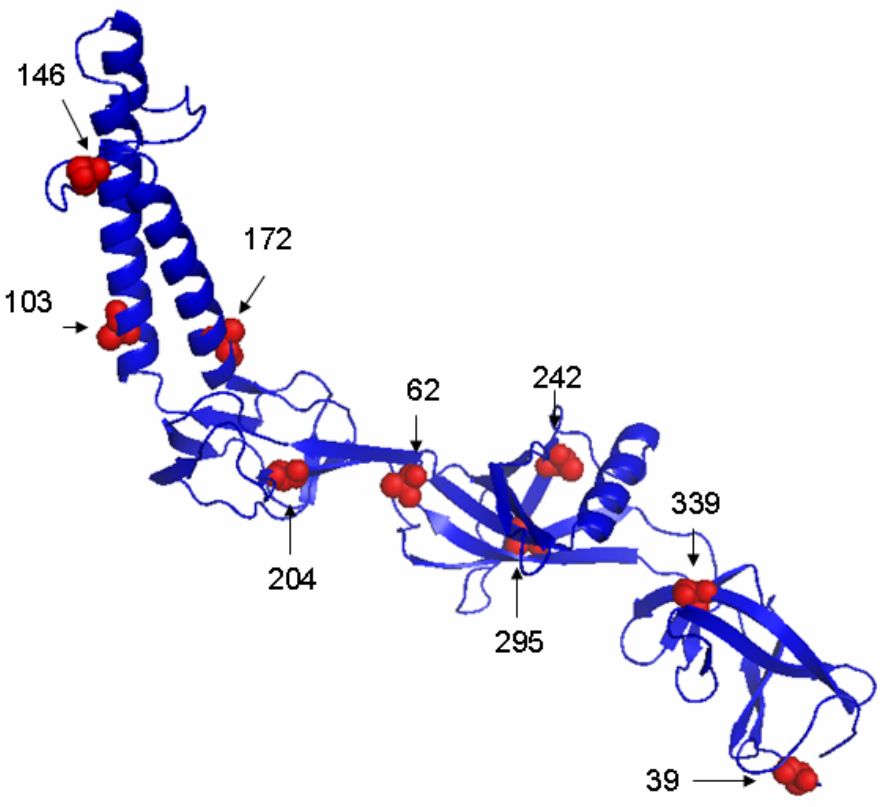

Figure 1.12 Positions of Cys substitutions in the homolog model of AcrA. This model was generated using Swiss-Model software (http://swissmodel.expasy.org//SWISS-MODEL.html) and the crystal structure of MexA as a template (62). Nine residues A39C, A62C, A103C, A146 C, A172C, A204C, A242C, A295C and A339C are labeled in red spheres. Note that residues for both A30C and A390C are not visualized in this structural model.

A

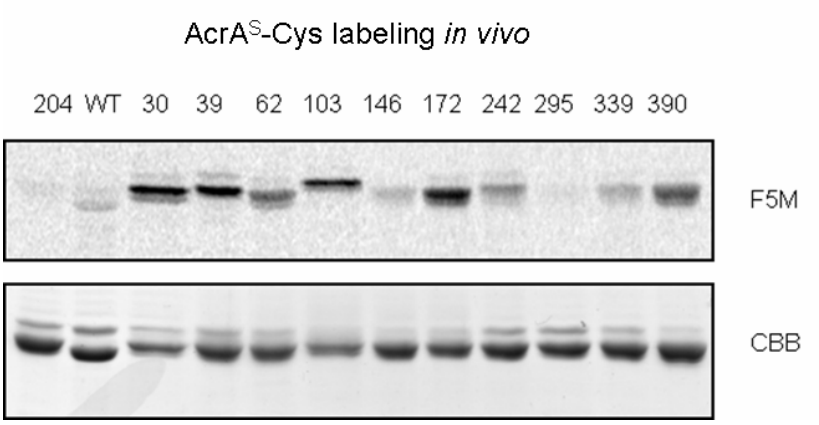

B

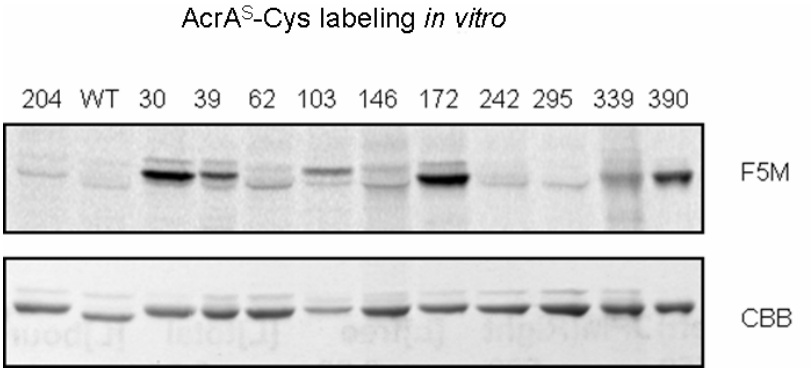

Figure 1.13 AcrA^S-Cys labeling *in vivo* and *in vitro*. F5M panels are fluorescence profiles of AcrA^S-Cys mutants, and CBB panels are corresponding protein profiles. (A) *In vivo* labeling of AcrA^S-Cys mutants and WT (AcrA without Cys mutation). Whole cells were incubated with 100 μM F5M in PBS for 30 min. Labeled AcrA^S-Cys variants and WT were purified and analyzed by SDS-PAGE (12%). Fluorescence was detected using Storm 840 Imager (Molecular Dynamics). The excitation wavelength and the emission wavelength were set at 450 nm and 520 nm, respectively. (B) *In vitro* labeling of AcrA^S-Cys. AcrA^S-Cys mutants and WT were purified and then labeled with 20 μM F5M. Fluorescence measurement was carried out as in (A).

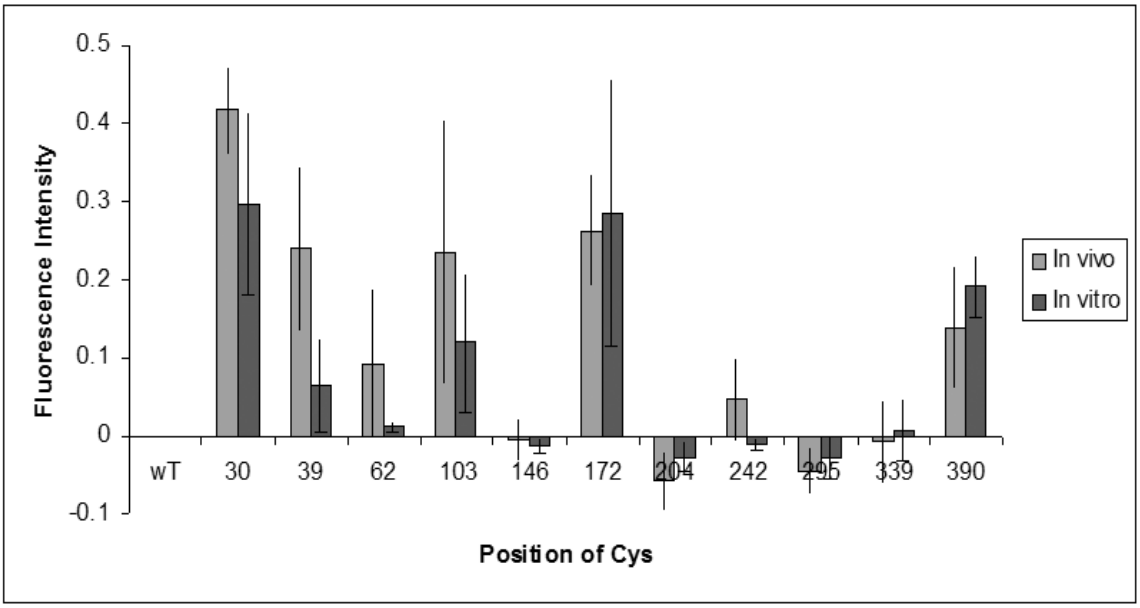

Figure 1.14 Quantification of fluorescence labeling of AcrA^{S}-Cys *in vivo* and *in vitro.* Fluorescence intensities and protein amounts of AcrA^{S}-Cys mutants and WT were quantified using Image Quant® program. The fluorescence intensity was normalized onto protein amounts. Error bars are standard deviations (n = 3)

Table 1.2 Fluoresceine-5-maleimide labeling of $AcrA^S$-Cys *in vivo* and *in vitro*.

"++" stands for accessible, "+" for partial accessible, "-" for inaccessible

Position of Cys	Domain	Labeling *in vivo*	Labeling *in vitro*
30	--	++	++
39	**MP**	**++**	**+**
62	**α, β-barrel**	**+**	**-**
103	**α-helical hairpin**	**++**	**+**
146	α-helical hairpin	-	-
172	α-helical hairpin	++	++
204	Lipoyl	-	-
242	**α, β-barrel**	**+**	**-**
295	α, β-barrel	-	-
339	MP	-	-
390	--	++	++

Chapter 2

Effect of AcrB and TolC on the Proteolytic Accessibility of AcrA

To understand the function mechanism of AcrA inside the cell, we characterized the structure of AcrA, especially the MP domain, *in vivo*. Here we used *in vivo* limited proteolysis to digest AcrA inside *E. coli* strains with different genetic backgrounds. Two strains were used: AG100AX in which both *acrA-acrB* and *acrE-acrF* multidrug efflux pumps are deleted from the chromosome, and ECM2112 lacking *acrA, acrB* and *tolC*. Using the identified AcrA fragments as a map, we characterized the the structure of over-produced $AcrA^{L}$-His *in vivo*, given that the over-produced $AcrA^{L}$-His functions well during the multi-drug efflux (38). For this purpose, we transformed the plasmid over-expressing $AcrA^{L}$-His into these two strains. The proteolytic profile of AcrA *in vivo* was analyzed by using anti-AcrA antibodies. Since TolC is expressed in AG100AX but not in ECM 2112 strain, comparison of cleavage profiles of AcrA from these two strains should reflect the effect of TolC on the accessibility of the over-expressed AcrA to trypsin. It should be noted that AcrB was not expressed in both strains.

Previous studies demonstrated that different complexes AcrA-AcrB, AcrA-TolC and AcrA-AcrB-TolC were formed inside the cells (32, 62, 66, 67, 73). In our experiments, *in vivo* limited proteolysis was used to characterize the conformations of AcrA in different complexes (AcrA-AcrB, AcrA-TolC, and AcrA-AcrB-TolC), which provides insight into the functional assembly of the multidrug efflux complex AcrAB-TolC. In particular, three stains were used: AG100, wild type (WT) producing the intact AcrAB-TolC complex; ZK796, delta TolC (ΔTolC) mutant expressing only AcrAB; and

AG102MB, delta AcrB (ΔAcrB) mutant producing AcrA and TolC. To make AcrA accessible to trypsin in the periplasm, we applied osmotic shock (20% sucrose Tris-EDTA buffer). This approach was previously shown to permeabilize the OM to trypsin (44).

2.1 Proteolytic profile of the overexpressed AcrA-His in cells is similar to that of purified $AcrA^{L}$-His

To reveal the function mechanism of AcrA *in vivo*, we used the limited proteolysis to characterize the conformations of the MP domain in the over-produced AcrA inside the cells. For this purpose, plasmid $pAcrA^{his}$ over-expressing $AcrA^{L}$-His was transformed into *E. coli* cells (AG100AX and ECM2112). Figure 2.1 (B) shows the trypsin cleavage profile of AcrA *in vivo* visualized by immunoblotting. Even without trypsin, some over-produced $AcrA^{L}$-His was degraded by endogenous periplasmic proteases. To identify the tryptic fragments of AcrA, we titrated whole cells with increasing amounts of trypsin. Several trypsin-specific bands of $AcrA^{L}$-His overexpressed in AG100AX were identified by comparison to the *in vitro* tryptic digestion (Figure 2.1 A): 37.4 kDa (T47-K396), 36.9 kDa (Q29-K374), 32.1 kDa (T47-K346), 28.9 kDa (T47-R315), and 26.5 kDa (T47-R294/R296). All these fragments were detected when AcrA was treated with trypsin *in vitro*. Thus, *in vivo* cleavage profile of $AcrA^{L}$-His was similar to that of the purified $AcrA^{L}$-His. Although the 26.5 kDa fragment (T47-R294/R296) was poorly detected by silver staining (Figure 1.7), this fragment can be clearly detected by immunoblotting in the $AcrA^{L}$-His digestion *in vivo.*

$AcrA^{L}$-His over-expressed in ECM2112 (ΔAcrAB-TolC) displayed the proteolytic profile similar to that in AG100AX cell (data not shown), suggesting that TolC does not

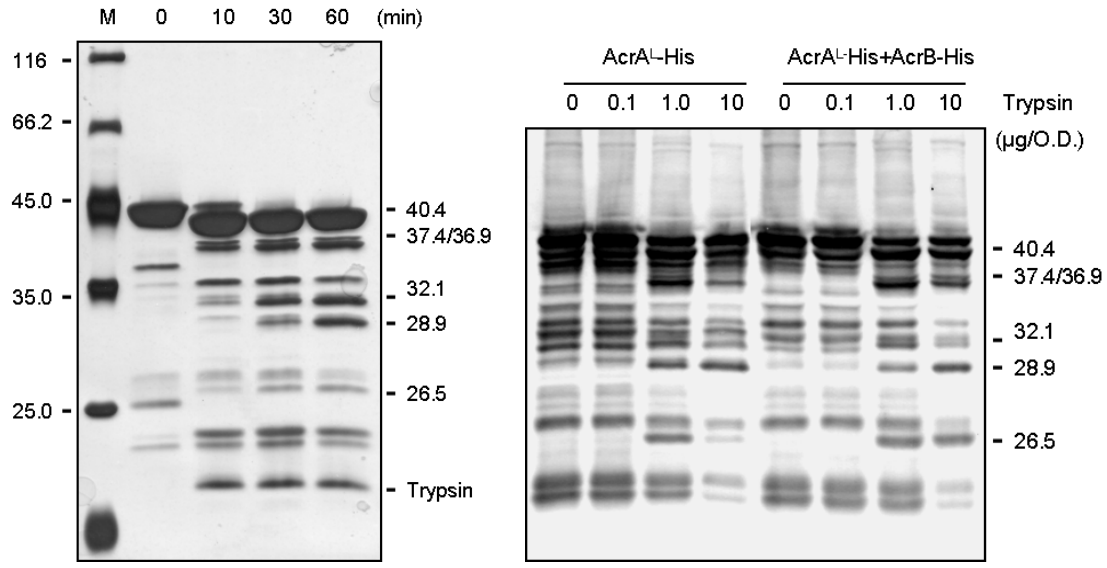

Figure 2.1 Tryptic digestion of overexpressed AcrA^{L}-His *in vivo* and *in vitro*. (A) Tryptic digestion of AcrA^{L}-His *in vitro*. Purified AcrA^{L}-His (1.95 μM) was treated with trypsin (0.10 μM). Tryptic fragments were resolved by SDS-PAGE (12%) and analyzed by silver staining. (B) Tryptic digestion of overproduced AcrA^{L}-His *in vivo*. AcrA^{L}-His was over-produced in *E. coli* AG100AX cells carrying pAcrA^{His} and pAcrA^{His}AcrB plasmids. After treatment with increasing concentrations of trypsin for 60 min at 37ºC, the whole cell proteins were resolved by SDS-PAGE (12%) and analyzed by immunoblotting with anti-AcrA antibody. O.D. - the optical density as determined by absorbance at 600 nm.

affect the tryptic cleavage of the over-produced AcrA^{L}-His inside the cell. We therefore concluded that over-expressed AcrA^{L}-His *in vivo* adopts the conformation similar to that of the purified AcrA^{L}-His.

We did not detect any changes in the tryptic cleavage of the purified AcrA^{L}-His in the presence of AcrB-His (Figure 1.9). We next examined whether AcrB-His inside the cell affects digestion of the over-produced AcrA^{L}-His. For this purpose, we used pAcrA^{his}AcrB plasmid which over-expressed both AcrA^{L}-His and AcrB-His under the native *acrA* promoter. This plasmid was transformed into AG100AX cells and the similar trypsin titration was conducted as described as above. As shown on Figure 2.1 (B), the same cleavage fragments of AcrA^{L}-His were obtained in the presence of AcrB-His, indicating that over-expression of AcrB-His together with AcrA^{L}-His did not significantly affect the tryptic cleavage profile of AcrA^{L}-His. Nevertheless, we found that, when treated with the high concentration of trypsin (10 µg/O.D.), the amount of the 26.5 kDa fragment (T47-R294/R296) was higher in cells over-producing AcrA^{L}-His and AcrB-His than in cells over-producing AcrA^{L}-His alone. This result suggested that AcrB-His interaction with AcrA^{L}-His inside the cells protects this 26.5 kDa fragment (T47-R294/R296) from further cleavage.

Taken together, these results showed that the overall structure of over-produced AcrA^{L}-His inside the cells is similar to that of purified AcrA^{L}-His and other components (AcrB and TolC) don't significantly affect the conformation of AcrA^{L}-His *in vivo*.

2.2 AcrB-His and TolC-His affect the trypsin accessibility to AcrA^{L}-His *in vivo*

Previous studies showed that AcrA-AcrB-TolC form a stable complex spanning

the two membranes in *E. coli* (66, 67). More recent studies further demonstrated that the lipoyl domain, β-barrel domain and MP domain in AcrA interact with the periplasmic domain of AcrB, whereas the N-terminal helix of AcrA packs against TolC helical coils (35, 62). Although the proposed docking model utilized computational energy minimization and site-specific *in vivo* cross-linking to optimize the AcrA-AcrB-TolC assembly, experimental evidence is still needed to further validate the putative conformational changes in AcrA during the complex assembly. For example, does interaction with AcrB or TolC induce different conformations of AcrA? How do the putative structural changes in AcrA as well as the protein-protein interactions (AcrA-AcrB or AcrA-TolC) coordinate during assembly of the functional tripartite complex (AcrA-AcrB-TolC)?

Here we used trypsin digestion of AcrA expressed in three strains AG100 (WT), AG102MB (ΔAcrB), and ZK796 (ΔTolC) to investigate the effect of AcrB and TolC on AcrA. First, the three strains were treated with increasing amounts of trypsin for five minutes and one hour (Figure 2.2). Although chromosomally produced AcrA was also cleaved by endogenous proteases in the periplasm, the amounts of cleaved fragments were much less than those of AcrA over-expressed from plasmids (Figure 2.1, B).

The comparison of the tryptic digestion profiles showed that similar AcrA fragments were produced in AG102MB (ΔAcrB) and ZK796 (ΔTolC) cells. When the trypsin concentration was increased, the amount of the 37.4 kDa (T47-K396), 36.9 kDa (Q29-K374), and 26.5 kDa (T47-R294/R296) decreased. On the other hand, some amount of the 28.9 kDa fragment (T47-R315) was detected. The profile of AG100 (WT) was different from those of AG102MB (ΔAcrB) and ZK796 (ΔTolC). Particularly, rapidly

A

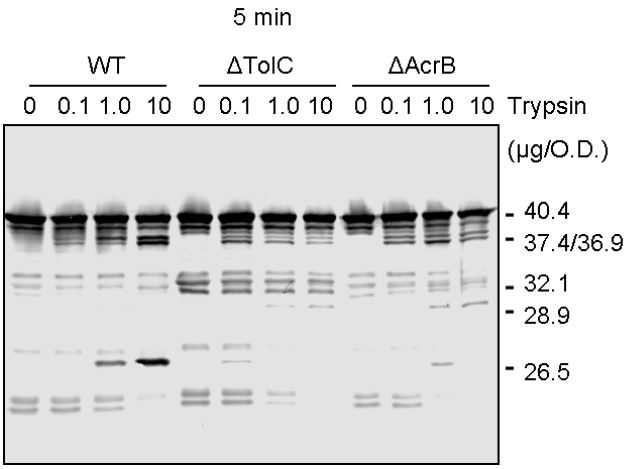

B

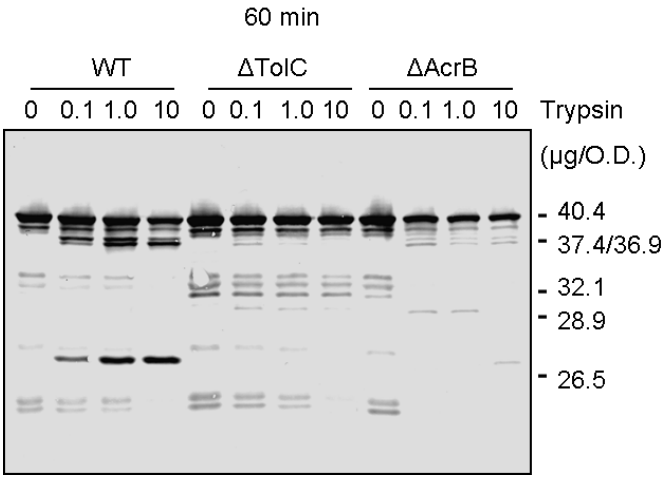

Figure 2.2 Tryptic digestion of chromosomally produced AcrA in *E. coli* cells with different genetic backgrounds. (A) WT, ΔTolC and ΔAcrB cells were treated with trypsin at indicated concentrations for 5 min. (B) WT, ΔTolC and ΔAcrB cells were treated with trypsin at indicated concentrations for 60 min. *E.coli* AG100 (WT), ZK796 (ΔTolC) and AG102MB (ΔAcrB) were grown to mid-exponential phase (A_{600} ~ 1.0). Cells were collected and treated with increasing concentrations of trypsin at 37ºC. Total proteins were resolved by 12% SDS-PAGE and AcrA fragments were visualized by anti-AcrA western blotting.

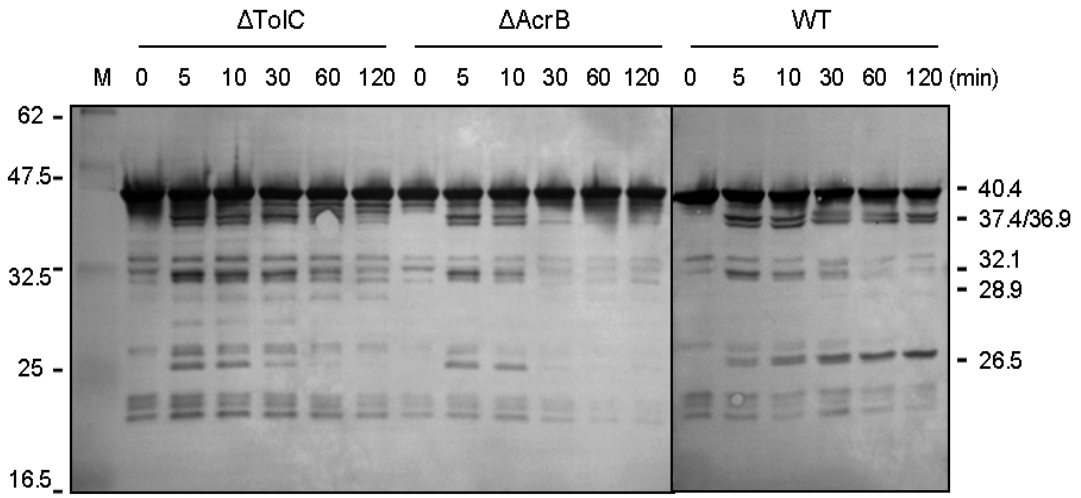

Figure 2.3 Time course of tryptic digestion of AcrA in *E. coli* strains with different genetic backgrounds. *E.coli* AG100 (WT), ZK796 (ΔTolC) and AG102MB (ΔAcrB) were grown to mid-exponential phase (A_{600}~ 1.0). Cells were collected and digested with trypsin (1.0 µg/O.D.). Aliquots were taken at 0, 5, 10, 30, 60, and 120 min and reactions were terminated by addition of SDS-sample buffer. Total proteins were resolved by 12% SDS-PAGE and AcrA fragments were visualized by anti-AcrA western blotting.

accumulated 37.4 kDa (T47-K396) and 36.9 kDa (Q29-K374) fragments were further cleaved in AG102MB (ΔAcrB) and ZK796 (ΔTolC) cells, whereas these fragments were resistant to further digestion in AG100 (WT) strain. Besides, the small amount of 28.9 kDa fragment (T47-R315) can be visualized in AG102MB (ΔAcrB) and ZK796 (ΔTolC) strains, compared to no evident 28.9 kDa band (T47-R315) in AG100 cells. Furthermore, at the high concentration of trypsin or after treatment extended to one hour, the 26.5 kDa fragment (T47-R296/R294) accumulated in AG100 (WT) strain. In contrast, this fragment was further cleaved in the other two strains (ΔAcrB and ΔTolC).

To further confirm that AcrA cleavage depends on genetic backgrounds of cells, we conducted the time course of trypsin proteolysis in these three strains. *E coli* cells were incubated with trypsin at concentration 1.0 µg/O.D and proteolysis was analyzed at 5, 10, 30, 60, and 120 minutes after addition of trypsin. Anti-AcrA immunoblotting showed the 40.4 kDa (N-K396), 37.6 kDa (T47-K396), 36.9 kDa (Q29-K374), 32.1 kDa (T47-K346), 28.9 kDa (T47-R315), and 26.5 kDa (T47-R294/R296) fragments (Figure 2.3). In agreement with the trypsin titration result, the cleavage profiles of AG102MB (ΔAcrB) and ZK796 (ΔTolC) were similar. On the other hand, the 37.4 kDa (T47-K396), 36.9 kDa (Q29-K374), and 26.5 kDa (T47-R294/R296) fragments were further digested in both AG102MB (ΔAcrB) and ZK796 (ΔTolC) strains. However, these three fragments were accumulated in AG100 (WT) strain during the time course. This result suggested that lack of any components, AcrB or TolC, resulted in the changes of AcrA accessibility to trypsin.

A

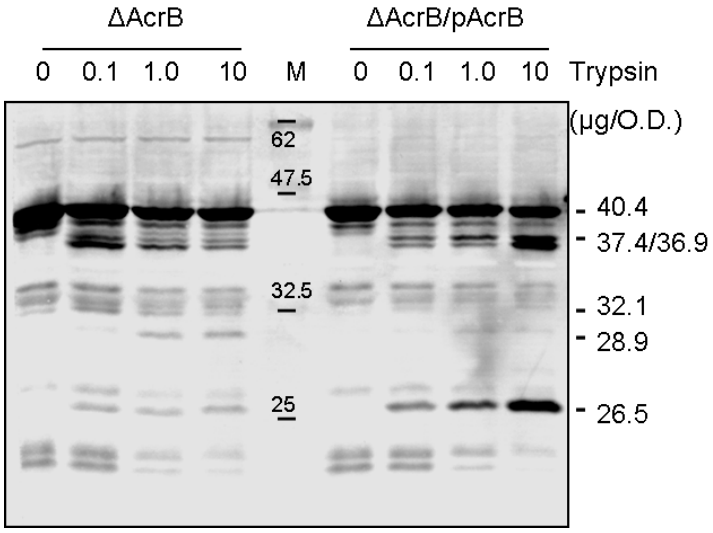

B

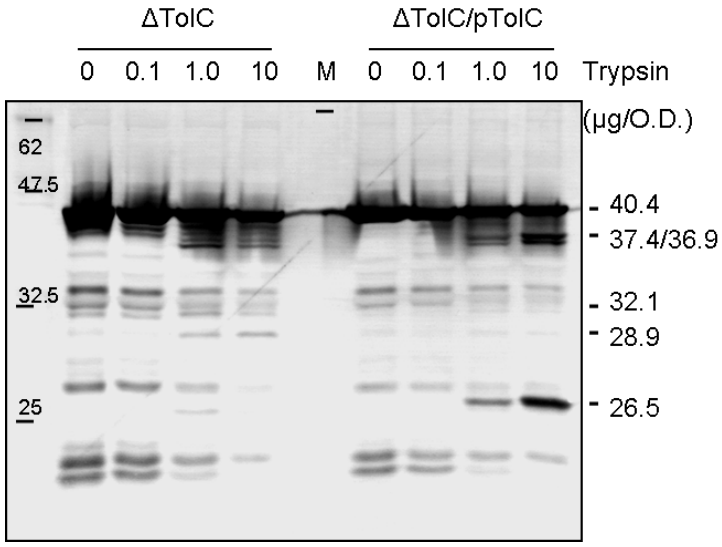

Figure 2.4 Effect of (A) AcrB and (B) TolC on the *in vivo* tryptic digestion of AcrA. ZK796 (ΔTolC) and AG102MB (ΔAcrB) cells were transformed with pTolC^{his} and pAcrB^{his} plasmids producing TolC and AcrB, respectively or with pUC18 vector alone. Cells were collected and treated with increasing concentrations of trypsin for 60 min at 37ºC. Total proteins were resolved by 12% SDS-PAGE and AcrA fragments were visualized by anti-AcrA immunoblotting.

2.3 AcrB-His and TolC-His protect the C-terminal domain of $AcrA^{L}$-His *in vivo*

To confirm that changes in proteolytic profiles of AcrA are caused by the lack of AcrB or TolC, we transformed plasmids expressing AcrB-His or TolC-His into AG102MB (ΔAcrB) or ZK796 (ΔTolC) strains respectively, and then investigated AcrA accessibility to trypsin (Figure 2.4). When the plasmid expressing AcrB-His was introduced in AG102MB (ΔAcrB) strain, the trypsin cleavage profile of AcrA became similar to that of AG100 (WT) strain: rapid digestion of 37.4 kDa (T47-K396)/36.9 kDa (Q29-K374) fragments and accumulation of the 26.5 kDa fragment (T47-R294/R296). When the plasmid borne TolC was produced in ZK796 strain (ΔTolC), the trypsin cleavage profile at 60 min was very similar to that of AG100 (WT) strain. This experiment demonstrated that, once AcrB or TolC is expressed in ΔAcrB cells or ΔTolC cells, respectively, to form the functional tripartite complex, AcrA accessibility to trypsin changed and the C-terminal domain of AcrA was protected from further digestion.

2.4 Trypsin digestion of AcrA in the presence of AcrB or TolC *in vitro*

The experiments described above demonstrated that the functional tripartite complex assembly protects the C-terminal domain of AcrA. We next performed trypsin digestion of the purified AcrA in the presence and absence of AcrB and/or TolC. The goal of these experiments was to establish whether AcrAB-TolC complex is assembled *in vitro*. AcrB-His and TolC-His were purified using metal-affinity chromatography as described in Methods. Figure 2.5 shows the SDS-PAGE analysis of the purified AcrB and TolC proteins. For limited trypsin proteolysis, purified $AcrA^{L}$-His was incubated with AcrB-His or TolC-His in the presence of *E. coli* polar lipid vesicles which were resuspended in

20 mM Hepes (pH7.0) buffer containing 3.2 mM TX and 100 mM NaCl. The cleavage fragments were resolved by SDS-PAGE and visualized by silver staining.

Figure 2.6 (A) shows the tryptic cleavage profiles of AcrA alone, AcrB alone, and AcrA-AcrB mixture. AcrB was rapidly degraded into several fragments with apparent molecular weights at 70 kDa, 55 kDa, 53 kDa, 52 kDa, and 40.5 kDa as estimated by comparison to the standard markers. Moreover, the 70 kDa fragment was further cleaved during the time course. When AcrA and AcrB were mixed together, AcrB was cleaved into the same fragments as AcrB alone. Similarly, the tryptic cleavage profile of AcrA was not affected by the presence of AcrB. This result suggested that incubation with AcrB *in vitro* does not induce conformational changes in AcrA or protection of cleavage sites in AcrA. This result is also consistent with that of proteoliposome cleavage (Figure 1.9).

Figure 2.6 (B) shows the tryptic digestion profiles of AcrA alone, TolC alone, and AcrA-TolC mixture. TolC was digested in 5 min into three major fragments with apparent MW at 50 kDa, 27 kDa, and 25 kDa as estimated by comparison to the standard markers. When AcrA and TolC were mixed together, TolC was digested into the same fragments as TolC alone. However, incubation with TolC resulted in the slower formation of the stable AcrA core (28.9 kDa). This slower accumulation could be due to protection of R315 of AcrA by interactions with TolC.

Previous studies have shown that AcrB and TolC bind to different domains of AcrA (35, 62). Here we demonstrated that AcrB and TolC affect the accessibility of AcrA to trypsin *in vivo*. Association with either AcrB or TolC results in the similar cleavage profile of AcrA *in vivo*. Interestingly, the accessibility of AcrA in the functional tripartite complex is different from that in either AcrA-AcrB or AcrA-TolC bipartite complexes.

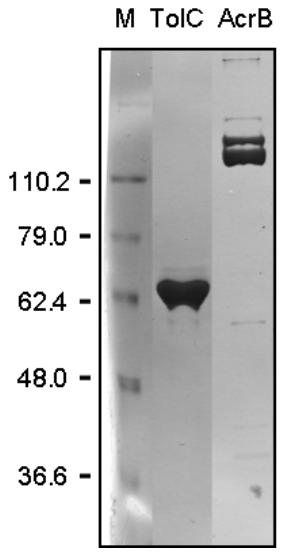

Figure 2.5 SDS-PAGE (12%) analysis of purified AcrB and TolC. Proteins were visualized by silver staining.

A

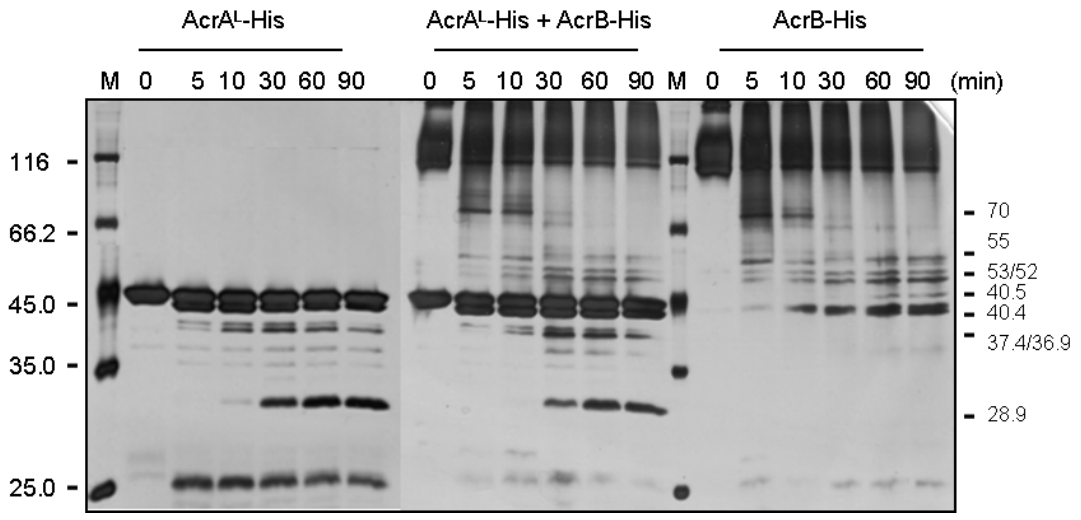

B

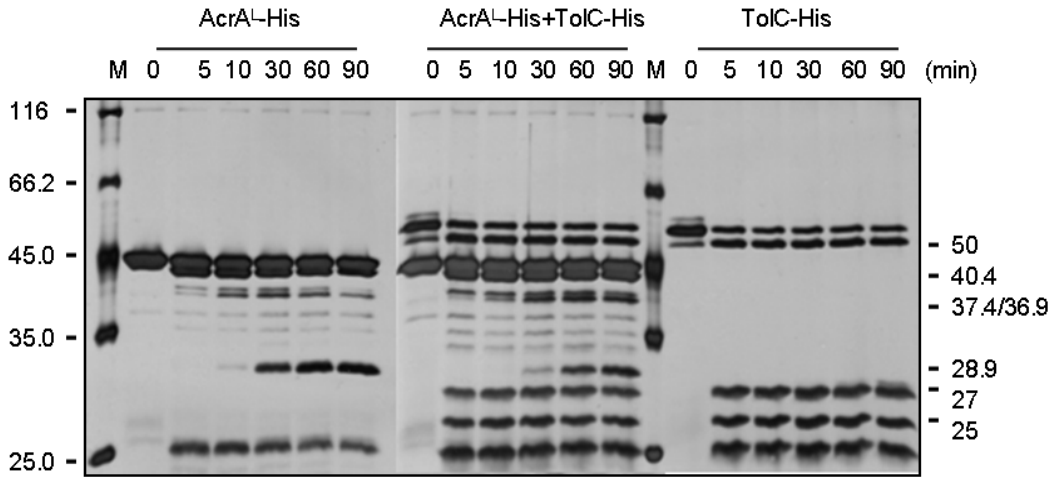

Figure 2.6 Effect of AcrB (A) and TolC (B) on the *in vitro* tryptic digestion of purified AcrA. Purified AcrA was incubated with purified AcrB or TolC in the presence of *E. coli* polar lipid vesicles, followed by trypsin digestion. Aliquots were taken at 0, 5, 10, 30, 60, and 90 min and reactions were terminated by SDS-sample buffer. The tryptic fragments were resolved by 12% SDS-PAGE and visualized by silver nitrate staining.

This specific AcrA profile in the functional tripartite complex was confirmed by the complementation experiment in which AcrB or TolC was introduced into the corresponding ΔAcrB or ΔTolC strains. The simplest interpretation for this result is that new interfaces which are formed during the assembly of the three component complex protect the C-terminal domain of AcrA (315-397 a.a). However, we can not exclude the possibility that AcrA undergoes conformational changes during the functional tripartite complex assembly. In addition, the effect of AcrB and TolC on the tryptic cleavage of AcrA *in vitro* was also investigated. We didn't detect the changes of AcrA cleavage due to AcrB. In contrast, the slower accumulation of the 28.9 kDa fragment (T47-R315) during the time course possibly results from the protection of R315 by AcrA-TolC interactions.

Chapter 3

Oligomerization of AcrA

3.1 AcrA^{S}-His forms oligomers in the presence of *E. coli* polar lipids

Oligomerization of MFPs including AcrA is a controversial topic. Even in the research of non-lipidated soluble AcrA, different oligomerization results were reported. A hydrodynamic study showed that AcrA^{S}-His predominantly exists as a monomer in solution (72). In contrast, an electron microscopy study demonstrated a dimer configuration of AcrA crystallized on lipid layers (2). Besides, a dimer of dimers was found in the X-ray crystal structure of AcrA core (53-299 a.a) (42). Interestingly, oligomers including trimers and dimers were detected in DSG cross-linking *in vivo* (74). To further address this "conflicting" oligomerization status of AcrA^{S}-His *in vivo* and *in vitro* and elucidate the assembly mechanism of the homo-oligomers, we used formaldehyde (FA) to cross-link oligomers of AcrA *in vitro*.

Formaldehyde (formula H_2CO) is one of the smallest and shortest cross-linkers. The structural study showed that the spacer arm of formaldehyde is about 2.3-2.7 Å (61). As shown in Figure 3.1, formaldehyde can bind a nitrogen atom or other atoms if two atoms are close within the spacer arm of formaldehyde, forming a cross-linked methylene bridge (-CH_2-). Thus, formaldehyde has been widely used in fixation and/or cross-linking to capture the fine structural details in light/electron microscopy studies and mass spectrometry experiments (61).

To investigate oligomerization of AcrA, we incubated AcrA^{S}-His with increasing concentrations of formaldehyde (Sigma) in 20 mM Hepes-KOH (pH 7.0) and 100 mM

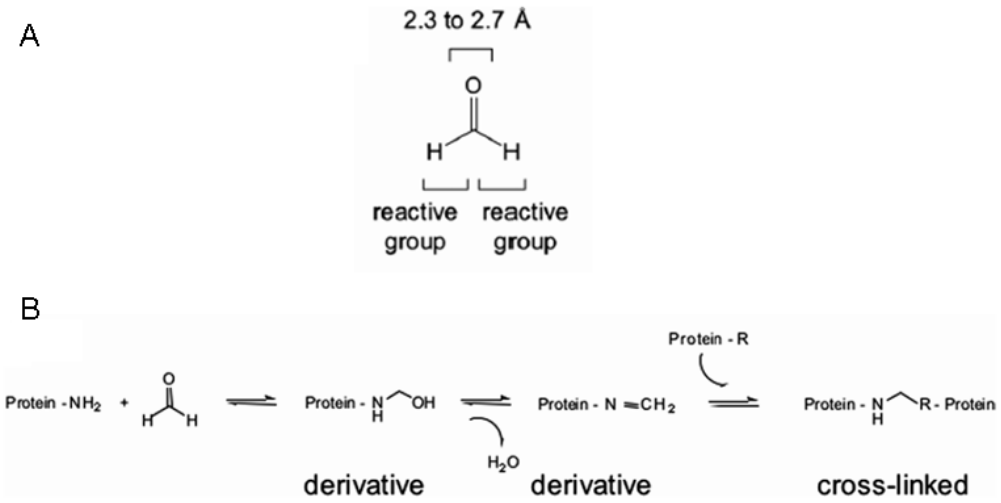

Figure 3.1 Mechanism of formaldehyde cross-linking (61). (A) Structure of formaldehyde. (B) Two step of cross-linking chemistry of formaldehyde.

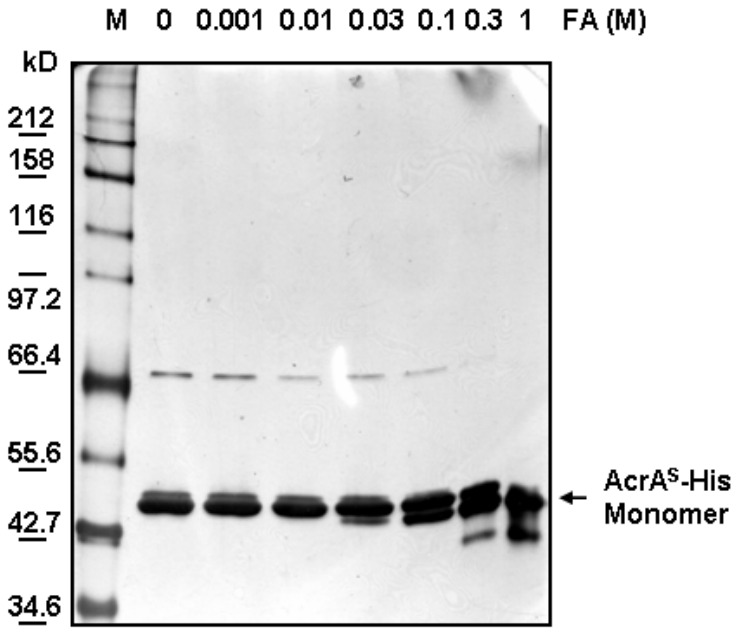

Figure 3.2 Cross-linking of AcrA^{S}-His with increasing concentrations of formaldehyde. After 30 min incubation at room temperature in 20 mM Hepes-KOH (pH 7.0), NaCl 100 mM, cross-linking was stopped by addition of 0.5 M glycine. The cross-linked AcrA was resolved by SDS-PAGE (8 %) and stained with silver nitrate.

A pH 7.0

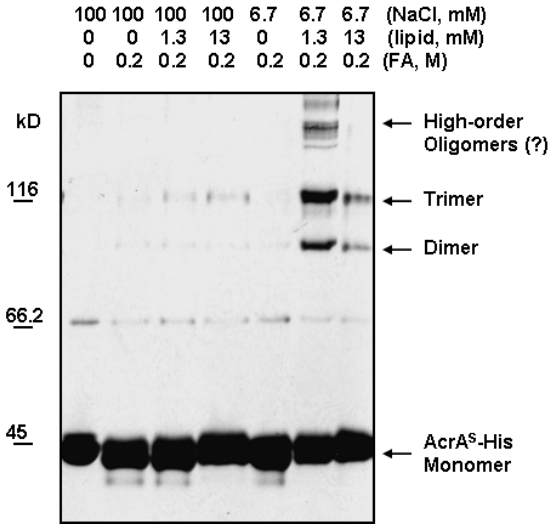

B pH 6.0

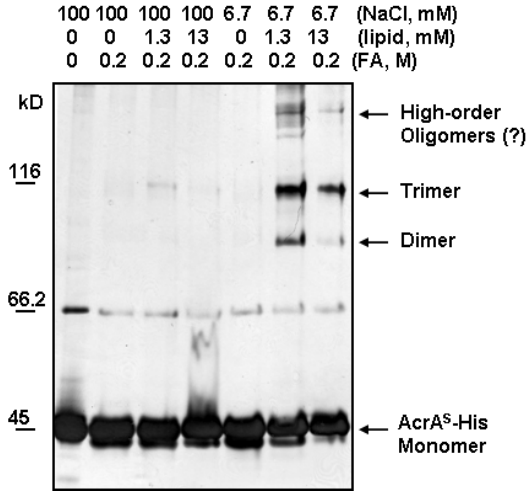

Figure 3.3 AcrA^S-His formed oligomers in the presence of *E. coli* polar lipids. (A) FA was incubated with AcrA^S-His in 20 mM Hepes (pH 7.0) buffers at various concentrations of lipids and NaCl. After termination of reactions by 0.5 M glycine, the cross-linked AcrA^S-His were resolved by SDS-PAGE (8%) and stained with silver nitrate. (B) FA cross-linking of AcrA^S-His in 20 mM Hepes (pH 6.0) buffers. Cross-linking was carried out as (A) except at pH 6.0.

NaCl for 30 minutes at room temperature. Cross-linking was terminated by addition of glycine at 0.5 M. Figure 3.2 shows the results of FA cross-linking of $AcrA^S$-His. Consistent with previous hydrodynamic studies (72), no oligomers were detected in this AcrA. The band with the mobility higher than that of the denatured monomeric $AcrA^S$-His was detected at formaldehyde concentration above 0.03M. The amount of this band increased with the concentration of formaldehyde. The entire AcrA was cross-linked at formaldehyde concentration 1M. This observation implied that significant intra-molecular cross-linking occurred. In addition, when formaldehyde concentration was above 0.3 M, there was a band shift on SDS-PAGE, suggesting that high concentration of formaldehyde interferes with electrophoresis and makes data interpretation difficult. Thus, 0.1-0.2 M formaldehyde was chosen in the subsequent experiments.

To examine the effect of *E. coli* polar lipids on the oligomerization of $AcrA^S$-His, we incubated $AcrA^S$-His with increasing concentrations of lipids before addition of formaldehyde. We did not detect $AcrA^S$-His oligomers in 20 mM Hepes-KOH (pH 7.0) buffer containing lipids and 100 mM NaCl. However, when the final concentration of NaCl was reduced to 6.7 mM, AcrA oligomers could be detected in the presence of lipids. By comparison to the molecular weight markers, we determined that both dimers and trimers of AcrA could be detected under these conditions (Figure 3.3 A). This result indicated that $AcrA^S$-His formed dimers and trimers in the presence of *E. coli* polar lipids.

As demonstrated in chapter 1, *E. coli* polar lipids phases affect the trypsin cleavage profile of $AcrA^L$-His. Here we investigated whether the micelle to vesicle transition of lipids affect oligomerization of $AcrA^S$-His. The concentration of TX was set constant at 3.2 mM. Before the FA cross-linking, purified $AcrA^L$-His was incubated with

increasing concentrations of lipids from 1.3 mM to 13 mM. The molar ratios of lipids/Trtion X-100 were 1:2.5 (lipid micelles) and 4:1 (lipid vesicles) respectively. As showed in Figure 3.3 (A), significant oligomers of $AcrA^S$-His were detected in the presence of both lipid vesicles and lipid micelles. This result suggests that lipid bilayers are not required for the oligomerization of $AcrA^S$-His.

Given that pH in the periplasm is about 6.0 (36), formaldehyde cross-linking was also carried out at pH 6.0. Results shown in Figure 3.3 (B) demonstrated that similar to pH 7.0 condition, $AcrA^S$-His formed oligomers at pH 6.0, indicating that pH does not affect the oligomerization of $AcrA^S$-His *in vitro*.

3.2 NaCl affects the oligomerization of $AcrA^S$-His *in vitro*

To analyze the effect of NaCl in more detail and further elucidate the oligomerization mechanism of $AcrA^S$-His, we performed formaldehyde cross-linking of $AcrA^S$-His at various concentrations of NaCl (Figure 3.4). When NaCl concentration increased from 6.7 mM to 60 mM, there was no significant change in $AcrA^S$-His oligomerization. However, no oligomerization was detected when NaCl concentration increased to 100 mM, indicating that high concentration of NaCl inhibits $AcrA^S$-His oligomerization. This result also suggested that the electrostatic interaction might be involved in AcrA-lipid interactions.

In summary, formaldehyde cross-linking results demonstrated that $AcrA^S$-His can form oligomers in the presence of *E. coli* polar lipids. Hence AcrA-lipid interaction promotes oligomerization of $AcrA^S$-His.

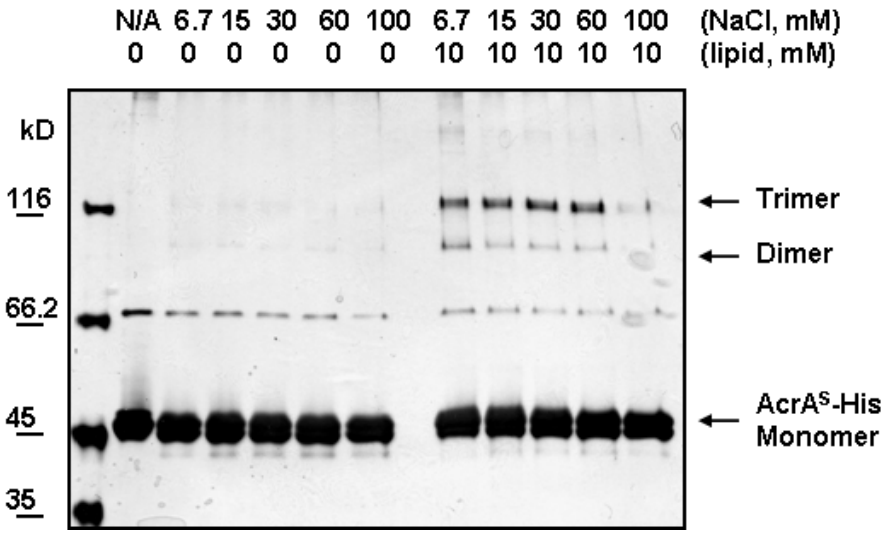

Figure 3.4 Oligomerization of AcrA^S-His is inhibited by 100 mM NaCl. AcrA^S-His was incubated with FA in 20 mM Hepes (pH 7.0) buffer containing increasing concentrations of NaCl (6.7 mM, 15 mM, 30 mM, 60 mM, and 100 mM). Reactions were terminated by addition of glycine (0.5 M). Cross-linked AcrA^S-His was resolved by SDS-PAGE (8%) and stained with silver nitrate.

3.3 Investigation of AcrA^{L}-His oligomerization by chemical cross-linking

Oligomerization of AcrA^{L}-His was investigated using formaldehyde cross-linking as described above for AcrA^{S}-His. Figure 3.5 (A) shows the results of cross-linking of AcrA^{L}-His with increasing concentrations of formaldehyde. At a formaldehyde concentration of 0.01 M, intra-molecular cross-linking was observed. As formaldehyde concentration was increased to 0.03 M, we detected oligomers (dimers and trimers) of AcrA^{L}-His. This result is different from the monomeric AcrA^{S}-His. Lipid modification at the N-terminus thus promotes the oligomerization of AcrA. Besides, we also found additional bands above trimer, indicating that there were some high-order oligomers. The time course of formaldehyde incubation with AcrA^{L}-His was also studied (Figure 3.5 B). As expected, at 0.1 M formaldehyde, AcrA^{L}-His was cross-linked into dimers and trimers even after 10 min of incubation. The amount of higher molecular weight bands increased with time of incubation. Overnight incubation with FA caused over-crosslinking of proteins without any clear bands. Once formaldehyde concentration was increased to 0.3 M and higher, the amount of high molecular weight bands increased. All these results demonstrated that AcrA^{L}-His exists as oligomers in solution.

Unlike the effect of NaCl on oligomerization of AcrA^{S}-His, AcrA^{L}-His cross-linking *in vitro* was not affected by NaCl concentrations (Figure 3.6). In addition, 3.2 mM TX did not completely dissociate the AcrA^{L}-His oligomers.

Since the lipid bilayers change the tryptic cleavage of AcrA^{L}-His (Figure 1.9), we also investigated the effect of lipids on oligomerization of AcrA^{L}-His (Figure 3.6). Cross-linking profiles did not change significantly when the lipid concentration increased from 1 mM (mixed micelle) to 10 mM (vesicles), suggesting that lipids do not affect the

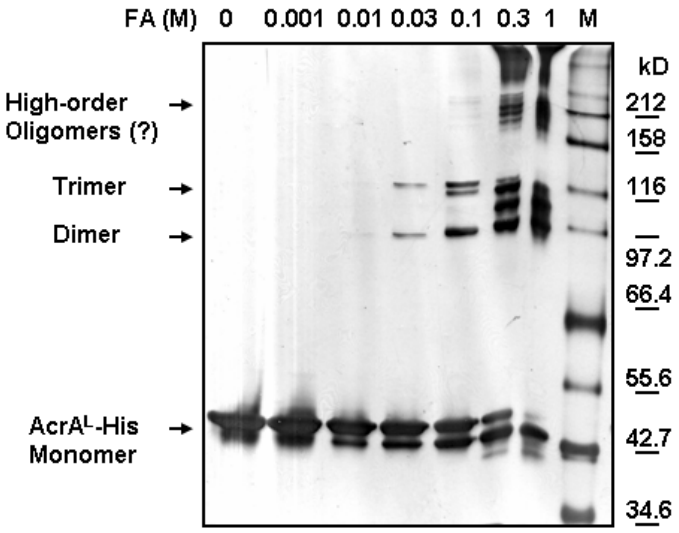

B

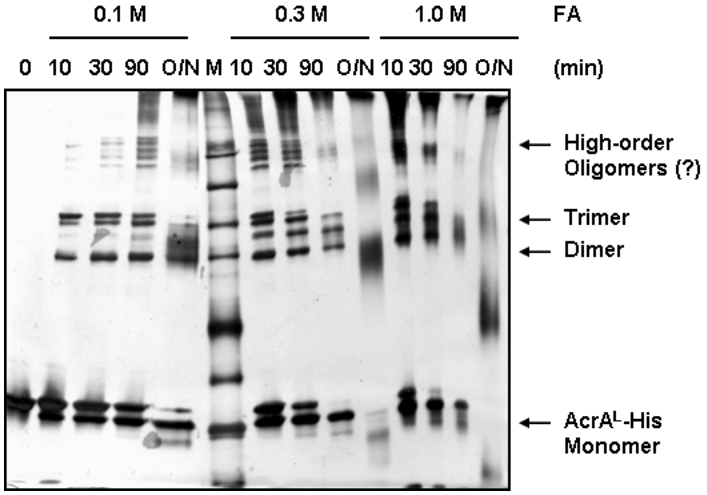

Figure 3.5 Cross-linking of AcrA^{L}-His with increasing concentrations of formaldehyde. (A) After 30 min incubation of AcrA^{L}-His with FA, cross-linking was terminated with glycine (0.5 M). The cross-linked AcrA was resolved by SDS-PAGE (8%). (B) Time course of formaldehyde cross-linking of AcrA^{L}-His *in vitro*. AcrA^{L}-His was incubated with FA (0.1 M, 0.3 M, and 1.0 M) for 10, 30, 90 minutes and overnight. Cross-linking was terminated with glycine (0.5 M). The cross-linked AcrA^{L}-His was resolved by SDS-PAGE (8%).

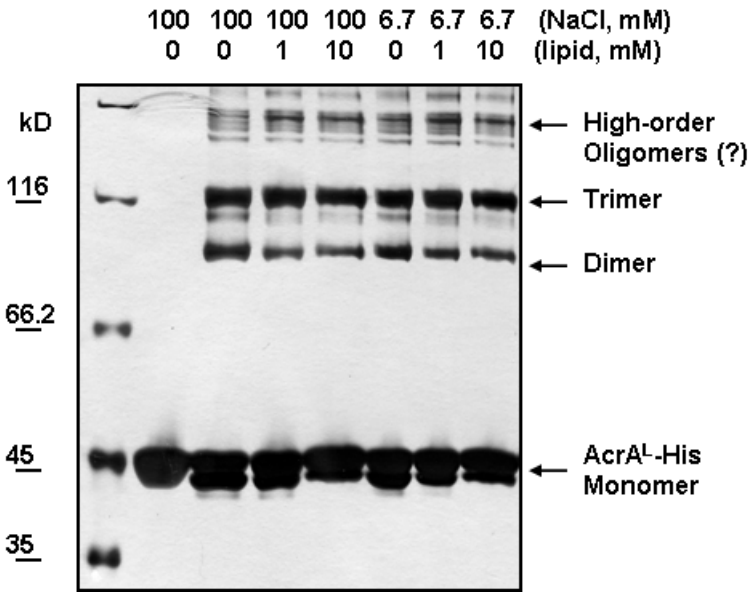

Figure 3.6 Formaldehyde cross-linking of AcrA^{L}-His *in vitro*. FA was incubated with AcrA^{L}-His for 30 min in 20 mM Hepes (pH 7.0) buffer containing 3.2 mM TX and increasing concentrations of *E. coli* polar lipids and NaCl. After termination by addition of 0.5 M glycine, cross-linked products were analyzed by 8% SDS-PAGE followed by silver nitrate staining.

oligomerization of $AcrA^{L}$-His. Taken together, our results showed that lipid modification stabilizes the association of $AcrA^{L}$-His protomers.

3.4 Characterization of $AcrA^{L}$-His oligomers by size exclusion chromatography

To characterize AcrA oligomerization, the molecular weight of AcrA was determined using size exclusion chromatography (SEC) coupled with static light scattering (SLS) and refractive index (RI) detectors. Size exclusion chromatography separates fragments on the basis of the molecular weight, whereas combination of static light scattering and refractive index allow to measure molecular weights of protein in solution.

Table 3.1 shows the calculated from a.a. composition and measured molecular weights of size markers. The measured molecular weight of amylase is about 190 kDa, slightly less than the calculated value 200 kDa. The measured molecular weight of BSA is about 72 kDa, a little larger than the theoretical value of 66.7 kDa. The measured molecular weight (30 kDa) of carbonic anhydrase is also very close to the calculated number (29 kDa). The differences between calculated and theoretical values in three proteins are within 10%.

$AcrA^{L}$-His was applied onto SEC column followed by SLS and RI in sequence. The three chromatography profiles are shown on Figure 3.7. The UV absorption showed that $AcrA^{L}$-His is separated into two peaks, peak 1 and peak 2. Combination of SLS and RI was used to calculate the molecular weights of proteins in these peaks. Table 3.2 demonstrated that peak 1 contains a protein with the molecular weight 436 ± 27 kDa, whereas peak 2 contains a protein with the molecular weight 128 ± 6 kDa. This result

Table 3.1 Molecular weights of standard markers measured by LS/SEC

Proteins	Mw(Cal.) (Dalton)	Mw* (Dalton)	Mn* (Dalton)	Mw/Mn	Mp* (Dalton)
Amy	200K	189100	188900	1.001	188400
BSA	66.7K	71720	71670	1.001	71610
CA	29K	29960	29760	1.007	31620

Note: 1. “Cal” is for calculated (from amino acid sequences) values.

2. Three molecular weight averages are defined as (35)

$$\text{Mw* (weight average molecular weight)} = \frac{\sum M_i^2 N_i}{\sum M_i N_i}$$

$$\text{Mn* (number average molecular weight)} = \frac{\sum M_i N_i}{\sum N_i}$$

Mp* is the molecular weight of the peak

In which, M_i stands for the molecular weight of ith molecules, N_i is the number of ith molecules with MW M_i.

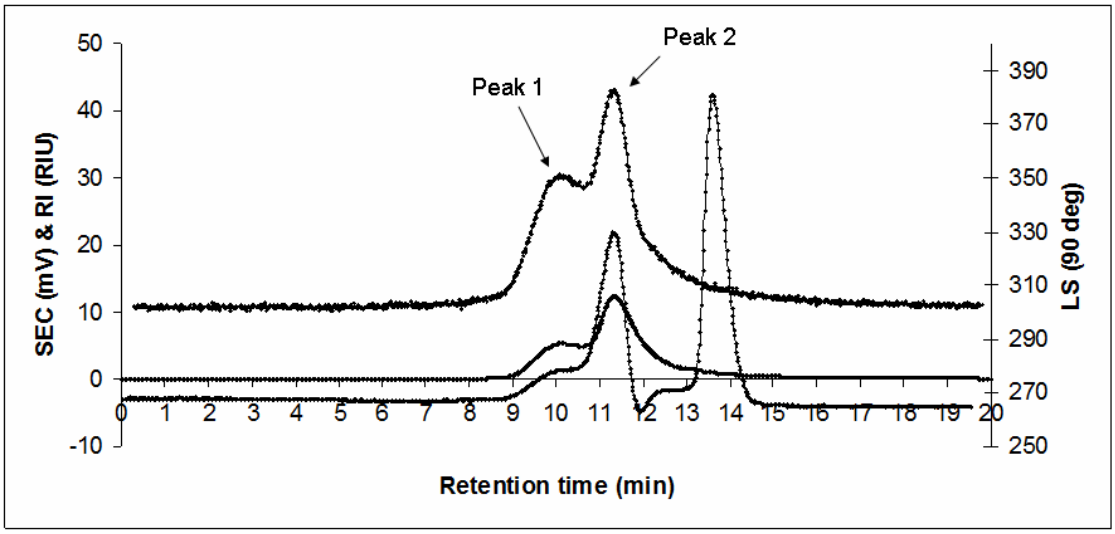

Figure 3.7 Size exclusion chromatography, refractive index profile, and light-scattering profile of $AcrA^{L}$-His. The primary Y-axis (left) is for SEC and RI, and secondary Y-axis (right) is for SLS. The flow rate of SEC was set at 1.0 ml/min. The running buffer contained 20 mM Tris-HCl (pH 7.0), NaCl 300 mM, and DDM (0.05%, w/v). 50 µg of AcrA (0.5 mg/ml) was loaded onto Diol-300 (YMC) column.

Table 3.2 Molecular weights of $AcrA^{L}$-His measured by LS/SEC

	Mw (Dalton)	Mn (Dalton)	Mw/Mn	Mp (Dalton)
peak 1				
1st Trial	407800	407600	1.001	412100
2nd Trial	461400	460700	1.001	467700
3rd Trial	439000	438900	1.000	436500
average	436067	435733	1.001	438767
peak 2				
1st Trial	128600	128600	1.000	125900
2nd Trial	120400	120300	1.000	118900
3rd Trial	136300	136200	1.000	133400
average	128433	128367	1.000	126067

A

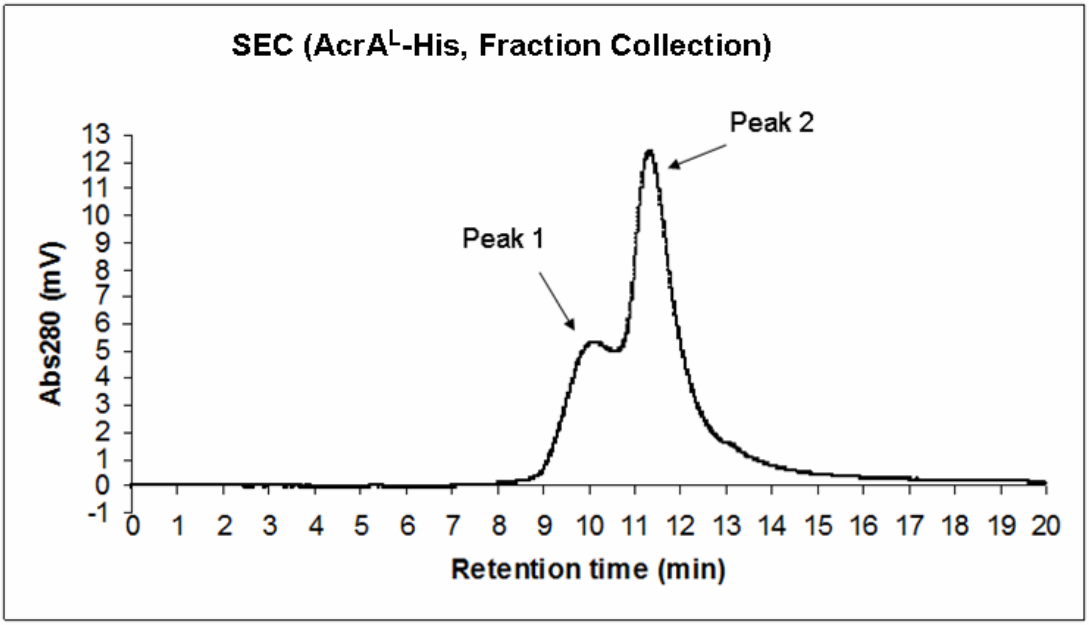

B

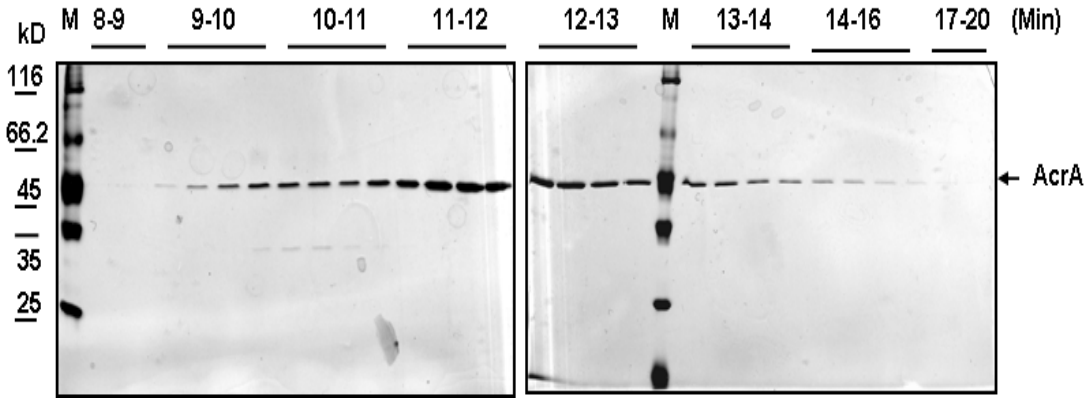

Figure 3.8 Fraction collection of AcrA^{L}-His separated by size exclusion chromatography. (A) Size exclusion chromatography of AcrA^{L}-His. Y axis is the UV absorption at 280 nm, and X-axis is time in min. The flow rate was set at 1.0 ml/min. (B) SDS-PAGE (12%) analysis of AcrA^{L}-His fractions separated by size exclusion chromatography. The numbers on the top of the SDS-PAGE are elution times in min.

suggested that peak 1 contains high-order oligomers of AcrA and peak 2 contains AcrA trimers. Previously AcrA trimers were detected in the *in vivo* DSG cross-linking experiment (74). The amount of AcrA in peak 2 (trimers) is much larger than that of peak 1 (high-order oligomers), we therefore concluded that $AcrA^{L}$-His exists as an oligomer, mostly a trimer *in vitro*.

To confirm that the peaks in the SEC profiles contain AcrA protein, fractions (0.25ml/aliquot) were collected under the same condition (Figure 3.8). The first peak was eluted from 9^{th} min to 10.5^{th} min. The amount of the second peak reached the top concentration at 11.5^{th} min and then slowly decreased until 17^{th} min. The silver staining of SDS-PAGE (12%) of the fraction collection is shown on Figure 3.8 (B). The profile suggests that the peaks in the UV absorption (280 nm) correspond to AcrA proteins rather than other contaminations. In addition, a 2-fold decrease of the loading amount of $AcrA^{L}$-His did not affect the separation results (data not shown). Moreover, similar results were obtained with two other independent AcrA preparations (data not shown). Thus, above consistent results suggest that lipidated AcrA form a stable oligomer.

3.5 Characterization of soluble forms of AcrA by size exclusion chromatography

When $AcrA^{S}$-His was applied onto SEC, we detected several small peaks from 6^{th} min to 16^{th} min (Figure 3.9, A). However, the collected fractions did not contain proteins. As shown on Figure 3.9 (B), $AcrA^{S}$-His was eluted from the column after 18^{th} min. Moreover, there were two peaks in the UV (280 nm) absorption profile. Since Diol-300 column has a specific separation range (10 kDa to several 100 kDa) and volume (15 ml), samples eluted at 15 min (flow rate: 1 ml/min) represent the included volume of the

column. The molecular weight of AcrA monomer is 41 kDa, which is within the separation range of Diol-300 column. We concluded that the abnormal chromatography of non-lipidated $AcrA^{S}$-His is likely due to non-specific binding of $AcrA^{S}$-His to column matrix.

Since the Diol-300 column could not be used to characterize the purified $AcrA^{S}$-His which is translocated into the periplasm with the aid of the cleavable signal peptide, we used the soluble form of mature AcrA-His. This soluble form of AcrA-His ($AcrA^{C}$-His, superscript C is for cytoplasmic) does not contain a signal peptide and is expressed in the cytoplasm. $AcrA^{C}$-His was purified as described previously (40). As shown on Figure 3.10, This $AcrA^{C}$-His was eluted at 13^{th} min. The MW analysis showed that this $AcrA^{C}$-His exists as a monomer (41 kDa) in solution.

Together, our FA cross-linking experiment showed the monomeric state of purified $AcrA^{S}$-His in solution. This result is in agreement with the hydrodynamic study (72). However, this $AcrA^{S}$-His can form oligomers in the presence of *E. coli* polar lipids, suggesting that the interaction between AcrA and lipids is one of the driving forces of oligomerization of $AcrA^{S}$-His. On the other hand, our study, especially the SEC result, demonstrated that $AcrA^{L}$-His exists as an oligomer, mostly a trimer, *in vitro*. This result indicates that lipid modification at the N-terminal Cys residue stabilizes the $AcrA^{L}$-His oligomers. We concluded that AcrA functions as a trimer inside the cell.

A

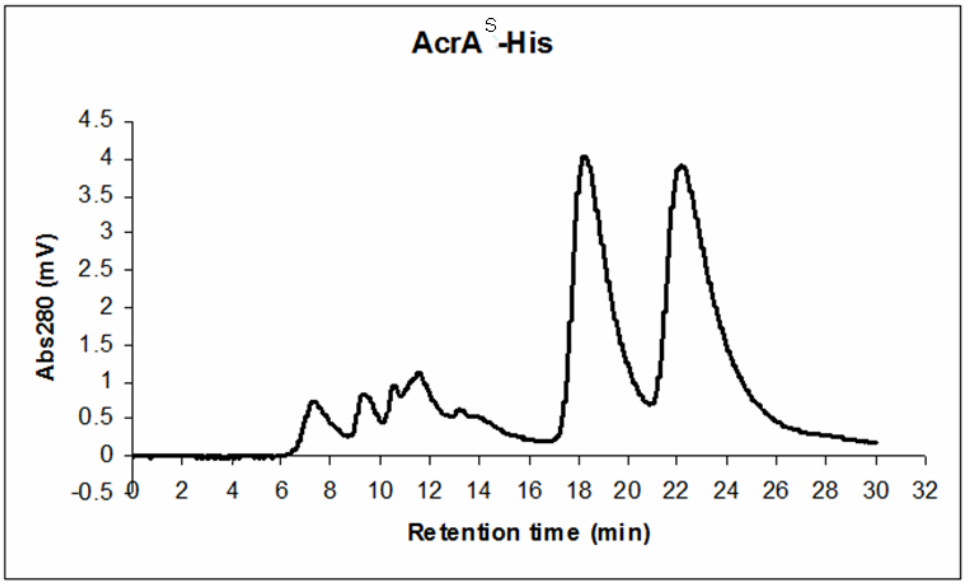

B

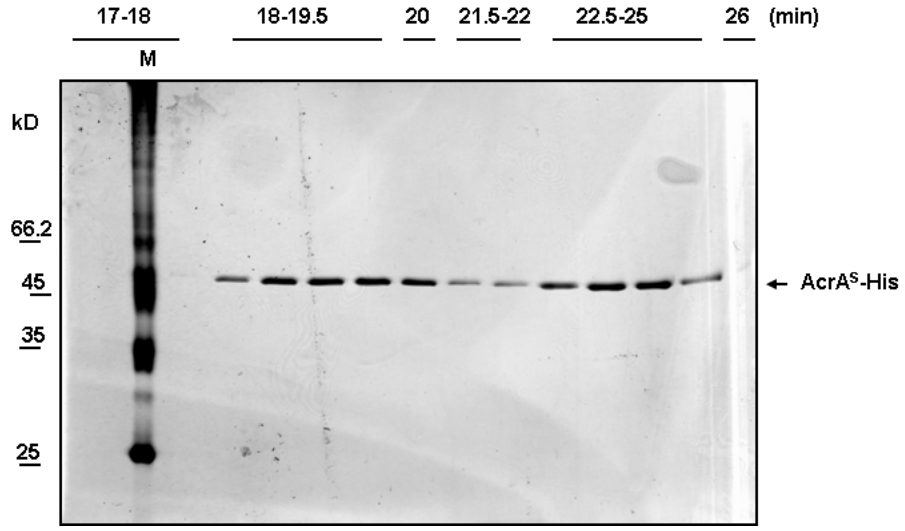

Figure 3.9 Fraction collection of AcrA^{S}-His separated by size exclusion chromatography. (A) Size exclusion chromatography of AcrA^{S}-His. Y axis is the UV absorption at 280 nm, and X-axis is time in min. The flow rate was set at 1.0 ml/min. (B) SDS-PAGE (12%) analysis of AcrA^{S}-His separated by size exclusion chromatography. The numbers on the top of the SDS-PAGE are elution times in min.

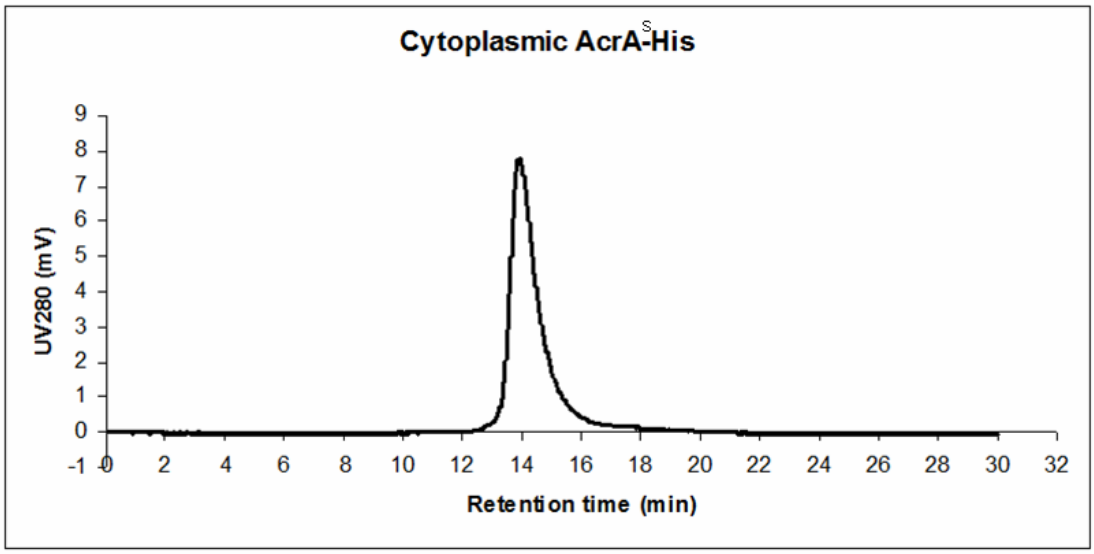

Figure 3.10 Size exclusion chromatography of purified cytoplasmic AcrA^{S}. Y axis is the UV absorption at 280 nm, and X-axis is time in min. The flow rate was set at 1.0 ml/min.

Chapter 4 Discussion

4.1 Lipid modification and lipid bilayer association affect the proteolytic accessibility of AcrA

Using limited proteolysis, we demonstrated that lipid modification and association of $AcrA^{L}$-His with lipid bilayers affect the accessibility of AcrA to proteases. In particular, different tryptic digestion profiles between $AcrA^{S}$-His and $AcrA^{L}$-His suggested that the lipid modification affects the accessibility of AcrA to trypsin. For example, R315 in $AcrA^{L}$-His is less accessible than that of $AcrA^{S}$-His. In addition, *E. coli* polar lipid vesicles cause changes of the accessibility of $AcrA^{L}$-His to trypsin.

AcrA is cleaved by trypsin into several fragments and the cleavage sites are located in the N- and C-terminal domains of AcrA which are folded together into the MP domain (Figure 1.6). The N-terminal strand directly passes through this MP domain, whereas the C-terminal residues form an up-down-up β-sheet. Structural model of the MP domain in AcrA shows that the cleavage site T47 is located on the loop between β-1 and β-2 strands (Figure 1.6). Cleavage sites R315 and K346 are positioned on the strand β-16 and the loop between β-18 and β-19 strands respectively. Another cleavage site K374 is located at the end of the MP domain and is exposed to external medium. During the tryptic digestion of $AcrA^{S}$-His and $AcrA^{L}$-His, the 32.1 kDa fragment (T47-K346) and 28.9 kDa fragment (T47-R315) are accumulated. However, the time course showed that these two fragments are formed with different kinetics depending on the presence of lipid modification. Compared to $AcrA^{S}$-His, the accumulation of the 32.1 kDa fragment (T47-K346) and the slower formation of the 28.9 kDa fragment (T47-R315) in $AcrA^{L}$-His

indicated that lipid moiety at the N-terminus of AcrA protects the residue R315 from trypsin cleavage, which results in the rapid accumulation of the 32.1 kDa fragment (T47-K346).

When $AcrA^{L}$-His binds to lipid bilayers, some amount of intact $AcrA^{L}$-His are not cleaved by trypsin. This indicates that the MP domain of AcrA is protected by lipid bilayers. In the periplasm the MP domain is proposed to be adjacent to the inner membrane. The association of AcrA, especially the MP domain, with lipid bilayers inhibits the access of these sites to trypsin. Thus the protection of the MP domain by lipid bilayers causes this trypsin-resistance.

In addition, the decrease in the amounts of the 32.1 kDa fragment (T47-K346) and increase of the 28.9 kDa fragment (T47-R315) in $AcrA^{L}$-His are coupled with the transition from lipid micelles to vesicles. This result suggests that R315 in $AcrA^{L}$-His becomes more accessible and/or flexible once lipid bilayers are introduced. One explanation is that association of $AcrA^{L}$-His with lipid bilayers induces the conformational changes of residue R315 on the β-16 strand of the MP domain, causing more exposure of R315 to external medium. The other interpretation is the steric hindrance of the N-terminal lipid modification. In this case, cleavage site R315, on the convex face of the MP domain, is masked by lipid moiety/modification in solution. Association of $AcrA^{L}$-His with lipid bilayers results in the insertion of the N-terminal lipid moiety into lipid bilayers, by which the mask effect of lipid moiety on R315 is decreased and thus R315 is more liable to be cleaved by trypsin.

Since the 32.1 kDa fragment (T47-K346) is the intermediate product during the trypsin proteolysis, the decreased amount of the 32.1 kDa fragment (T47-K346) in the

presence of lipid bilayers can be explained by the faster further cleavage to produce the stable 28.9 kDa fragment (T47-R315). Another interpretation is that the accessibility of K346 on the flexible loop (between β-18 and β-19 strands) of the MP domain is decreased due to the structural variations induced by lipid bilayers. Although association of $AcrA^{L}$-His with lipid bilayers affects the trypsin accessibility at R315 and K346, other experiments are needed to further investigate the effect of the lipid modification interference on the tryptic digestion of $AcrA^{L}$-His.

In conclusion, our results demonstrate that lipid modification results in the decrease of the accessibility of R315 to proteases, possibly due to the protection by the lipid moiety or structural changes in the β-16 strand of the MP domain. Association of $AcrA^{L}$-His with lipid bilayers increases the accessibility of R315 by decreasing the steric hindrance or conformational variations. On the other hand, the decrease of the 32.1 kDa fragment (T47-K346) in the presence of lipid bilayers indicates that this fragment is rapidly cleaved to form the stable 28.9 kDa core (T47-R315) or the accessibility of the cleavage site K346, located on the flexible loop of the MP domain, is decreased due to steric hindrance of lipid bilayers or the structural changes in AcrA.

4.2 The MP domain of AcrA is protected in the AcrAB-TolC complex

AcrA-AcrB-TolC is a stable multidrug efflux complex and the substrates do not affect the complex assembly *in vivo* (66, 67). Several lines of evidence have shown that, as a periplasmic adaptor protein, AcrA bridges AcrB and TolC to form the stable complex (32, 62, 67). Using the *in vivo* cross-linking and the structural modeling, Symmons et al proposed that the lipoyl domain, β-barrel, and MP domain of AcrA associate with AcrB,

whereas the α-helical haripin of AcrA is involved in the interaction with TolC (62). Our *in vitro* proteolysis experiments showed that the MP domain of the purified AcrA is flexible and rapidly cleaved by trypsin. Therefore we examined the tryptic profiles of AcrA *in vivo* in the presence and absence of AcrB and TolC. The overexpressed from plasmid AcrA was cleaved *in vivo* into the same set of fragments as *in vitro*. However, the proteolytic profiles of chromosomal AcrA depended on the genetic background of *E. coli* strains. Our result showed that the deletion of any of the two components AcrB or TolC results in the tryptic cleavage of AcrA, which is different from that in the functional tripartite complex. In particular, the 28.9 kDa fragment (T47-R315) was not detected but the 26.5 kDa fragment (T47-R294 or T47-R296) was accumulated in the AG100 (WT) cells in which the functional tripartite complex is formed. In contrast, both fragments were formed and then rapidly cleaved in the cells AG102MB and ZK796, in which AcrA associates with either TolC or AcrB, respectively (Figure 2.2). On the other hand, expression of the respective missing component AcrB or TolC from plasmids introduced into AG102MB (ΔAcrB) or ZK796 (ΔTolC) cells, correspondingly, restored the tryptic cleavage profile of AcrA as in the tripartite complex. This result suggests that the MP domain of AcrA is protected when the functional multidrug efflux complex AcrAB-TolC is assembled.

Furthermore, the lack of the 28.9 kDa fragment (T47-R315) in AG100 cells (WT) can be explained by the protection of R315. In the structural modeling of AcrA, R315 is located on the β-16 strand. Thus, the assembly of the tripartite complex AcrAB-TolC causes the change of accessibility of the β-16 strand, at least the burial of the residue R315. This residue is adjacent to the residue D320 which was reported to be directly

cross-linked to AcrB (62). On the other hand, the assembly of the tripartite complex also prevents the 26.5 kDa fragment (T47-R294 or T47-R296) from further digestion. Moreover, the 36.9 kDa fragment (Q29-K374) is accumulated in AG100 (WT) but further cleaved in AG102MB (ΔAcrB) and ZK796 (ΔTolC). Our structural model of AcrA including the MP domain shows that the cleavage site (R294 or R296) is located at the end of α-β-barrel domain, which is linked to the MP domain by a short β-linker, whereas another cleavage site K374 terminates the MP domain. Therefore the MP domain is folded as an integrated domain and protected in the functional tripartite complex.

In the docking model of the AcrAB-TolC complex (62), these cleavage sites in AcrA (R294/R296, R315, and K374) are adjacent to the AcrA-AcrB interfaces (PC1 and PN2 domains in AcrB). It is likely that the functional assembly of the tripartite complex rather than bipartite complexes (AcrA-AcrB and AcrA-TolC) *in vivo* induces the folding changes in the MP domain of AcrA, which protect this domain from trypsin attack.

Furthermore, the functional study shows that the MP domain is essential for the drug efflux in *E. coli* (12). Dr. Yoichi Yamada performed the site-specific mutagenesis on the conserved twelve residues in the MP domain. The MIC data showed that one AcrA mutant, G363C, significantly impaired the drug efflux activity by AcrAB-TolC pump. Although the reason for the functional defect in G363C is still unclear, it is likely that G363C causes the structural defect in the assembled tripartite complex. The failure of the complex assembly due to this substitution is supported by the tryptic cleavage profile of this mutant which was similar to that of overproduced AcrA-His in the absence of AcrB. Indeed, previously Krishnamoorthy et al demonstrated that the misfit between components of the tripartite complex impaired the drug efflux function (29).

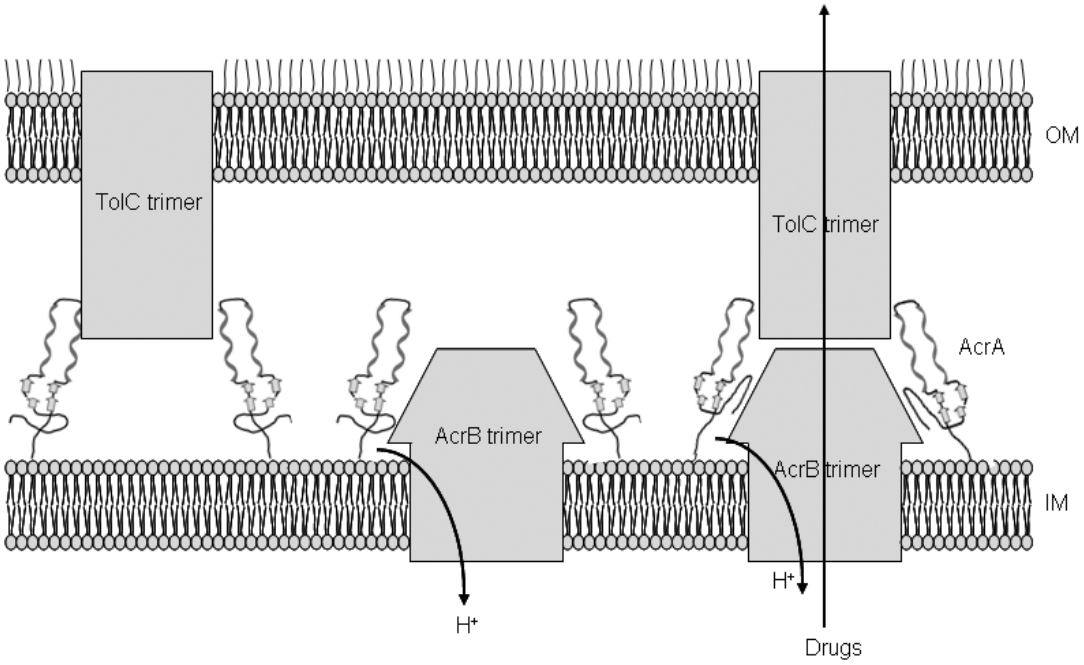

Figure 4.1 Schematic representation of the mechanism of assembly of AcrAB-TolC complex. The lipoyl and β-barrel domains of AcrA interact with AcrB, whereas the α-helical hairpin docks against TolC. In the bi-partite complexes, the MP domain is unstructured and readily cleaved by trypsin. However, upon assembly of the functional tri-partite AcrAB-TolC complex this domain is trypsin-resistant.

Taken together, above results suggest that the MP domain of AcrA is required for the functional assembly of AcrAB-TolC complex. Moreover, the lack of the 28.9 kDa fragment (T47-R315) and the accumulation of the 36.9 kDa (Q29-K374) and 26.5 kDa (T47-R294/R296) fragments in the trypsin digestion of AcrA assembled into the functional complex indicates that, compared to either AcrA-AcrB or AcrA-TolC bipartite complexes, the MP domain of AcrA is structured and resists the further digestion in the functional tripartite complex (Figure 4.1).

4.3 AcrA forms oligomers *in vitro*

Oligomerization of AcrA is a controversial issue. Monomer, dimer, trimer, and dimer of dimers have been proposed in different studies (2, 40, 72, 74). In particular, $AcrA^{S}$-His is a monomer in solution, whereas it forms oligomers *in vivo* (74). Using chemical cross-linking, we found that monomeric $AcrA^{S}$-His forms oligomers in the presence of *E. coli* polar lipids. Thus AcrA-lipid interaction promotes $AcrA^{S}$-His oligomerization. This also provides the interpretation for the purified $AcrA^{S}$-His existing as a monomer in solution but forming oligomers *in vivo* (72, 74). It should be noted that low concentration of NaCl (less than 100 mM) is also necessary for $AcrA^{S}$-His oligomerization in solution. Indeed, the *in vitro* formed $AcrA^{S}$-His oligomers dissociated into monomers again when NaCl concentration was increased to 100 mM, which explains why $AcrA^{S}$-His exist as monomers in solution containing high concentrations of NaCl (more than 100 mM). This result also suggests that other factors are required for the oligomerization of $AcrA^{S}$-His *in vivo*.

Lipidated $AcrA^{L}$-His, on the other hand, was reported to form oligomers *in vivo*

(74). Interestingly, we found that unlike the monomeric $AcrA^{S}$-His, $AcrA^{L}$-His exists as an oligomer in solution. This result strongly indicates that lipid modification stabilizes the AcrA oligomers *in vitro*. Unlike the weak interaction among $AcrA^{S}$-His protomers, $AcrA^{L}$-His protomers form stable oligomers, even in the presence of mild detergents such as TX and DDM. The proteolytic profile of the oligomeric $AcrA^{L}$-His is similar to that of monomeric $AcrA^{S}$-His. This result suggests that oligomerization does not protect the MP domain of AcrA from trypsin attack. This in turn indicates that oligomerization of AcrA involves other domains of AcrA. In the crystal structure of AcrA core, there are intensive contacts involving the α-helical hairpin, lipoyl domain and α-β-barrel domain in the parallel association of AcrA dimers (40).

In the SEC experiment, we detected and identified two forms of AcrA oligomers. The major peak contains AcrA trimers, whereas the second peak contains high-order oligomers in which there are about 10-12 AcrA protomers. The amount of AcrA trimers is much larger than that of the high-order oligomers as shown in Figure 3.7. This result is consistent with the previous *in vivo* cross-linking study, which showed that AcrA trimers is the predominant form of AcrA *in vivo* (74). The high-order AcrA oligomers are likely to be protein aggregates. We noticed that the amount of AcrA in this peak increases with time.

On the other hand, dimers of AcrA were detected in our formaldehyde cross-linking experiments (Figure 3.3) and the previous DSG cross-linking study (74). Since the chemical cross-linking is time dependent, the dimers of AcrA possibly represent intermediate products of the reaction.

In the crystal structure, AcrA is a dimer of dimer. However, this structure contains

only the core of AcrA (45-312 a.a). This dimer of dimer arrangement possibly does not reflect the oligomerization of the whole AcrA protein. Indeed, MexA, AcrA homolog in *P. aeruginosa*, was crystallized as a whole protein molecule (21, 62). MexA protomers associate to form unusual six- and seven-membered superhelical rings in a head-to-head manner. In this crystal structure, the MP domain was not structured in most MexA protomers, but in some protomers (for example, B and F chain) was crystallized and resolved (62). Inter-molecular hydrogen-bond network is involved in the formation of the wide part of the funnel structure, whereas the narrow (central) part consists of the conventional coiled-coils (21).

Taken together, our study shows that lipid modification and AcrA-lipid are involved in the oligomerization of AcrA. Our results, especially SEC data, suggest that AcrA forms oligomers, mostly trimers. Although we have found that lipid modification contributes to the oligomerization of AcrA, we still don't know how lipid modification at the N-terminal Cys residue can affect the oligomerization of AcrA. One possibility is that lipid modification stabilizes the MP domain, which is required for the oligomerization of AcrA. In addition, it remains unclear: what is the oligomeric number of AcrA *in vivo*? How do these AcrA oligomers form and cooperate with AcrB and TolC to assemble a functional tripartite complex? Answering these questions in the future will further improve our understanding of the molecular mechanism of AcrAB-TolC complex assembly.

References

1. **Akama, H., T. Matsuura, S. Kashiwagi, H. Yoneyama, S. Narita, T. Tsukihara, A. Nakagawa, and T. Nakae.** 2004. Crystal structure of the membrane fusion protein, MexA, of the multidrug transporter in Pseudomonas aeruginosa. J Biol Chem **279:**25939-42.
2. **Avila-Sakar, A. J., S. Misaghi, E. M. Wilson-Kubalek, K. H. Downing, H. Zgurskaya, H. Nikaido, and E. Nogales.** 2001. Lipid-layer crystallization and preliminary three-dimensional structural analysis of AcrA, the periplasmic component of a bacterial multidrug efflux pump. J Struct Biol **136:**81-8.
3. **Barth, H. G., C. Jackson, and B. E. Boyes.** 1994. Size Exclusion Chromatography. Analytical Chemistry **66:**595-620.
4. **Borges-Walmsley, M. I., J. Beauchamp, S. M. Kelly, K. Jumel, D. Candlish, S. E. Harding, N. C. Price, and A. R. Walmsley.** 2003. Identification of oligomerization and drug-binding domains of the membrane fusion protein EmrA. J Biol Chem **278:**12903-12.
5. **Buchanan, S. K., B. S. Smith, L. Venkatramani, D. Xia, L. Esser, M. Palnitkar, R. Chakraborty, D. van der Helm, and J. Deisenhofer.** 1999. Crystal structure of the outer membrane active transporter FepA from Escherichia coli. Nat Struct Biol **6:**56-63.
6. **Elkins, C. A., and K. E. Beenken.** 2005. Modeling the tripartite drug efflux pump archetype: Structural and functional studies of the macromolecular constituents reveal more than their names imply. Journal of Chemotherapy **17:**581-592.
7. **Elkins, C. A., and H. Nikaido.** 2003. Chimeric analysis of AcrA function reveals the importance of its C-terminal domain in its interaction with the AcrB multidrug efflux pump. J Bacteriol **185:**5349-56.
8. **Ferguson, A. D., E. Hofmann, J. W. Coulton, K. Diederichs, and W. Welte.** 1998. Siderophore-mediated iron transport: crystal structure of FhuA with bound lipopolysaccharide. Science **282:**2215-20.
9. **Fernandez-Recio, J., F. Walas, L. Federici, J. Venkatesh Pratap, V. N. Bavro, R. N. Miguel, K. Mizuguchi, and B. Luisi.** 2004. A model of a transmembrane drug-efflux pump from Gram-negative bacteria. FEBS Lett **578:**5-9.
10. **Fontana, A., P. P. de Laureto, B. Spolaore, E. Frare, P. Picotti, and M. Zambonin.** 2004. Probing protein structure by limited proteolysis. Acta Biochim Pol **51:**299-321.
11. **Fralick, J. A.** 1996. Evidence that TolC is required for functioning of the Mar/AcrAB efflux pump of Escherichia coli. J Bacteriol **178:**5803-5.
12. **Ge, Q., Y. Yamada, and H. Zgurskaya.** 2009. The C-terminal domain of AcrA is essential for the assembly and function of the multidrug efflux pump AcrAB-TolC. J Bacteriol **191:**4365-71.
13. **George, A. M., and S. B. Levy.** 1983. Amplifiable resistance to tetracycline, chloramphenicol, and other antibiotics in Escherichia coli: involvement of a non-plasmid-determined efflux of tetracycline. J Bacteriol **155:**531-40.
14. **Gerken, H., and R. Misra.** 2004. Genetic evidence for functional interactions between TolC and AcrA proteins of a major antibiotic efflux pump of Escherichia

coli. Mol Microbiol **54:**620-31.
15. **Gilson, L., H. K. Mahanty, and R. Kolter.** 1990. Genetic analysis of an MDR-like export system: the secretion of colicin V. Embo J **9:**3875-84.
16. **Green, E. A., S. Pietrokovski, S. Henikoff, P. Bork, T. Attwood, L. Hood, and A. Bairoch.** 1997. Genome maps 8. Building gene families. Wall chart. Science **278:**615-30.
17. **Guan, L., and T. Nakae.** 2001. Identification of essential charged residues in transmembrane segments of the multidrug transporter MexB of Pseudomonas aeruginosa. J Bacteriol **183:**1734-9.
18. **Gupta, S. D., and H. C. Wu.** 1991. Identification and subcellular localization of apolipoprotein N-acyltransferase in Escherichia coli. FEMS Microbiol Lett **62:**37-41.
19. **Hantke, K., and V. Braun.** 1973. Covalent binding of lipid to protein. Diglyceride and amide-linked fatty acid at the N-terminal end of the murein-lipoprotein of the Escherichia coli outer membrane. Eur J Biochem **34:**284-96.
20. **Helmut Blum, Hildburg Beier, and Hans J. Gross.** 1987. Improved silver staining of plant proteins, RNA and DNA in polyacrylamide gels. Electrophoresis **8:**93-99.
21. **Higgins, M. K., E. Bokma, E. Koronakis, C. Hughes, and V. Koronakis.** 2004. Structure of the periplasmic component of a bacterial drug efflux pump. Proc Natl Acad Sci U S A **101:**9994-9.
22. **Hubbard, S. J.** 1998. The structural aspects of limited proteolysis of native proteins. Biochim Biophys Acta **1382:**191-206.
23. **Husain, F., M. Humbard, and R. Misra.** 2004. Interaction between the TolC and AcrA proteins of a multidrug efflux system of Escherichia coli. J Bacteriol **186:**8533-6.
24. **Hussain, M., S. Ichihara, and S. Mizushima.** 1980. Accumulation of glyceride-containing precursor of the outer membrane lipoprotein in the cytoplasmic membrane of Escherichia coli treated with globomycin. J Biol Chem **255:**3707-12.
25. **Ip, H., K. Stratton, H. Zgurskaya, and J. Liu.** 2003. pH-induced conformational changes of AcrA, the membrane fusion protein of Escherichia coli multidrug efflux system. J Biol Chem **278:**50474-82.
26. **Johnson, J. M., and G. M. Church.** 1999. Alignment and structure prediction of divergent protein families: periplasmic and outer membrane proteins of bacterial efflux pumps. J Mol Biol **287:**695-715.
27. **Jonsson, A. P.** 2001. Mass spectrometry for protein and peptide characterisation. Cell Mol Life Sci **58:**868-84.
28. **Koronakis, V., A. Sharff, E. Koronakis, B. Luisi, and C. Hughes.** 2000. Crystal structure of the bacterial membrane protein TolC central to multidrug efflux and protein export. Nature **405:**914-9.
29. **Krishnamoorthy, G., E. B. Tikhonova, and H. I. Zgurskaya.** 2008. Fitting periplasmic membrane fusion proteins to inner membrane transporters: mutations that enable Escherichia coli AcrA to function with Pseudomonas aeruginosa MexB. J Bacteriol **190:**691-8.
30. **Lai, S. H., W. M. Philbrick, and H. C. Wu.** 1980. Acyl moieties in phospholipids are the precursors for the fatty acids in murein lipoprotein of

Escherichia coli. J Biol Chem **255:**5384-7.
31. **Levy, S. B.** 1992. Active efflux mechanisms for antimicrobial resistance. Antimicrob Agents Chemother **36:**695-703.
32. **Lobedanz, S., E. Bokma, M. F. Symmons, E. Koronakis, C. Hughes, and V. Koronakis.** 2007. A periplasmic coiled-coil interface underlying TolC recruitment and the assembly of bacterial drug efflux pumps. Proc Natl Acad Sci U S A **104:**4612-7.
33. **Locher, K. P., B. Rees, R. Koebnik, A. Mitschler, L. Moulinier, J. P. Rosenbusch, and D. Moras.** 1998. Transmembrane signaling across the ligand-gated FhuA receptor: crystal structures of free and ferrichrome-bound states reveal allosteric changes. Cell **95:**771-8.
34. **Lopez, O., A. de la Maza, L. Coderch, C. Lopez-Iglesias, E. Wehrli, and J. L. Parra.** 1998. Direct formation of mixed micelles in the solubilization of phospholipid liposomes by Triton X-100. FEBS Lett **426:**314-8.
35. **Lovell, R. J. Y. a. P. A.** 1991. Introduction to Polymers.
36. **Lynch, C., P. Courvalin, and H. Nikaido.** 1997. Active efflux of antimicrobial agents in wild-type strains of enterococci. Antimicrob Agents Chemother **41:**869-71.
37. **Ma, D., D. N. Cook, M. Alberti, N. G. Pon, H. Nikaido, and J. E. Hearst.** 1995. Genes acrA and acrB encode a stress-induced efflux system of Escherichia coli. Mol Microbiol **16:**45-55.
38. **Ma, D., D. N. Cook, M. Alberti, N. G. Pon, H. Nikaido, and J. E. Hearst.** 1993. Molecular cloning and characterization of acrA and acrE genes of Escherichia coli. J Bacteriol **175:**6299-313.
39. **Mazzariol, A., Y. Tokue, T. M. Kanegawa, G. Cornaglia, and H. Nikaido.** 2000. High-level fluoroquinolone-resistant clinical isolates of Escherichia coli overproduce multidrug efflux protein AcrA. Antimicrob Agents Chemother **44:**3441-3.
40. **Mikolosko, J., K. Bobyk, H. I. Zgurskaya, and P. Ghosh.** 2006. Conformational flexibility in the multidrug efflux system protein AcrA. Structure **14:**577-87.
41. **Miyamae, S., O. Ueda, F. Yoshimura, J. Hwang, Y. Tanaka, and H. Nikaido.** 2001. A MATE family multidrug efflux transporter pumps out fluoroquinolones in Bacteroides thetaiotaomicron. Antimicrob Agents Chemother **45:**3341-6.
42. **Murakami, S., R. Nakashima, E. Yamashita, T. Matsumoto, and A. Yamaguchi.** 2006. Crystal structures of a multidrug transporter reveal a functionally rotating mechanism. Nature **443:**173-9.
43. **Murakami, S., R. Nakashima, E. Yamashita, and A. Yamaguchi.** 2002. Crystal structure of bacterial multidrug efflux transporter AcrB. Nature **419:**587-93.
44. **Neu, H. C., and L. A. Heppel.** 1965. The release of enzymes from Escherichia coli by osmotic shock and during the formation of spheroplasts. J Biol Chem **240:**3685-92.
45. **Nikaido, H.** 1998. Antibiotic resistance caused by gram-negative multidrug efflux pumps. Clin Infect Dis **27 Suppl 1:**S32-41.
46. **Nikaido, H.** 1998. The role of outer membrane and efflux pumps in the resistance of gram-negative bacteria. Can we improve drug access? Drug Resist Updat **1:**93-

8.
47. **Nishino, K., and A. Yamaguchi.** 2001. Analysis of a complete library of putative drug transporter genes in Escherichia coli. J Bacteriol **183:**5803-12.
48. **Okusu, H., D. Ma, and H. Nikaido.** 1996. AcrAB efflux pump plays a major role in the antibiotic resistance phenotype of Escherichia coli multiple-antibiotic-resistance (Mar) mutants. J Bacteriol **178:**306-8.
49. **Pautsch, A., and G. E. Schulz.** 1998. Structure of the outer membrane protein A transmembrane domain. Nat Struct Biol **5:**1013-7.
50. **Piao, S., Y. Xu, and N. C. Ha.** 2008. Crystallization and preliminary X-ray crystallographic analysis of MacA from Actinobacillus actinomycetemcomitans. Acta Crystallogr Sect F Struct Biol Cryst Commun **64:**391-3.
51. **Piddock, L. J.** 2006. Multidrug-resistance efflux pumps - not just for resistance. Nat Rev Microbiol **4:**629-36.
52. **Poole, K.** 2001. Multidrug resistance in Gram-negative bacteria. Curr Opin Microbiol **4:**500-8.
53. **Putman, M., H. W. van Veen, and W. N. Konings.** 2000. Molecular properties of bacterial multidrug transporters. Microbiol Mol Biol Rev **64:**672-93.
54. **Rigaud, J. L.** 2002. Membrane proteins: functional and structural studies using reconstituted proteoliposomes and 2-D crystals. Braz J Med Biol Res **35:**753-66.
55. **Sankaran, K., S. D. Gupta, and H. C. Wu.** 1995. Modification of bacterial lipoproteins. Methods Enzymol **250:**683-97.
56. **Sankaran, K., and H. C. Wu.** 1994. Lipid modification of bacterial prolipoprotein. Transfer of diacylglyceryl moiety from phosphatidylglycerol. J Biol Chem **269:**19701-6.
57. **Schulz, G. E.** 1996. Porins: general to specific, native to engineered passive pores. Curr Opin Struct Biol **6:**485-90.
58. **Seeger, M. A., A. Schiefner, T. Eicher, F. Verrey, K. Diederichs, and K. M. Pos.** 2006. Structural asymmetry of AcrB trimer suggests a peristaltic pump mechanism. Science **313:**1295-8.
59. **Stegmeier, J. F., G. Polleichtner, N. Brandes, C. Hotz, and C. Andersen.** 2006. Importance of the adaptor (membrane fusion) protein hairpin domain for the functionality of multidrug efflux pumps. Biochemistry **45:**10303-12.
60. **Stewart, J. B., and M. A. Hermodson.** 2003. Topology of RbsC, the membrane component of the Escherichia coli ribose transporter. J Bacteriol **185:**5234-9.
61. **Sutherland, B. W., J. Toews, and J. Kast.** 2008. Utility of formaldehyde cross-linking and mass spectrometry in the study of protein-protein interactions. J Mass Spectrom **43:**699-715.
62. **Symmons, M. F., E. Bokma, E. Koronakis, C. Hughes, and V. Koronakis.** 2009. The assembled structure of a complete tripartite bacterial multidrug efflux pump. Proc Natl Acad Sci U S A.
63. **Tamura, N., S. Murakami, Y. Oyama, M. Ishiguro, and A. Yamaguchi.** 2005. Direct interaction of multidrug efflux transporter AcrB and outer membrane channel TolC detected via site-directed disulfide cross-linking. Biochemistry **44:**11115-21.
64. **Thanabalu, T., E. Koronakis, C. Hughes, and V. Koronakis.** 1998. Substrate-induced assembly of a contiguous channel for protein export from E.coli:

reversible bridging of an inner-membrane translocase to an outer membrane exit pore. EMBO J **17:**6487-96.

65. **Tikhonova, E. B., V. K. Devroy, S. Y. Lau, and H. I. Zgurskaya.** 2007. Reconstitution of the Escherichia coli macrolide transporter: the periplasmic membrane fusion protein MacA stimulates the ATPase activity of MacB. Mol Microbiol **63:**895-910.
66. **Tikhonova, E. B., and H. I. Zgurskaya.** 2004. AcrA, AcrB, and TolC of Escherichia coli Form a Stable Intermembrane Multidrug Efflux Complex. J Biol Chem **279:**32116-24.
67. **Touze, T., J. Eswaran, E. Bokma, E. Koronakis, C. Hughes, and V. Koronakis.** 2004. Interactions underlying assembly of the Escherichia coli AcrAB-TolC multidrug efflux system. Mol Microbiol **53:**697-706.
68. **Vaccaro, L., V. Koronakis, and M. S. Sansom.** 2006. Flexibility in a drug transport accessory protein: molecular dynamics simulations of MexA. Biophys J **91:**558-64.
69. **Ye, L., Z. Jia, T. Jung, and P. C. Maloney.** 2001. Topology of OxlT, the oxalate transporter of Oxalobacter formigenes, determined by site-directed fluorescence labeling. J Bacteriol **183:**2490-6.
70. **Yoneyama, H., H. Maseda, H. Kamiguchi, and T. Nakae.** 2000. Function of the membrane fusion protein, MexA, of the MexA, B-OprM efflux pump in Pseudomonas aeruginosa without an anchoring membrane. J Biol Chem **275:**4628-34.
71. **Yum, S., Y. Xu, S. Piao, S. H. Sim, H. M. Kim, W. S. Jo, K. J. Kim, H. S. Kweon, M. H. Jeong, H. Jeon, K. Lee, and N. C. Ha.** 2009. Crystal Structure of the Periplasmic Component of a Tripartite Macrolide-Specific Efflux Pump. J Mol Biol.
72. **Zgurskaya, H. I., and H. Nikaido.** 1999. AcrA is a highly asymmetric protein capable of spanning the periplasm. J Mol Biol **285:**409-20.
73. **Zgurskaya, H. I., and H. Nikaido.** 1999. Bypassing the periplasm: reconstitution of the AcrAB multidrug efflux pump of Escherichia coli. Proc Natl Acad Sci U S A **96:**7190-5.
74. **Zgurskaya, H. I., and H. Nikaido.** 2000. Cross-linked complex between oligomeric periplasmic lipoprotein AcrA and the inner-membrane-associated multidrug efflux pump AcrB from Escherichia coli. J Bacteriol **182:**4264-7.

Appendix 1

Abbreviations

ABC	ATP Binding Cassette
BSA	Bovine Serum Albumin
CA	Carbonic Anhydrase
CBB	Coomassie Brilliant Blue
DDM	n-Dodecyl-β-D-Maltoside
DTT	Dithiothreitol
EDTA	Ethylenediaminetetraacetate
F5M	Fluorescein-5-Maleimide
FA	Formaldehyde
HEPES	N-2-Hydroxyethylpiperazine-N'-2-ethanesulfonic acid
IM	Inner Membrane
IPTG	Isopropyl-β-D-thiogalactopyranoside
kDa	Kilodalton
LB	Luria-Bertani
LS	Light Scattering
MALDI-TOF	Matrix-Assisted Laser Desorption/Ionization coupled Time-Of-Flight
MATE	Multidrug And Toxic Compound Extrusion
MFP	Membrane Fusion Protein
MFS	Major Facilitator Superfamily

MIC	Minimal Inhibitory Concentration
MS	Mass Spectrometry
MW	Molecular Weight
OD	Optical Density
OM	Outer Membrane
OMF	Outer Membrane Factor
ORF	Open Reading Frame
PBS	Phosphate Buffered Saline
PK	Proteinase K
PL	Proteoliposomes
POE	Polyoxyethylene
PMSF	Phenylmethylsulfonyl fluoride
RI	Refractive Index
RND	Resistance-Nodulation-Cell Division
RT	Room Temperature
SDS-PAGE	Sodium Dodecyl Sulfate-Polyacrylamide Gel Electrophoresis
SEC	Size Exclusion Chromatography
SMR	Small Multidrug Resistance
TX	Triton X-100
UV	Ultraviolet
WT	Wild type